PROBING THE DARK SECTOR

A Dissertation

Presented to the Faculty of the Graduate School

of Cornell University

in Partial Fulfillment of the Requirements for the Degree of

Doctor of Philosophy

by

Istvan Laszlo

May 2012

© 2012 Istvan Laszlo
ALL RIGHTS RESERVED

PROBING THE DARK SECTOR

Istvan Laszlo, Ph.D.

Cornell University 2012

Cosmology today is in a golden era, data is pouring in and exciting and challenging questions are being raised. We know that we live in an accelerating Universe populated largely by dark matter and dark energy, yet we have little information on the nature of either of these mysterious components. Theories abound and data is coming in with far greater quantity and precision than ever before and promises to enable distinguishing between these theories, however as we improve instruments we find ourselves plagued with how to effectively model signatures of the theories, and also how to truly interpret the data. Uncertainties in the nonlinear regime of theoretical predictions and in handling astrophysical systematics in observables are now emerging as leading issues that hinder constraining power. This thesis investigates the dark sector, considering first how one can approach the generation of correct nonlinear predictions for growth where gravity is modified (MG) in an attempt to explain the acceleration of the Universe. Next, we examine a possible Yukawa type self coupling of dark matter, motivated by the problems in small scale ΛCDM simulations of growth of structure, such as the cuspiness of halo density profiles and over production of small haloes. Finally, forecasts of constraining power for future surveys are made, in light of a key astrophysical systematic in weak lensing observations, namely the actual alignment of galaxies that form in the same halo which mixes in with the lensing signal in two ways, both generically summed up as Intrinsic Alignments(IA). We find that the standard approach of using fits developed in ΛCDM to generate nonlinear predicted matter power spectra for MG

theories is valid, at least to mildly nonlinear scales. In the context of dark matter, there is no evidence against an interaction, yet also no preference for one. Finally for future survey forecasts, we find that previous forecasts were optimistic, and without a strong model for IA, additional probes will be required to compliment the weak lensing shear results and arrive at constraints similar to those derived from a survey in the absence of or with perfectly known IA contamination.

BIOGRAPHICAL SKETCH

Istvan Laszlo was born in 1982 in Budapest, Hungary, but his family soon moved to the United States and he has always called this his home. Living in Maryland, Istvan completed all of his schooling there, through his undergraduate years at the University of Maryland, College Park. Graduating from UMD with degrees in Computer Science, Astronomy, Physics and Mathematics in 2004, Istvan spent 1 year searching to enter the gaming industry as game programmer, but found he desired a greater challenge, and began his graduate studies in cosmology at Cornell University, in the Department of Astronomy, in 2005.

To my sister, who has always been by my side,

to my mother, for her unwavering encouragement,

to my father, whose guidance led me to where I am,

to my daughter-to-be, Ebony, who keeps me young and smiling, and

to my fiancee, Robyn, whose love and support lead me to my future.

ACKNOWLEDGEMENTS

Thanks to Rachel Bean, my advisor, for her infinite patience and guidance. Thanks also to my collaborators Sarah Bridle, Donnacha Kirk, Eanna Flannagan, and Mark Trodden for their patience and excellent insights, to my many friends and colleagues at Cornell, in particular Nishant Agarwal and Greg Sloan, for useful discussions and support. Also many thanks to Anatoly Klypin and Jon Holtzman for kindly making their PM code publicly available and Olivier Doré, Hans Stabenau and Ira Wasserman for valuable discussions in the course of this work. The work of IL and RB presented in chapter 2 is supported by the National Science Foundation under grants AST-0607018 and PHY-0555216. RB's, EF's and MT's work in chapter 3 is supported by NASA ATP grant NNX08AH27G. RB and IL's work in the same chapter is supported by NSF grants AST-0607018 and PHY-0555216 and Research Corporation, EF's by NSF grants PHY-0457200 and PHY-0555216 and MT's by NSF grant PHY-0653563 and by Research Corporation.

Further thanks to the Aspen Center for Physics for support and for hosting two coincident workshops on "Wide-Fast-Deep Surveys: New Astrophysics Frontier" and "Testing General Relativity in the Cosmos" in 2009 where the work in chapter 4 was conceived, and the Kavli Royal Society International Centre for hosting the "Testing general relativity with cosmology" workshop in 2011 that supported fruitful discussion and collaboration.

Also we (the authors of the work in chapter 4) thank Filipe Abdalla, Adam Amara, David Bacon, Scott Dodelson, Ole Host, Martin Kilbinger, Andrew Jaffe, Bhuvnesh Jain, Benjamin Joachimi, Ofer Lahav, Rachel Mandelbaum, Anais Rassat, Alexandre Refregier and Jochen Weller for helpful discussions. RB's and IL's research for the work in chapter 4 is supported by NSF CAREER grant AST0844825, NSF grant PHY0968820, NASA Astrophysics Theory Pro-

gram grants NNX08AH27G and NNX11AI95G and by Research Corporation and SLB thanks the Royal Society for support in the form of a University Research Fellowship and acknowledges support from European Research Council in the form of a Starting Grant with number 240672.

CONTENTS

LIST OF FIGURES

LIST OF TABLES

CHAPTER 1

INTRODUCTION

1.1 Cosmology Today

Cosmology is in a golden era, a wealth of cosmological data is pouring in and more missions to improve and add to the wealth of information are planned and undergoing. A clear picture of the universe is emerging and we believe the Universe is

- *homogenous*: Averaged over large scales the Universe is uniform
- *isotropic*: Averaged over large scales the Universe is the same in all directions
- *expanding*: The space time of our universe is stretching
- *accelerating*: The expansion of the Universe is speeding up

The first two points are statements that our visible Universe is a representative sample of the Universe as a whole and that the physical laws which govern it are the same as they would be for other observers anywhere else. The third point hints at the origin of the Universe, extrapolating backward in time an expanding Universe must at one point have been a singularity of space-time (the very fabric of the Universe, the canvas upon which we paint matter and energy), which we term the Big Bang. The fourth point while stated as simply as the others, is the most surprising and exciting. Under typical assumptions the first three points and our sampling of the matter and energy in the Universe would imply that by general relativity the matter in the Universe should slow and eventually reverse

the expansion of space-time, yet this is not the case. Instead, some mysterious force or material or physics drives the expansion on.

This thesis considers some theories for each dark component, some current data and the constraints it sets on those theories and models, and future survey prospects. In the context of future missions important systematics arise, where the sensitivity is reaching levels that we are limited by astrophysical systematics that figure in as noise in the signal at present, but might in the future become probes of cosmology themselves once better understood. The second half of this text deals with considering one key such systematic and its interplay with models for dark energy.

Before delving into these topics, the next sections continue to introduce cosmology as it stands today, explain the underlying physical framework, discuss the observations utilized to shape our understanding of the Universe, and describe the accepted model of the Universe. Then this introduction turns to a discussion of the dark sector, with descriptions of some evidence for, and rationale behind, each of the dark components, along with some of the leading theories for what these components are. Finally the introduction concludes with a discussion of how additional observations and combinations of observables can be used to learn about the

Then, the thesis will turn to more detailed descriptions of how we can simulate observables in these theories (2), how well we can constrain some theories (3), and finally how future data and systematics will impact constraints on these theories((4). Finally (5) will summarize the findings presented in the preceding chapters and discuss future directions and prospects.

1.1.1 The Physics of Cosmology

Understanding how the background expansion history and growth of perturbations proceeds arise simply from Einstein's general relativity.

We begin with the (perturbed) Friedman-Robertson-Walker metric written in the conformal Newtonian (or longitudinal) gauge,

$$ds^2 = a(\tau)^2 \left[-(1+2\psi)d\tau^2 + (1-2\phi)dx_j dx^j\right] \tag{1.1}$$

where a is the expansion or scale factor, τ is the conformal time, x is the comoving coordinate (j=1,2,3 spatial directions) and ϕ and ψ are the two gravitational potentials, arising from perturbations, that for ΛCDM are equal[2].

The scale factor, a, describes by what factor the Universe was smaller than its present size today, as $a = 1$ today. This expansion of the Universe means there are two types of distances; the comoving distance which neglects expansion, and physical distance which we as observers would measure, that includes 'added' distance of expansion. The two are related simply;

$$physical\ distance = a * comoving\ distance. \tag{1.2}$$

Comoving distance can be thought of as measured on an expanding coordinate system that expands in step with the Universe, thus if things aren't moving except due to the expansion of the Universe, their coordinates in that comoving system are unchanging, and so the comoving distance between them remains constant. Whereas the physical distance, as they expand away from one another, increases. The usefulness of comoving distances should be apparent, changes in comoving distances are due to 'real' motions of the objects, separating out any motion due to expansion.

The conformal time, τ, can best be understood by noting that light travels a physical distance $d = ct$, and $d\tau = dt/a$ so the comoving distance is as one expects $dx = cd\tau$. Integrating this from t=0, the Big Bang, to the present day then gives the maximum distance light can have traveled, the comoving horizon. As time goes on, this increases monotonically and so, dropping the factor of c can be used as a time variable itself. This new time variable is the conformal time, and in some sense can be considered as a time coordinate in the expanding frame, where as t, the physical time is the time measured by observer accounting for expansion.

Finally, ϕ and ψ can be treated as $\phi(\vec{x}, \tau)$ and $\psi(\vec{x}, \tau)$ and represent the perturbations in the gravitational potentials.

Einstein's Equations relate combinations of the elements of the metric above in the form of the Einstein tensor, $G_{\mu\nu}$, and hence the potentials, to the matter and energy content of the Universe described by the energy momentum tensor, $T_{\mu\nu}$,

$$G_{\mu\nu} = 8\pi T_{\mu\nu}, \tag{1.3}$$

where

$$T^{\mu}{}_{\nu} = \begin{pmatrix} -\rho & 0 & 0 & 0 \\ 0 & P & 0 & 0 \\ 0 & 0 & P & 0 \\ 0 & 0 & 0 & P \end{pmatrix} \tag{1.4}$$

where ρ is the energy density and P is the pressure of the component being considered. Evaluating this in absence of the perturbations gives the background equations, the familiar Friedmann and acceleration equations for a flat universe(eg [2]):

$$\mathcal{H}^{\in}(\dashv) \;=\; \frac{8\pi G}{3} a^2 \rho \tag{1.5}$$

and

$$\frac{d}{d\tau}(\mathcal{H}) = -\frac{\triangle\pi}{\ni}\mathcal{G}\dashv^{\in}(\rho + \ni\mathcal{P}). \tag{1.6}$$

Where $\mathcal{H} = \dashv\mathcal{H} = \frac{\lceil\dashv}{\frac{\lceil\tau}{\dashv}}$ and ρ includes all the components of the Universe; for example for Universe with matter, radiation, and a cosmological constant the Friedmann equation becomes

$$H^2(a) \;\; = \;\; H_0^2\left[\frac{\Omega_m}{a^3} + \frac{\Omega_\gamma}{a^4} + \Omega_\Lambda\right], \tag{1.7}$$

where H_0 is Hubble's constant, Ω_m and Ω_γ are the fractional energy densities today in non-relativistic matter (baryonic and cold dark matter) and any relativistic species (eg radiation) respectively.

H is a key element in considering a theory as it contains in it the evolution of the expansion of the universe. Comoving distances as a function of time, or scale factor (which can be viewed as a time variable since the Universe has and always will expand, so that a is monotonically increasing with time), are based on the expansion history of the Universe,

$$\chi(a) = \int_a^1 \frac{da'}{a'^2 H(a')} \tag{1.8}$$

and so determining $H(a)$ is of great importance. The other thing one needs from a theory beyond predicting general expansion history, is to also predict the assembly of galaxies and galaxy clusters.

The physics behind the growth is general relativity, since although the initial perturbations on on scales described by Newtonian physics, the density perturbations seeded after the Big Bang are enlarged by inflation to super horizon scales. Thus understanding how a theory will impact growth is achieved by evaluating Einstein's equations for the metric perturbations which relate the potentials to

fractional perturbations in density, $\delta_s \equiv \delta\rho_s/\rho_s$, peculiar velocity, $v_{(s)}$, and intrinsic shear σ_s for a matter component 's'. These equations in the conformal newtonian gauge are

$$k^2\phi + 3\mathcal{H}(\dot{\phi} + \mathcal{H}\psi) = -\frac{3\mathcal{H}^2}{2}\sum_s \Omega_s\delta_s, \tag{1.9}$$

$$k^2(\dot{\phi} + \mathcal{H}\psi) = \frac{3\mathcal{H}^2}{2}\sum_s (1+w_s)\Omega_s(ik^j v_{(s)j}) \quad , \textit{ and} \tag{1.10}$$

$$\phi - \psi = \frac{9\mathcal{H}^2}{2}\sum_s (1+w_s)\Omega_s\sigma_s, \tag{1.11}$$

where $\Omega(a)$ is the fractional energy density, and $w(a)$ is the equation of state for the fluid.

The first two equations above can be combined to find the Poisson equation,

$$k^2\phi = -\frac{3\mathcal{H}^2}{2}\sum_s \Omega_s\left(\delta_s + 3\mathcal{H}(1+w_s)ik^j\frac{v_{(s)j}}{k^2}\right), \tag{1.12}$$

$$= -\frac{3\mathcal{H}^2}{2}\sum_s \Omega_s\Delta_s \tag{1.13}$$

where Δ_s is a gauge invariant density variable defined in the rest frame of the matter components [3].

This relates the potentials to the perturbations, to understand then the total evolution of growth, one turns to the perturbed fluid equations to describe the evolution of the density and velocity perturbations,

$$\dot{\delta} = -(1+w)(ik^j v_j - 3\dot{\phi}) - 3\mathcal{H}(c_s^2 - w)\delta, \tag{1.14}$$

$$ik^j\dot{v}_j = -\left[\mathcal{H}(1-3w) + \frac{\dot{w}}{1+w}\right]ik^j v_j + \frac{c_s^2}{1+w}k^2\delta - k^2\sigma + k^2\psi \tag{1.15}$$

where c_s^2 is the sound speed for the fluid.

Thus, the two things a theory must predict are expansion history and growth of perturbations. To then compare to our universe, we must understand the im-

pact each of these has on the look of our Universe in terms of the cosmological observables we utilize to study the Universe.

1.1.2 Observations Used to Characterize Background Expansion

Since expansion history is related to distances, it is natural that distance determinations are a key probe of cosmology. Just as there are two distances in theoretical descriptions there are two observable distances, luminosity distance and angular diameter distance. For an object at distance, d, large compared to its physical size, l, its angular size,θ will appear $\theta = l/d$. Using this then we can determine the distance to an object if l is known,

$$d_A = l/\theta = a\chi(a) \tag{1.16}$$

where χ is the comoving distance to the object, determined from its redshift, and the second equality stems from noting that the angular size subtended by the object will be its comoving size (l/a) divided by the comoving distance to that object.

Luminosity distance assumes we know the luminosity of the object, and uses the fact that the distance determines the flux received from the object, $F = \frac{L}{4\pi d_L^2}$ which in expanding universe becomes $F = \frac{La^2}{4\pi\chi^2}$ so that setting the two equal defines d_L:

$$d_L = \frac{\chi(a)}{a} \tag{1.17}$$

From the above it is clear that measuring distances based on standard candles or standard rulers can tell us about $\chi(a)$ if we know the expansion factor at the

time the light was emitted by the object. This is determined by measuring the redshift of the object (the Doppler shift induced by recession of the object from us), and assuming that the recessional velocity is due to the Hubble flow (to the expansion of the Universe). Then the redshift, z, can be used to determine the expansion factor

$$a = \frac{1}{1+z} \tag{1.18}$$

Thus, we can use the observed distances and redshifts understand the expansion history of the Universe. If we have some means of determining the luminosity or size of a distant object.

Standard candles are groups of objects that owing to the nature of the source of emission all share the same luminosity and hence can be used to make luminosity distance measurements, an example is Type IA Supernovae discussed below. Standard rulers analogously are objects or rather features for which we know the actual length scale and thus enable us to make measurements of the angular diameter distance, Baryon Acoustic Oscillations produce a cosmological sound horizon that is such a standard ruler.

Supernova Observations

The most common example of a standard candle is type IA supernovae; the result of accretion onto a white dwarf pushing it over the Chandrasekhar mass limit [1]. Since these supernovae start from the same mass as they explode, they produce the same

[1]Really, the mechanism for type IA supernovae is more complicated, there is evidence that they in fact explode over the mass limit, due to intricacies of the process of mass transfer and ignition and collapse. Despite this, they are more or less standard, and can be calibrated based on rise and fall of their light curves

luminosity and as such serve as known luminosity probes, or standard(izeable) candles.

Baryon Acoustic Oscillations

One standard ruler comes from the cosmological sound horizon set by baryon acoustic oscillations. In the early Universe the high temperature and pressure result in baryons and photons being coupled, so that in a density perturbation where initially all matter (dark and baryonic) are clumped, the baryons move out from the center carried by the photons. This results in a spherical shell of baryonic material around a dark matter center where the original perturbation was, supported against gravity by the radiation pressure. As photons and baryons decouple as the expansion decreases pressures and things are able to cool, growth can proceed with structure collecting both on the dark matter perturbation at the center and along the baryonic spherical shell. The photon-baryon mix moves at calculable speed, roughly half the speed of light, and so knowing the time to decoupling translates into knowing how far out the shell advances. Thus, baryon acoustic oscillations set a calculable scale, and this is imprinted on the cosmic microwave background(CMB) and on Large Scale Structure.

Cosmic Microwave Background

The cosmic microwave background(CMB) is one of the most versatile and informative probes of cosmology, providing not only distance scale measurements to use to understand background expansion but also clues of the fractional density of each component.

The CMB is a frozen in picture of the structure of the Universe very early in its history, at a time called recombination. It is the first light able to travel significant distances. Just after the Big Bang the Universe is a hot plasma of protons, electrons, and photons, and cooling as time goes on. As it cools protons and free electrons combine to form neutral hydrogen, enabling photons to travel much farther before being absorbed; this is what is meant by recombination. From this time on, the light can actually travel and thus can be seen today when looking far enough away, resulting in a Big Bang afterglow.

The observable of interest is the small anisotropies due to the initial perturbations that seed structure growth. Expressed in terms of the variance of the coefficients of the fluctuations in temperature expanded in a basis of spherical harmonics

$$C_\ell \equiv < |a_{\ell m}|^2 > \equiv \frac{1}{2\ell+1} \sum_{m=-\ell}^{+\ell} |a_{\ell m}|^2 \tag{1.19}$$

$$\frac{\delta T}{T}(\theta,\phi) = \sum_{\ell=2}^{+\infty} \sum_{m=-\ell}^{+\ell} a_{\ell m} Y_{\ell m}(\theta,\phi), \tag{1.20}$$

C_ℓ contains all the information of the CMB maps if temperature fluctuations are Gaussian. By considering the angular power spectrum, C_ℓ(or rather $\ell(\ell+1)C_\ell/2\pi$) as a function of ℓ, one can set constraints on the input cosmology (the fractional densities) quite well. This is because the location of peaks and relative peak heights of the power spectrum are very sensitive to the cosmology. The CMB contains a signature of baryon acoustic oscillations, and even information on post processing of the perturbations due to changing potentials as the light travels to us due to the (integrated) Sachs-Wolfe effect.

1.1.3 Observations Used to Characterize Growth

All of the aforementioned observables probe the general expansion history of the Universe, revealing how the background density evolves. On top of this background evolution of space time, perturbations exist and grow giving rise to the CMB temperature anisotropies at recombination and galaxies and galaxy clusters today. Large scale structure (LSS) surveys (e.g. [4, 5, 6]) provide probes of the growth of perturbations in density that give rise to the structure of the Universe.

The structures in the Universe represent the result of the growth of primordial perturbations in the density of matter and radiation by gravitational instability. Studying these structures in detail probe the gravitational physics of the Universe as function of time. These probes thus provide complimentary information, and become the key for understanding a bit more about dark energy.

Growth observables include looking at luminous matter distributions and total matter distributions, and are at first level always characterized in terms of the two point correlation functions (or their Fourier space average, the power spectra).

That is for some three-dimensional field X we observe a two-dimensional projection in a direction $\hat{\mathbf{n}}$ which can be written

$$X(\hat{n}) = \int_0^\infty dz W_X(z) \mathcal{X}(\hat{\mathbf{n}} r(z), z), \tag{1.21}$$

where the window function ($W_X(z)$) is used to select the range of z which affects the observable.

In this work we characterize observations by the observed two-dimensional angular power spectrum of two fields X and Y

$$C_\ell^{XY} = \int_0^{\chi_\infty} \frac{d\chi}{\chi^2} W_X(\chi) W_Y(\chi) S_X(k_\ell, \chi) S_Y(k_\ell, \chi) \tag{1.22}$$

where $k_\ell = \ell/\chi$, the W are window functions, while S represent source functions for the fields.

The power spectrum of two fields then, P_{XY} is given by

$$P_{XY} =< S_X S_Y > . \tag{1.23}$$

The observables in large scale structure basically contain information on the potentials ϕ and ψ, and ultimately can be related to the perturbations in density δ of the matter.

Thus understanding how to evolve the perturbations in simulations is key to generating simulated observables against which to compare observations. The perturbations are treated to linear order in perturbation theory, and evolved according to the linearized equations already given in equation 1.11. Typically, the density considered is that of the dark matter, as baryon fractions are low, and baryonic processes matter at lower scales than commonly used.

Matter Power Spectrum

The matter power spectrum is the simplest and in some sense most fundamental observable of interest upon which large scale structure depends and in terms of which one can formulate galaxy clustering and velocity measurements. It is the power spectrum of the actual matter (over)density perturbations, $\delta = n/\bar{n} - 1$ and as such is sourced by the perturbations themselves, so that

$$(2\pi)^3 P(k)\delta^3(\vec{k} - \vec{k}') =< \delta(\vec{k})\delta(\vec{k}') > . \tag{1.24}$$

Of course, astronomers cannot observe the total matter distribution to arrive at this, instead one probes the luminous matter via galaxy surveys and assumes a

mass to light bias factor b to relate the observed galaxy power spectrum to the underlying matter power spectrum,

$$P_{gg}(k,\chi) = b^2(k,\chi)P_{\delta\delta}(k,\chi) \tag{1.25}$$

Characterizing growth of structure in terms of the scales that do show structure, or in terms of the power of correlations on various scales has become the norm. Galaxy redshift surveys and galaxy peculiar velocities, provide information on the matter power spectrum, and the Newtonian potential arising from matter. However, these probes suffer from bias, being derived only from luminous matter, and are often only considered in linear theory. Yet, the matter power spectrum has clearly non-linear evolution at small scales. For standard GR, a typical approach is to use analytical fits based on N-body simulations of ΛCDM [7, 8] and $wCDM$ [9, 10, 11] scenarios to apply the non-linear correction to a linear power spectrum.

Simulations of modified gravity models are for the most part lacking, however. With the exception of [1, 12], analyses often proceed by applying the ΛCDM based analytical non-linear fits to modified linear power spectra, e.g. [13, 14]. Recently an analytical approach to estimating non-linear growth in modified gravity, including those with anisotropic stress, [15] was proposed and it was noted that there were currently no simulations against which to test the ansatz. Thus, testing how to extend mater power spectra to mildly non linear regimes is the focus of chapter 2.

Convergence Power Spectrum and Weak Lensing

Addressing the fact that matter power spectrum observables, are based only on luminous matter, one considers also probes of total mass, such as shear or convergence power spectra, derived from weak lensing measurements. Weak lensing gives

two-point and higher statistical correlations of the true or total density field [16], potentially in tomographic redshift slices [17, 18].

Note the usefulness of weak lensing measurements, lies in the fact that modified gravity models can introduce extrinsic anisotropic shear stresses (see e.g. [19]) that modify the relationship between the weak lensing potential and the matter over density that might be detectable by contrasting weak lensing with other large scale structure observations [20, 14].

Restating this in terms of the Newtonian potentials, there are two to consider, ϕ the standard gravitational potential, that determines how matter gives rise to the potential, and ψ which basically describes how things respond to the potential. Weak gravitational lensing (WL) is a particularly useful probe of gravity because it is sensitive to $\phi + \psi$, the sum of the metric potentials, while most matter power spectra observables depend on ϕ alone. That is, the shear field sourcing the shear angular power spectrum is the sum of the two Newtonian potentials, $\psi+\phi$, while for instance the galaxy power spectrum is actually sourced by ϕ (and related directly to the perturbations by application of the Poisson equation).

Thus weak lensing and cosmic shear measurements are the key addition to our cosmological dataset that will enable us to constrain dark energy theories([21, 22].)

Cosmic shear was first detected a decade ago ([23, 24, 25, 26]), and has blossomed over the years, with data from the Hubble Space Telescope COSMOS survey ([27, 28]), and the Canada-France-Hawaii Telescope Legacy Survey (CFHTLS) ([29]). In addition the 100 square degree survey ([30]) combines data from several smaller surveys ([31, 32, 33, 31]). These datasets have shown the additional power gained by such measurements and spur on new plans.

Upcoming "Stage III" projects include Kilo-degree Survey (KIDS) on the Very Large Telescope (VLT) Survey Telescope (VST), the Panoramic Survey Telescope and Rapid Response System (Pan-STARRS) project, the Subaru Meaurement of Images and Redshifts (SuMIRe) survey using HyperSUPRIMECam(HSC), the Dark Energy Survey (DES) on the Blanco Telescope. More ambitious "Stage IV" imaging projects are the Large Synoptic Survey Telescope (LSST) ground-based project and in space the proposed European Space Agency mission *Euclid* and the NASA proposed Wide-Field Infrared Survey Telescope (WFIRST).

1.1.4 The Universe Today and the Concordance Model

The above observations all paint a picture consistent with the physics laid out if we consider as the standard starting point is a Universe whose components are

- *radiation and relativistic neutrinos*: energy in the form of photons and relativistic neutrinos
- *matter*: the everyday baryonic material from which we and stars are made
- *dark matter*: a mysterious gravitating component, that behaves as normal matter gravitationally, but does not otherwise interact
- *cosmological constant/dark energy/modified gravity*: the component responsible for the acceleration of the Universe

The standard model of the Universe, the ΛCDM model, mixes radiation, baryonic matter, cold dark matter(CDM), and a cosmological constant (Λ), as its choice for the accelerating component. In ΛCDM gravity is described GR, and current constraints ([34]) suggest 22% of the energy content of the Universe is in the form

of CDM and 73% as the cosmological constant, and the rest is neutrinos and radiation and baryons. This model enables simulations of Universes that result in statistically similar Universes to our own, and uses but a few parameters, and as such has become the concordance model.

Though the model does reasonably well, it does face a few challenges when comparing to fine details of observations and especially when considering its theoretical footing. Simulations of structure in ΛCDM are prone to producing an over abundance of structure on small scales, too many low mass satellite haloes, or over dense central regions in galaxies and clusters. These are referred to as the missing satellite and cuspiness problems. The degree to which these considerations are problems is somewhat debated; observations are detecting more low mass haloes, and mechanisms for avoiding high central densities are being discovered and added to simulations, however at present tension between theory and observation remains.

Beyond simulation mismatches, it must be noted that though the behavior of the components is known (to a certain degree), their origins are not at all understood. For instance, attempting to use vacuum energy as the source of the cosmological constant requires a fine-tuning of its value to many orders of magnitude smaller than theory can motivate(Fine-tuning problem), e.g.[35], analogous tuning is required to explain why the cosmological constant is just now becoming dominant and important (Coincidence Problem). Admitting that tuning is an issue, perhaps alternative descriptions are needed for the accelerating component, termed dark energy.

In light of this, perhaps the most interesting thing to note about ΛCDM is that neither the nature of dark energy nor of dark matter are understood. Thus, there seems both a need and an opportunity, to extend beyond the vanilla cosmology of

ΛCDM. As a result, quite a few theories exist to attempt to explain these dark components.

The general expansion history of the Universe is well constrained and studied and, as such, is the main criteria for testing and guiding theories. However, it alone cannot distinguish between the many theories, which predict variations in the way structure assembles in over dense regions. What makes this time truly the golden era of cosmology is that we are now poised to collect high quality data on this growth of structure. In particular deep and wide angular scale data sets on large scale structure in many forms, eg galaxy counts, galaxy shear, and galaxy velocity surveys, will probe both the luminous matter and total matter (luminous plus dark) distributions and as such provide crucial information on the assembly of structure in the Universe, which will provide a lever arm with which to truly discriminate between various theories. These surveys include for example KIlo-Degree Survey (KIDS), Pan-STARRS [2], Subaru Measurement of Images and Redshifts survey using HyperSUPRIMECam(HSC), [3] DUNE [36], JDEM/SNAP [37], the Dark Energy Survey (DES) [4],the Large Synoptic Survey Telescope (LSST,[38]) [5], and prospective space based surveys Euclid[6] and Wide Field Infra-Red Space Telescope (WFIRST)[7].

[2] http://pan-starrs.ifa.hawaii.edu
[3] http://sumire.ipmu.jp/en/
[4] http://www.darkenergysurvey.org
[5] http://www.lsst.org
[6] http://sci.esa.int/euclid
[7] http://wfirst.gsfc.nasa.gov

1.2 The Dark Sector

The dark sector is the term used to describe the 95% of the Universe that isn't our everyday experience, e.g. that isn't baryonic matter or radiation. Despite being the largest part of the energy density of the Universe today, the components of the dark sector are the least understood. Dark matter (23% of the energy content of the Universe) is a gravitating and but otherwise non-, or extremely weakly, interacting component, but what it is remains a mystery. Dark energy is 72% of the Universe's energy content and is really only understood at the level of being known to exist and being known to cause the accelerated expansion of the Universe.

The case for these dark components is clear, many observations confirm the need for such seemingly bizarre additions to our Universe, yet at the same time the underlying physics of the dark sector remains for all real purposes unknown. Thus, a wide variety of possible candidates and theories exist for describing what these dark components are, and generally tend to be new extensions of the standard model of particle physics treating the dark components as actual material of some form or other, extensions of field theory in the form of new scalar fields, or alterations of the way gravity works at relevant scales in ways to mimic the effects of these dark components. The next few sections will review the evidence and theories for each dark component in turn.

1.2.1 Dark Matter: Observational Evidence

The mysterious dark (extremely weakly or non-interacting, aside from gravitationally) matter makes up some 23% of the Universe's energy content, and as such $\sim$ 85% of the total matter in the Universe, yet its nature is not all understood. For

the very reason we term it dark, this component of the Universe is difficult to study, namely the only way we know to detect it is indirectly through its gravitational effect. To probe the gravitational potential of a region we need some test particles moving in that potential. Fortunately, we have many candidates; the motion of stars, gas, and galaxies themselves, and even light all react to the potentials in or through which they move.

Galactic rotation curves and X-ray mapping of galaxies and clusters all serve to test the gravitational dynamics of galaxies and clusters by studying how these test particles move. Weak lensing studies on the other hand utilize light as the test particle. Each of these is described briefly below.

Galactic Rotation Curves

Originally, dark matter arose from observations of galactic rotation curves, extensive luminous studies of galaxies made it known that the density of (luminous) material fell off as one got further from the center of a galaxy. If the galaxy is in virial equilibrium then it is expected that the rotation (orbital) velocity of material at a radius r should be

$$v \propto \sqrt{\frac{GM(r)}{r}} \tag{1.26}$$

where M(r) is the mass enclosed by the orbit. For centrally concentrated mass, $M(r)$ does not increase as one increases r, and so one expects the velocity to decrease as r increases. However, when spectroscopy is employed to determine the motion of material at various radii it is found the velocity does not fall off as expected, instead it remains more or less constant, suggesting a more distributed mass component ($M(r) \propto r$) that somehow the luminous surveys had missed as in[39, 40].

X-ray Gas Distributions

Beyond mapping rotation profiles of galaxies, one can map the density and temperature of the gas in a galaxy and determine the total mass needed to keep that gas bound under the assumption of hydrostatic equilibrium. The result is a strong indicator that there is far more mass than we detect in the galaxies. For example, adding the X-ray gas component to the visible component accounts for only 6% of the total mass inferred for M87[41]. Other galaxies and even galaxy clusters show similar discrepancies based on the gas in them.

Gravitational Lensing

Weak gravitational lensing occurs when light from a background galaxy is distorted by passing a massive object such as a galaxy and results in the distortion of that image (as opposed to strong lensing which results in generation of multiple images or rings or arcs). When the lens is not a galaxy but rather a cluster, the multiple lensing events of the single background galaxy enables a mapping of the actual mass distribution of the cluster. This can be used to infer the total mass and thus can be compared to the gas and luminous component to reveal need for dark matter. This reconstruction is not often done in practice, instead the multiple lensing events are used with many background images and in this way allows one to constrain the total mass fraction in the Universe and the dark energy component as well eg [42, 43]. This estimate of the total matter contribution can be compared with other estimates of baryonic contribution to show that in fact there is much more matter in the Universe than baryons.

Further, one can use weak lensing to determining just how far the halo of a

galaxy extends, and there by estimate the contribution from the dark halo to the total matter fraction as in [44].

Colliding Galaxies

Still newer evidence comes from observations of colliding galaxies as in the case of Bullet Cluster where X-ray observations can map the baryonic content, and lensing maps can reconstruct the total mass distribution. The baryonic material is shocked by the collision and thus sits at the center of the system(the galaxies having passed by each other), while their dark matter content is un-shocked and moves freely past revealing indeed that the luminous matter does not describe the location of most of the mass of the galaxies and essentially giving a picture of the dark matter haloes of the galaxies ([45]).

Abell 520 is another system that shows evidence for some odd location of mass concentrations, namely a peak in X-ray derived gas density at a location where there is no significant luminous counterpart to give rise to a constraining potential, suggesting a dark core eg [46].

While seeing the gravitational silhouette of dark matter is a potent indicator of its presence, it does not tell us anything about the source of that gravitation. Thus, many possibilities are explored.

CMB

Further evidence comes from the same cosmological probes we use to determine background expansion history, as though we can estimate the baryonic content of the Universe, we find it far too little to match observations, e.g. matching the

ISW contribution to the CMB, which is sensitive to the balance of radiation and total (luminous and dark) matter, and matching CMB multipole peak locations. As well as the scale of the sound horizon at recombination (set by baryon acoustic oscillations) and the signal for peaks in structure at the center of each BAO wave.

1.2.2 Dark Matter: Challenges

It is interesting to note that a more detailed analysis suggests that treating dark matter as a real component that interacts only via gravity has some difficulties, which are made manifest using the same sorts of observations.

Using this minimalist interpretation of dark matter, ie treating the Universe as a ΛCDM Universe, halo density profiles from simulations suggest divergent density profiles as one nears the center of a galaxy[47]. By looking at density profiles determined by weak lensing or galactic rotation curve observations we can really get to the nature of a CDM halo and find that, when considering LSB galaxies (low surface brightness galaxies with low mass to light ratios) these tend to be more shallow profiles, while those of cluster haloes without luminous galaxies have flat profiles[47]. Note that in the case of LSB it is possible that beam smearing distorts the observations and if corrected for would give LSBs with steeper central profiles (eg. [48])

Rotation curves, which can constrain slope or concentration (or both in extremely well done cases), also point to discrepancies between simulations and observations. This suggests some key small scale physics is missing.

Indeed the failure of ΛCDM on small scales extends to small scale structure, ΛCDM simulations consistently result in excess structure on smaller scales (as

reflected by an excess of subclumps and subhalos)[47]. There are also an excess of dwarf galaxies predicted in CDM simulations of the local group [49, 50].

When one looks at the success of the Tully Fisher relation in relating luminosity to maximum rotation speed, one can explain this by appealing to gravitational interactions between the disk and the Halo [51], which sets limits on the concentration of the halo that is again smaller than concentrations implied by the simulations [47]. Bar Stability arguments similarly require a low density core, otherwise a bar would not persist[47].

It is worth noting that, one may think simulations just get the center profile wrong, but resolution and determination of the true center of the galaxy would only tend to soften divergence, not enhance it, so its not likely to be an artifact[47].

Indeed these various points each may be argued individually, but when looked at as a whole suggest one key symptom, namely excessive concentrations on smaller scales and in central areas in CDM simulations [52].

1.2.3 Dark Matter: Theory

What the preceding has emphasized is that we see that a Newtonian gravity applied to the luminous material that we are able to catalogue does not explain observed kinematics and dynamics of galaxies and galaxy clusters. This can be explained either by missing material or missing physics.

If it is missing material, then our physics is correct but we are lacking in our particle model some particle that is in fact the dark matter, otherwise the idea is that just as Newtonian gravity fails for certain high density scales and is replaced

by GR, perhaps it also fails on galactic and cluster scales, and some extended version of gravity must be used. A discussion of particle candidates is provided below, while extended physics is described in 3 and in the context of dark energy theories below.

Particle candidates

Interpreting dark matter as actual missing material, and considering the added problems of even basic ΛCDM, theorists have a variety of theories for what the nature and properties of dark matter might be. Therefore, quite a few fundamental dark matter particle candidates are proposed, [53] provides a nice review.

It is important to that while it may at first seem tempting to say that it must be simple baryonic material that we miss, the above observations, (e.g. presence of Baryon Acoustic oscillations centered on dark matter densities, or CMB constraints on Ω_m adn Ω_b, as well as constraints from Big Bang nucleosynthesis on baryon content clearly show that baryons are not the total matter in the Universe. Thus, though it is possible to attribute some dark matter to hidden baryons, there is a need for non-baryonic dark matter.

The candidates can be classed as cold, warm or hot dark matter, based on their speeds of motion and resultant properties. Cold dark matter moves slowly and results in bottom up formation of structure, hot dark matter is ultra relativistic and as such cannot give rise to density perturbations on small scales required to seed galaxy formation. Warm dark matter is intermediate to the two and will give rise to bottom-up structure formation above its free streaming length, and top-down for larger scales.

The candidates considered are many and various, see eg [53] for a more complete review, some generic ones are highlighted here:

- *neutrinos*-a warm dark matter candidate, these standard model particles are known to exist, but it can be shown that even assuming the largest mass allowed by constraints ([54] neutrinos can only contribute at most at the level $\Omega_\nu h^2 \lesssim 0.07$. CMB limits on neutrino fraction are even more restrictive, $\Omega_\nu h^2 < 0.0067$.
- *WIMPs*-Weakly Interacting Massive Particles, because of their large masses considered as warm or more often cold dark matter candidates, these like neutrinos do not interact via strong or electromagnetic forces, hence remaining dark. However unlike neutrinos, owing to their mass, WIMPs can easily build structure. Also unlike neutrinos, these particles are non-standard model candidates as no standard model particle with required masses would remain stable. A possible WIMP would be the supersymmetric netralino.
- *MACHOs*-Massive Compact Halo Objects, cold dark matter candidates, and in fact typically thought of as baryonic candidate, such as collapsed stars (black holes and neutron stars) or failed stars, brown dwarfs or even rogue planets. These objects however are unlikely to give the smooth widely distributed haloes of galaxies that rotation curves and gas dynamics imply.
- *Axions*-a cold dark matter candidate, are light particles proposed in particle physics to solve CP violation. While determining the amount of axions expected has high uncertainties deriving from assumptions on how they are produced, it is possible to create a Universe in which axions could explain dark matter [55].

Extended Physics

Others propose Modified Newtonian Dynamics(MOND) or other theories of Modified Gravity (MOG), such as TeVes, GIA and BIMOND (see e.g. [56] for a review), the idea being that just as Einstein corrected Newton's gravity, perhaps when galactic scales are considered gravity once more requires modifications.

Detection Experiments

The key to distinguishing between these lies in assessing how each affects growth in the Universe, in particular due to their additional properties. Each candidate can have some interactions, though weak, other than simply interacting via gravity,[57, 58, 59, 60, 61, 62, 63, 64, 65, 66] .

Such interactions can have astrophysical consequences, for example, the prospect of dark matter interactions, such as self-annihilation, that could give rise to the 511 keV emission [67]; the 'WMAP haze' [68, 69, 70]; implications for tidal streams in galactic systems [71, 72], as well as modifications to dark matter halo profile [73, 74, 52], dark matter halo mass function [75] or altered dark matter motion in cluster collisions, such as the Bullet Cluster [76].

Thus, several attempts exist to test for WIMPs or other particle candidates based on these interactions.

Direct Detection Experiments focus on detecting dark matter via the weak interactions it may have with standard model particles[77]. Typically considering scattering, using scintillation, photon emission, ionization due to the scattering (or combinations of these measurements) as the means of detection these set upper

limits on the scattering cross section[53].

There are many searches, like the Xenon-100 Experiment [78] and various searches at the Large Hadron Collider (LHC, as in e.g. [77]), which follow on the Cryogenic Dark Matter Search(CDMS,[79]), EDELWEISS[80, 81], ZEPLIN series (eg[82]),and DAMA[83] experiments. It should be noted that DAMA claimed a detection of scattering not jsut set limits, but that this detection remains un-verified and in tension with other experiments as discussed in[53] and references therein.

Beyond such direct detections of scattering events, one can search for modulations in the detection rates, owing to the motion of the Earth as it orbits the sun with respect to the galaxies frame of reference, which is expected to create a $\sim 7\%$ effect.

Still other experiments focus on indirectly detecting dark matter via detecting high energy products of dark matter annihilation. These products include neutrinos, positrons, anti protons and gamma-rays. Searches focus their attentions at over dense regions since the annihilation rate is proportional to density, and so strongest signals come from dense regions, like galaxy centers or clusters.

Neutrinos observations are attempted by neutrino telescopes like (AMANDA,[84]), (ANTARES,[85]) and (IceCube,[86]). Positron and anti-proton experiments include the High-energy Antimatter Telescope (HEAT,[87]), Balloon borne Experiment Superconducting Solenoidal spectrometer (BESS,[88, 89]), Cosmic AntiParticle Ring Imaging Cherenkov Experiment (CAPRICE, [90]) and the Payload for Antimatter Matter Exploration and Light-nuclei Astrophysics experiment (PAMELA, e.g. [91]).

Gamma-rays should be detectable by space based experiments such as the

Energetic Gamma Ray Experiment Telescope (EGRET,[92]) and Fermi Large Area Telescope (FermiLAT, e.g. [93], formerly GLAST).

Note that while gamma rays from such annihilations are expected to have an energy in the range of GeV to TeV resulting in an interaction length much smaller than the extent of Earth's atmosphere and so would not be expected to reach the ground one can measure these indirectly from the ground [53]. To make indirect observations, one can attempt to detect the particle shower and Cherenkov light created by the interaction of gamma rays passing through the atmosphere. The first application of this technique to detect cosmic gamma-rays via their Cherenkov light was the detection of such emission from the Crab Nebula from Whipple observatory ([94]). Other detections and probable sources of cosmic gamma-rays have since been identified as in [95], and many such searches exist, e.g. MAGIC ([96]), the Collaboration of Australia and Nippon (Japan) for a GAmma Ray Observatory in the Outback (CANGAROO-III, [97]),the High Energy Stereoscopic System (H.E.S.S., [98]), and the Very Energetic Radiation Imaging Telescope Array System (VERITAS, [99]).

To date, no detection of dark matter has conclusively been claimed but limits on the cross section for scattering with standard model particles and on the annihilation cross section are being made and refined, and with increasing sensitivity there is an ever increasing hope to make a detection.

1.2.4 Acceleration: Observational Evidence

The larger portion of the dark sector is the mysterious component behind the unexpected acceleration of the expansion of the Universe. The case for acceleration

is now irrefutable; a diverse range of observations are showing consistent evidence for the acceleration of the universe's expansion, for example supernovae observations(SN) [100, 101, 102, 103, 104, 105], cosmic microwave background(CMB) temperature and polarization fluctuations [106, 107, 108, 109, 110, 111, 112, 113, 114], and baryon acoustic oscillations(BAO) [115, 116].

The nature of these observations and how they provide measurements of the back ground expansion via yielding distance information has already been presented in 1.1.2.

Supernovae observations can be understood in a more direct and conceptual manner as well. Simply put if the expansion of the Universe were at a constant rate, then the Hubble constant would in fact be a constant and equal at all times to its value today. Then ignoring the peculiar velocities of galaxies, galaxies would recede from us with velocity, V,

$$V = H_0 D. \tag{1.27}$$

Thus, plotting spectroscopically determined velocities of galaxies as a function of distance to the galaxy should produce a line. However, if the expansion is decelerating or accelerating, then the result is a curve which lies above or below this line respectively. More often then not, it is apparent magnitude and redshift which are plotted, but magnitude is proxy for distance and redshift for recession velocity, so this means basically switching the axes and the scaling since magnitude goes as log of distance. In this case then, the accelerating universe lies above the constant expansion curve and the decelerating universe lies below. When this plot is made, the supernova lie in the accelerating region, and moreover one can use the exact location to set constraints on the amount of total matter and accelerating component present in the Universe.

The CMB observations also reveal the need for dark energy of one form or another, through the location of the first peak, which implies a flat Universe, which further implies that the total fractional energy density of the Universe must be around 1 where as the observed fractional energy density of matter even with added dark matter is only 0.3.

Large scale structure (LSS) surveys [4, 5, 6] also show evidence requiring some dark energy component, and provide complimentary information to the background expansion probes, and in fact are the key for understanding a bit more about dark energy. These also have already been discussed, in 1.1.3.

The imprinted scale of BAO in both CMB and LSS data is yet another strong indicator, even cluster abundances in LSS data reveals that the Universe is not merely matter alone.

1.2.5 Acceleration: Theoretical Origins

As for dark matter, theories of this accelerating component fall into two main categories aside from cosmological constant, and again these categories are interpreting this as a new particle, fluid or field, or alternatively as a sign that general relativity is incorrect or incomplete, adding new physics or new interactions to the vanilla cosmology.

Cosmological Constant

Einstein's original formulation of his equations included a constant Λ, which in fact with an appropriate choice of value serves to stabilize the universe (which is

why he originally added it) and for other values to accelerate the Universe (which is why we consider it today). It is this constant that ΛCDM appeals to to explain the acceleration, however using the cosmological constant has certain theoretical difficulties. The first is that attempting to define why the value is the one we observe. If one assumes that the origin of the constant is the vacuum energy of space, then one finds that any theoretical value we can motivate for the vacuum energy and hence the cosmological constant is many orders of magnitude larger than the cosmological constant required to match observations. This is called the fine tuning problem, i.e. the value of the constant must be fine tuned and the tuning is not motivated by any underlying physics that we know. The second largest difficulty, one which in fact is inherent in most theories for an accelerating component is why it happens to be the case that the accelerating component just happens to become important recently, and thus the driving force behind the recent expansion history. Ideally, one would want a theory that can explain this coincidence, hence this is referred to as the coincidence problem. Which is simply a statement that in theories we don't like to live at a special time or location; we don't like coincidences or lucky finds, rather we prefer to find physically motivated reasons behind such apparent coincidences.

To this end we consider many alternative explanations for the acceleration, and we characterize them in terms of contributions to Einstein's equations, either adding to the energy momentum tensor as new material present in the universe or as contributions to the Einstein Tensor as new physics.

Considering the addition of an actual fluid is best done via speaking of its Lagrangian, or rather the resulting action. That is, Einstein's equations like most physics are obtained via minimization of an action, which in this case is the integral of the Ricci curvature scalar, R, formed as usual from the metric, g,

$$S = \int d^4x \sqrt{|g|} R. \tag{1.28}$$

Here, R, is in fact the Lagrangian density for the normal matter content of the Universe, so that Lagrangians and actions are related via

$$S = \int d^4x \sqrt{|g|} \mathcal{L}_M. \tag{1.29}$$

Minimizing with respect to the metric, results in the Einstein Equations, and shows the relationship already stated for the energy momentum tensor.

Further usefulness of the Lagrangian density comes from the Euler-Lagrange equation,

$$\frac{\partial \mathcal{L}(t)}{\partial q} - \partial_\alpha \frac{\partial \sqrt{|g|} \mathcal{L}(t)}{\partial_\alpha q} = 0. \tag{1.30}$$

Evaluating the Euler-Lagrange equation leads results in the derivation of the fluid equations describing the evolution of the density of the fluid whose action S we are considering.

Thus, one can add a dark energy component by making simple additions to the Lagrangian, i.e. extending it beyond the normal matter term.

One such addition is that made by Quintessence theories (e.g. [117, 118]), a scalar field typically considered to be slow rolling (analogous to or perhaps in fact

the same as the inflationary field). For theories of quintessence the idea is to add to the action a quintessence Lagrangian,

$$\mathcal{L}_Q = -\frac{1}{2}(\nabla_\mu Q)(\nabla^\mu Q) - V(Q) \tag{1.31}$$

where the potential V and the field Q obey

$$\Box Q = V_{,Q} \tag{1.32}$$

where $\Box$ is the d'Alembertian. Given this the field contributes to the energy momentum tensor as

$$T_{\mu\nu} = (\nabla_\mu Q)(\nabla_\nu Q) + g_{\mu\nu}\mathcal{L}_Q \tag{1.33}$$

Finally the equation of motion for such a quintessence field is

$$\ddot{Q} + 3H\dot{Q} + V_{,Q} = 0. \tag{1.34}$$

The term $3H\dot{Q}$ is Hubble friction. The requirement for acceleration to arise from a component is that its equation of state, $w = P/\rho$, must be less than $-1/3$, this is true for the quintessence field if $\dot{Q} < V$.

While the idea of Cosmological Constant treats dark energy as a fluid. This addition of more exotic material or fields is what is really meant by the term dark energy.

Modified Gravity

The previous section explained dark energy by adding additional terms to the Lagrangian density, this changes the energy momentum tensor in Einstein's Equation, yet at the same time one can consider changes to the Einstein tensor. This is a fundamental change of physics rather than of the matter-energy content of

the Universe. These are modified gravity Theories, and are however typically expressed as modified action theories again, but rather than simply adding a term to the Lagrangian, they out right replace the part of the action corresponding to the Einstein-Hilbert action introduced earlier, $S = \int d^4x\sqrt{|g|}R$.

Rather than invoke dark energy per se (in the form of some fluid or field), this thesis focuses on the alternative explanation for cosmic acceleration, that our standard theory of gravity is incomplete and that a correct theory of gravity would explain cosmic acceleration at late times and large scales in a universe populated by matter with positive pressure.

Such extensions of GR, or entirely new physics can be proposed with relative freedom, the only stringent tests at present coming from background expansion. In fact, precision measurements of gravity only exist for scales $< 10^{13}$ m (e.g.[119]). All of these are discussed in more detail in chapters 2 and 4.

Higher dimensional theories couple gravity to extra dimensions allowing for a leaking of gravity into the extra dimensions, thus enabling acceleration of the expansion of the Universe; still more attempt to work directly in the context of GR directly adding small modifications with cutoff scales. There is much overlap between such theories and indeed in terms of effective theories can be described analogously, a large family of them can be described simply using two parameters.

There are a large number of theoretically motivated modified theories of gravity, see [117, 120] for reviews, or [121, 122, 123, 124, 19, 125, 126, 127, 128, 129, 130, 131, 132, 133, 134, 135, 136] for additional discussions.

A prominent class of these theories are scalar-tensor theories. For these theories

the Einstein-Hilbert action is replaced by

$$S = \int d^4x\sqrt{|g|}[b(\lambda)R - \frac{1}{2}h(\lambda)g^{\mu\nu}(\partial_\mu\lambda)(\partial_\nu\lambda) - U(\lambda)] \tag{1.35}$$

where λ is the new scalar field. The presence of b couples the field to gravity, making Newton's gravitational constant depend on $b(\lambda)$ and the rest of the terms are just the kinetic and potential energy terms for the field. varying with respect to the metric, as in the case of the Einstein-Hilbert action gives the equation of motion, which for this case is

$$G_{\mu\nu} = b^{-1}[\frac{1}{2}T^{(m)}_{\mu\nu} + \frac{1}{2}T^{(\lambda)}_{\mu\nu} + \nabla_\mu\nabla_\nu b - g_{\mu\nu}\Box b] \tag{1.36}$$

where I've included normal matter contribution (so that infact the action had a term for the matter Lagrangian) to show that b plays a part in it as well. The energy momentum tensor for the scalar field is given by

$$T^{(\lambda)}_{\mu\nu} = h(\lambda)(\nabla_\mu\lambda)(\nabla_\nu\lambda) - g_{\mu\nu}[\frac{1}{2}h(\lambda)g^{\rho\sigma}(\nabla_\rho\lambda)(\nabla_\sigma\lambda) + U(\lambda)] \tag{1.37}$$

A specific case of this class is Brans-Dicke Theory, for which $b(\lambda) = \lambda/2,\ h(\lambda) = w/\lambda$, and $U(\lambda) = 0$, where w is jsut a constant parameter.

A more general case of this class is that known as $f(R)$ theories. These use an action

$$S = \int d^4x\sqrt{|g|}f(R). \tag{1.38}$$

The equivalence can be seen immediately as $f(R)$ theories are basically scalar-tensor theories that have no kinetic term[117].

Further theories exist, using higher order derivatives in the action as in Gauss Bonnet, or higher dimensions like DBI and DGP.

Most theories require some masking to hide modifications on smaller solar system scales where general relativity is well tested via things like lunar laser ranging

and the anomalous precession of Mercury. A common choice is the chameleon mechanism [137, 138] but varies in each case.

As mentioned before for the cosmological constant, in almost all cases a coincidence problem remains, however, it is possible to physically motivate the onset of acceleration if some interactions exist between the dark sector elements tying the acceleration to properties of a matter dominated Universe [139, 140, 58, 141, 142, 143, 62, 144, 145, 133], though such interactions do introduce dynamical instabilities in the growth of structure [146, 147, 148, 149, 150, 151]. Such interactions are explored and discussed in further detail in 3.

This thesis, however, assumes that solar system tests are passed, and that coincidence is not an issue, and works mostly with a generic two parameter MG theory.

Rather than considering a specific theory, one can consider a phenomenological parameterization for how the gravitational metric perturbations are related to the underlying matter distribution and motion, such as was discussed in [152, 153, 1, 154, 155, 156, 14, 157, 158, 159, 160, 161, 162, 163, 164, 161, 165, 117, 166, 167, 168, 169, 170, 171, 172, 173, 174, 175, 176, 177, 178, 179, 180, 181, 182, 183, 184, 185]. One parameterization in particular is well suited to contrasting information about galaxy positions with weak lensing measurements. It specifies how the evolution of the two scalar metric perturbations in the conformal Newtonian gauge, the "Newtonian potentials", is distinct from that predicted by GR. While galaxy distributions are sensitive to just one of the potentials, lensing is sensitive to the sum of both. This parameterization allows constraints to be quickly set for families of models and also for simple null tests searching for deviations from general relativity.

1.3 Distinguishing Between Theories

This thesis focuses on how cosmologists can go about narrowing down this vast landscape of theories and candidates for dark matter and dark energy or modified gravity, and how best to utilize observations of the CMB, SN, BAO, and LSS to this end. Cosmological observations in general provide either distance measures which serve as probes of background expansion history or probes of the growth of structure. Theories today by and large have been crafted to fit the expansion history, which is well constrained by present data, but predict a wide range of variations in the assembly of structure and the scales on which most structures are found, thus large scale structure observations are key in testing the theories that pass the background expansion tests [186, 14, 187].

This thesis deals with each of the above topics in turn, chapter 2 discusses how well analytical fits of the matter power spectrum by Peacock and Dodds and Smith et. al. are able to predict the non-linear growth found in the simulations involving modified gravity, including specific theories and the two parameter model. Chapter 3 discusses models where there exists a dark matter interaction and constrains the interaction strength using recent supernovae, large scale structure and cosmic microwave background data. Chapter 4 forecasts constraints on joint MG/IA models. Finally, chapter 5 summarizes all the findings and proceeds to consider future possibilities.

CHAPTER 2

NON-LINEAR GROWTH IN MODIFIED GRAVITY

(Published as Istvan Laszlo and Rachel Bean [156])

Theoretical differences in the growth of structure offer the possibility that we might distinguish between modified gravity theories of dark energy and ΛCDM. A significant impediment to applying current and prospective large scale galaxy and weak lensing surveys to this problem is that, while the mildly non-linear regime is important, there is a lack of numerical simulations of non-linear growth in modified gravity theories. A major question exists as to whether existing analytical fits, created using simulations of standard gravity, can be confidently applied.

This chapter addresses this, presenting results of N-body simulations of a variety of models where gravity is altered including the Dvali, Gabadadze and Porrati model. We consider modifications that alter the Poisson equation and also consider the presence of anisotropic shear stress that alters how particles respond to the gravitational potential gradient. We establish how well analytical fits of the matter power spectrum by Peacock and Dodds and Smith et. al. are able to predict the non-linear growth found in the simulations from $z = 50$ up to today, and also consider implications for the weak lensing convergence power spectrum. We find that the analytical fits provide good agreement with the simulations, being within 1σ of the simulation results for cases with and without anisotropic stress and for scale dependent and independent modifications of the Poisson equation. No strong preference for either analytical fit is found.

We first consider the applicability of standard gravity non-linear fits to modified gravity theories in which just the Poisson equation is modified, considering the 5D gravity form considered by [188], complementing the work of [1, 12] who con-

sidered non-linear growth when a Yukawa-like gravitational coupling is introduced [189]. We then address the impact of anisotropic stress on non-linear growth to assess if existing analytical non-linear fits are adequate to model evolution in these scenarios. We consider the non-linear growth in the Dvali, Gabadadze, and Porrati (DGP) 5D model [121] and in toy models that contrast the effects of anisotropic stress with those of a modified Poisson equation.

We first establish the framework for investigating modified gravity theories in section 2.1, and outline the specific models we consider with scale independent and dependent modifications and the presence and absence of anisotropic shear. The details of our simulations and implementation, including the two standard analytic fits are presented in 2.2. The approach to weak lensing is discussed in 2.3. The results showing dimensionless power spectra and the success of analytic fits are discussed in 2.4.

2.1 Modified Gravity Theories

We first outline the effect that the general modifications to gravity we study have on the perturbed Einstein's equations. Following the notation of [2], in the conformal Newtonian (or longitudinal) gauge, the metric is written as

$$ds^2 = a(\tau)^2 \left[-(1+2\psi)d\tau^2 + (1-2\phi)dx_j dx^j\right] \tag{2.1}$$

where a is the expansion factor, τ is the conformal time, x is the comoving coordinate (j=1,2,3 spatial directions) and ϕ and ψ are the two gravitational metric perturbations.

Einstein's equations relate the metric perturbations to fractional perturbations in density, $\delta_s \equiv \delta\rho_s/\rho_s$, peculiar velocity, $v_{(s)}$, and intrinsic shear σ_s for a matter

component 's',

$$k^2\phi + 3\mathcal{H}(\dot{\phi} + \mathcal{H}\psi) = -\frac{3\mathcal{H}^2}{2} Q \sum_s \Omega_s \delta_s, \tag{2.2}$$

$$k^2(\dot{\phi} + \mathcal{H}\psi) = \frac{3\mathcal{H}^2}{2} \sum_s (1 + w_s)\Omega_s (ik^j v_{(s)j}) \tag{2.3}$$

$$\phi - \psi = \frac{9\mathcal{H}^2}{2} \sum_s (1 + w_s)\Omega_s \sigma_s + \sigma_0 \tag{2.4}$$

where $\mathcal{H} = \dot{a}/a$, $\Omega(a)$ is the fractional energy density, and $w(a)$ is the equation of state for the fluid. We have introduced the function $Q(k, a)$ as a modification in the relationship between the gravitational potentials and matter density in the $\delta T_0{}^0$ equation, (2.2), and $\sigma_0(k, a)$ as an extrinsic anisotropic stress in addition to the intrinsic anisotropic stresses from the matter components (predominantly radiation) in the equation for $\delta T_i{}^j$, $i \neq j$, (2.4). For standard gravity $Q = 1$ and $\sigma_0 = 0$.

Equations (2.2) and (2.3) combine to give

$$k^2\phi = -\frac{3\mathcal{H}^2}{2} Q \sum_s \Omega_s \left(\delta_s + 3\mathcal{H}(1 + w_s) ik^j \frac{v_{(s)j}}{k^2} \right), \tag{2.5}$$

$$= -\frac{3\mathcal{H}^2}{2} Q \sum_s \Omega_s \Delta_s \tag{2.6}$$

where Δ_s is a gauge invariant density variable defined in the rest frame of the matter components [3].

Density and velocity perturbations evolve according to the perturbed fluid equations which are unchanged by the gravitational modifications,

$$\dot{\delta} = -(1 + w)(ik^j v_j - 3\dot{\phi}) - 3\mathcal{H}(c_s^2 - w)\delta, \tag{2.7}$$

$$ik^j \dot{v}_j = -\left[\mathcal{H}(1 - 3w) + \frac{\dot{w}}{1 + w} \right] ik^j v_j + \frac{c_s^2}{1 + w} k^2 \delta - k^2\sigma + k^2\psi \tag{2.8}$$

where c_s^2 is the sound speed for the fluid.

We will consider a universe dominated by pressureless matter, $w = c_s^2 = \sigma = 0$, and scenarios in which $\psi \sim \phi$, so that on subhorizon scales $|k^2\psi| \gg |3\mathcal{H}\dot{\phi}|, |3\ddot{\phi}|$, and

$$\ddot{\delta} + \mathcal{H}\dot{\delta} + k^2\psi \approx 0 \tag{2.9}$$

Using (2.8), we define the peculiar acceleration, g,

$$g_j \equiv \frac{1}{a}\frac{d}{d\tau}(av_j) = -ik_j\psi. \tag{2.10}$$

Following the notation of [14], we relate the anisotropic stress to ϕ through a function η,

$$\eta \equiv \frac{\sigma_0}{\phi}. \tag{2.11}$$

Q and η here are equivalent to q and η in [190].

Making a subhorizon approximation, and $\mathcal{H}v/k \ll \delta$, assuming $v \lesssim \delta$, the modified Poisson equation and peculiar acceleration equations are

$$k^2\phi = -\frac{3\mathcal{H}^2}{2}Q\Omega_m\delta, \tag{2.12}$$

$$g_j = -ik_j(1+\eta)\phi. \tag{2.13}$$

while the matter perturbation equation is

$$\ddot{\delta} + \mathcal{H}\dot{\delta} - \frac{3\mathcal{H}^2}{2}Q(1+\eta)\Omega_m\delta = 0. \tag{2.14}$$

Note that, we can describe the evolution of δ in terms of the linear growth factor, D, with respect to some reference scale, a_i, $\delta(k,a) \equiv D(a)\delta(k,a_i)$ where D is scale independent for standard gravity, but could be scale dependent if gravity is so modified.

We can relate the Fourier space modification to a real space interaction in the form of a Green's function,

$$\phi(\mathbf{r}) = -G\rho_m(a)a^2 \int d^3\mathbf{r}'\delta(\mathbf{r}')f(\mathbf{r}-\mathbf{r}') \quad (2.15)$$

$$g(\mathbf{r}) = -\nabla\left[(1+\eta(\mathbf{r}))\phi(\mathbf{r})\right] \quad (2.16)$$

with $f(\mathbf{r}) = 1/|\mathbf{r}|$ recovering standard gravity. Using the convolution theorem we find,

$$Q(k,a) = \frac{k^2}{4\pi}f(k,a). \quad (2.17)$$

The effect of modified gravity in weak lensing statistics is described in [191] where they show that the weak lensing distortion is dependent upon the sum of the two gravitational potentials, $\Phi \equiv \phi + \psi$. As in [14], we introduce the parameter $\Sigma(Q,\eta)$ to describe the deviation of the weak lensing potential from standard gravity

$$k^2\Phi = -3\mathcal{H}^2\Sigma\Omega_m\delta, \quad (2.18)$$

$$\Sigma \equiv \left(1+\frac{\eta}{2}\right)Q. \quad (2.19)$$

with $\Sigma = 1$ for standard gravity.

2.1.1 5D Gravity

We consider a model, motivated by 5-dimensional gravity theories in which gravity is Newtonian on small scales but modified on scales larger than a characteristic scale r_s [192, 193, 188]. This model is characterized by the form

$$f(\mathbf{r}) = \frac{1}{|\mathbf{r}| + \frac{r^2}{r_s}} \quad (2.20)$$

and

$$Q(\mathbf{k},a) = \frac{kr_s}{2}\left[-2\left(\int_{kr_s}^{\infty}\frac{\cos(t)}{t}dt\right)\sin(kr_s) + \cos(kr_s)\left(\pi - 2\int_0^{kr_s}\frac{\sin(t)}{t}dt\right)\right] \quad (2.21)$$

with $\eta(k,a) = 0$. We are principally interested in the effect that modifications to gravity could have on the transition from linear to non-linear regime, typically occurring over comoving scales $1-10Mpc$. For our analysis, therefore, we consider evolution for values of the parameter r_s of $20h^{-1}\ Mpc$, $10h^{-1}\ Mpc$, and $5h^{-1}\ Mpc$, which alters the behavior in the relevant scales. We do not consider here smaller values of the modification which would alter behavior in the wholly non-linear regime. We leave it for future study to assess whether such changes are well modeled by analytical fits describing the properties of collapsed halos.

2.1.2 DGP

A physical model that serves as an excellent example of the effects of anisotropic shear is the Dvali, Gabadadze, and Porrati (DGP) model [121] that is based on 5D gravity, wherein at some large scale, r_c (comparable to the horizon scale), gravity is sensitive to the presence of an additional dimension.

The extra dimension alters the 4D background evolution to that described by the modified Friedmann equation,

$$H(a) = \frac{1}{2r_c} + \sqrt{\left(\frac{1}{2r_c}\right)^2 + \frac{8\pi G}{3}\rho_m(a)} \quad (2.22)$$

where $H = \mathcal{H}/a$, with late time acceleration being triggered when the universe's horizon $\sim r_c$.

The modification also alters the growth of fluctuations in density and motion of matter. As well as a modification to the Poisson equation as discussed in 2.1.1, this model also results in an anisotropic shear such that the two potentials are given by [194, 195, 196, 14]:

$$k^2\phi = -\frac{3\mathcal{H}^2}{2}\left(1-\frac{1}{3\beta}\right)\Omega_m\delta \tag{2.23}$$

$$k^2\psi = -\frac{3\mathcal{H}^2}{2}\left(1+\frac{1}{3\beta}\right)\Omega_m\delta \tag{2.24}$$

where

$$\beta \equiv 1-\frac{2H^2(a)r_c^2}{2H(a)r_c-1}. \tag{2.25}$$

In contrast to 2.1.1, this gives a scale independent modification to the Poisson equation,

$$Q(a) = 1-\frac{1}{3\beta} \tag{2.26}$$

and non-negligible anisotropic stress,

$$\eta(a) = \frac{2}{3\beta-1}, \tag{2.27}$$

and $\Sigma = 1$.

For our analysis, with a background cosmology with Hubble constant, $H_0, = 70kms^{-1}Mpc^{-1}$, fractional matter density, $\Omega_m, = 0.3$, and consistent with the observational constraints found in [196] (2.22), $r_c = 6.1Gpc$.

2.1.3 Twin Toy Models

Finally, we consider a set of twin models that provide a simple way to further explore the effects of anisotropic stress on non-linear growth. We consider two

different modifications that both yield the same form for the weak lensing potential, with $\Sigma = 1 + \Sigma_0 a$, such that they reduce to standard gravity at early times and become modified at late times. This form of Σ is equivalent to model GDE1 of [14]. The twin models ('TM') we study have two contrasting, simple forms in terms of Q and η :

$$\text{TM 1}: \quad Q = 1, \quad \eta = 2\Sigma_0 a, \tag{2.28}$$

and

$$\text{TM 2}: \quad Q = 1 + \Sigma_0 a, \quad \eta = 0. \tag{2.29}$$

In TM1, the Poisson equation is the same as for standard gravity, however the peculiar acceleration of the matter particles responding to the gradient of the potential is affected by the anisotropic stress. In TM2, in contrast, the peculiar acceleration is the same as for standard gravity but the gravitational potential at late times has a different relation to matter over/under densities. We consider values of $\Sigma_0 = \pm 0.008, \ \pm 0.016$ consistent with 1 and 2σ Fisher-matrix constraints for a prospective DUNE-like weak lensing survey [14].

2.2 N-Body Simulations

To obtain fully non-linear results in each of the models, we obtain N-body simulations via a Particle Mesh(PM) Code, taking as an initial form the code of [197]. For scale independent modifications we make simple modifications to the code, described in 2.2.1. For scale dependent modifications we have to alter the potential and motion calculations as described in 2.2.2.

2.2.1 Standard Gravity and Scale-independent Modifications

The PM code is reviewed in detail in [197] but we provide some highlights in order to set the framework for discussing the modifications we make to the code.

PM codes operate by defining a simulation area as a box of size L on a side, assuming it is closed so that we have periodic boundary conditions, subdividing it into a mesh or grid of N^3 cells (of size L/N on a side), and defining all quantities on that mesh. The simulation is then initialized at some early redshift (z_i) and ${N_P}^3$ particles are placed according to model dependent power spectra fits provided with the code (based on the cosmological parameters: the scalar spectral index, n_s, the amplitude of fluctuations in $8h^{-1}Mpc$, σ_8, the fractional density from curvature, Ω_K, baryons, Ω_b and cold dark matter, Ω_{cdm}, and the Hubble constant $H_0 = 100hkms^{-1}Mpc^{-1}$). The evolution is then carried out by advancing time in equal steps of the expansion factor, a_{step}. At each step in expansion factor the code determines a density in each cell, uses that density to compute the potential ϕ in each cell, and finally moves particles according to the gradient of the potential.

Defining the Density

Defining the density can be done in a variety of ways, the code uses the Cloud-In-Cell scheme depicted in fig. 2.1, wherein a particle is taken to be a cube with dimensions equal to that of the cells and with a corner positioned at the location of the particle. The particle contributes to each cell it extends into a mass equal to the particle's total mass weighted by the fraction of the particle's volume in the cell under consideration. Once the mass in each cell is determined it is effectively

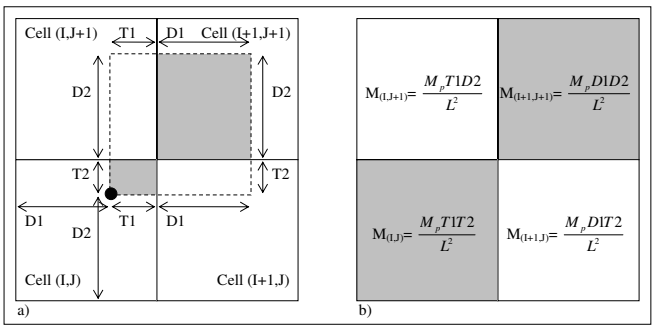

Figure 2.1: A two dimensional description of cloud in cell density assignment. a) The definition of the variables in relation to the particle's actual position. The particle is the black dot, but it is extended to be a square particle denoted by the dotted lines, thus it lies in four cells. The sides of the cells and the size of the particle square are $L = D1 + T1 = D2 + T2$. b) The resultant mass distribution in each cell. Note that the mass is not retained in the original particle's area, but rather smeared over the cell it occupies.

smeared over the entire cell.

Obtaining the Potential

For standard gravity, the code uses (2.12) with $Q = 1$, with the dimensionless variables of [197], $\tilde{r} \equiv r/x_0$ and $\tilde{\phi} \equiv \phi/(x_0 H_0)^2$ and writing $\delta \equiv \rho(x,a)/\bar{\rho}(a) - 1$,

$$\tilde{\nabla}^2 \tilde{\phi} = \frac{3}{2} \frac{\Omega_{m,0}}{a} \delta. \tag{2.30}$$

To evaluate (2.30), we use the discretized Poisson equation over cells, $n = 0, N-1$. In one dimension, the discrete Laplacian is given by

$$\nabla^2 \phi_n \approx \phi_{n+1} + \phi_{n-1} - 2\phi_n. \tag{2.31}$$

Defining the discrete Fourier transform,

$$\tilde{\phi}_k = \Sigma_{n=0}^{N-1} \phi_n e^{i2\pi nk/N}, \tag{2.32}$$

the discretized Poisson equation is

$$\nabla^2\tilde{\phi}_k = \tilde{\phi}_k \times 2\left[\cos\left(\frac{2\pi k}{N}\right) - 1\right]. \tag{2.33}$$

Generalizing to three dimensions one obtains the '7-point crest template',

$$\begin{aligned}\nabla^2\phi_{i,j,k} \approx \quad & \phi_{i+1,j,k} + \phi_{i-1,j,k} + \phi_{i,j+1,k} \\ + \quad & \phi_{i,j-1,k} + \phi_{i,j,k+1} + \phi_{i,j,k-1} - 6\phi_{i,j,k},\end{aligned} \tag{2.34}$$

with

$$\nabla^2\tilde{\phi}_k = \tilde{\phi}_k \times G_k,$$

where G_k is given by

$$G_k = 2\left[\cos\left(\frac{2\pi k_x}{N}\right) + \cos\left(\frac{2\pi k_y}{N}\right) + \cos\left(\frac{2\pi k_z}{N}\right) - 3\right]. \tag{2.35}$$

Combining (2.35) and (2.30) the Poisson equation used in the code is,

$$\tilde{\phi}_k = \frac{3}{2}\frac{\Omega_{m,0}}{a\ G_k}\delta. \tag{2.36}$$

The code calculates $\delta(\mathbf{r})$, Fourier transforms to $\delta(\mathbf{k})$, divides by G_k and then transforms back to real space to obtain $\phi(i,j,k)$.

In the case of scale-independent modifications (2.36) is purely modified by

$$G_{k,alt}(k,a) \equiv \frac{G_k}{Q(a)} \tag{2.37}$$

Advancing the Particles

Once we have the potential ϕ we advance the particles according to (2.16). In standard gravity, component wise on the grid we have only to compute

$$\begin{aligned} g_x &= -(\phi_{i+1,j,k} - \phi_{i-1,j,k})/2 \\ g_y &= -(\phi_{i,j+1,k} - \phi_{i,j-1,k})/2 \\ g_z &= -(\phi_{i,j,k+1} - \phi_{i,j,k-1})/2. \end{aligned}$$

In the presence of anisotropic stress modifications,

$$g_{j,alt} = [1 + \eta(a)]g_j \tag{2.38}$$

2.2.2 Scale-dependent Modifications

In order to incorporate the scale dependent modifications to gravity we follow the convolution approach in (2.15). To do this we multiply by $f(\mathbf{k}, a)$ at each step in a rather than $1/G_k$.

Defining the Radius r for $g(\mathbf{r})$

In scale dependent theories, by definition, we now convolve with functions involving the actual scale r, and we must therefore define explicitly a radius on the grid. The mass is smeared over the entire cell it lies in, so that the distances simply become those between cells. The Fourier transforms involve periodic boundary conditions, so we define the radius for one origin at $(0, 0, 0)$, and wrap the radius around the grid. Since the code uses the dimensionless radii to compute the function we have called $f(\tilde{\mathbf{r}})$, the cell indices can be used to construct the radius and we define $\tilde{r}_i$ to be the index of the relevant cell in the i^{th} direction (i=1,3).

The periodic boundary conditions require a change to the basic prescription presented above, namely to include the periodic boundary condition we must set up a 1D radius of the form [0 1 2... $N/2-1$ $N/2$ $N/2-1$ ... 2 1] where N is the number of cells making up the grid in a dimension. Thus, the radii in the i-th

dimension can be defined as

$$\tilde{r}_i(n) = \begin{cases} n & n \leq N_i/2 \\ N_i - n & n > N_i/2 \end{cases} \tag{2.39}$$

The final 3-dimensional radius, $\tilde{r}$, is computed trivially as

$$\tilde{r}^2 = \sum_{i=1}^{3} \tilde{r}_i^2 \tag{2.40}$$

There remains one final subtlety in computing the radius. Since $\tilde{r}[1,1,1] = 0$, division by $\tilde{r}$ requires us to make a change to avoid infinities. To avoid these singularities we take the standard approach of 'softening' r (e. g. [198]), that is adding a small non-zero term to all the values of $\tilde{r}$ used in operations that would give a singularity. For instance if we consider $g(\tilde{r}) = 1/\tilde{r}$ we instead compute $g(\tilde{r}) = (\tilde{r}^2 + \epsilon^2)^{-1/2}$. Note that, for consistency, all values of r in the division are softened, not only the actual one that gives a singularity ($\tilde{r}[1,1,1]$). Further, note in the case of well defined modifications, e.g. $g(\tilde{r}) = e^{-\tilde{r}}/\tilde{r}$ the exponent need not be softened, so that we compute $e^{-\tilde{r}}(\tilde{r}^2 + \epsilon^2)^{-1/2}$.

2.2.3 Obtaining Analytic Spectra

We compare the non-linear spectra from simulations to predicted spectra from analytical mappings of linear power spectra using the Smith et. al. fit (SP) [8], and the Peacock and Dodds (PD) fit [7].

Analytical Linear Spectra

We evolve a linear spectrum forward in time using the modified equation for the growth of the over-density (2.14) from an epoch at which non-linear corrections are

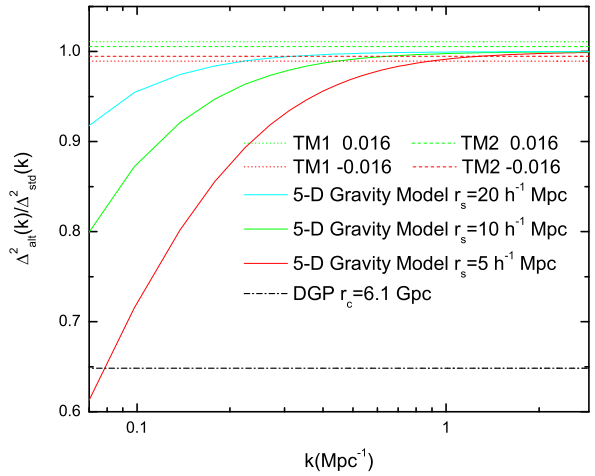

Figure 2.2: The ratio of the linear power spectrum in the modified theories to those of standard gravity for the models discussed in section 2.1: the 5-D gravity model of Uzan and Bernadeau (solid), TM1 (dotted), TM2(dashed) and DGP (dot-dashed).

inconsequential and the modification scale is large compared to the simulation box size, so that standard gravity is effectively recovered on the relevant scales, through the modified gravity era to today. Specifically, we find it appropriate to begin with a linear ΛCDM power spectrum obtained with CAMB [199], that includes effects from baryon photon coupling at early times, at $z = z_i = 50$.

Analytical Non-Linear Fits

We briefly review the physical ingredients of the PD [7] and SP [8] analytical fits against which we compare the simulations.

The PD fit is based on the assumption of stable clustering [200], the hypothesis that the correlation function on scales smaller than those of virialized structures decouple from the expansion. The fit utilizes a linear to non-linear mapping pro-

posed by Hamilton et al. (HKML) [201]

$$k_L = [1 + \Delta^2_{NL}(k_{NL})]^{-1/3} k_{NL} \tag{2.41}$$

which can be intuitively seen from noting that a density contrast $(1+\delta)$ can arise from collapse by a factor $(1+\delta)^{1/3}$. Peacock and Dodds generalized the HKML method to estimate the resulting non-linear power spectrum through a universal scaling relation, f_{NL},

$$\Delta^2_{NL}(k_{NL}) = f_{NL}[\Delta^2_L(k_L)], \tag{2.42}$$

$$f_{NL}(x) = x \left[\frac{1 + B\beta x + [Ax]^{\alpha\beta}}{1 + ([Ax]^\alpha g^3(a)/[Vx^{1/2}])^\beta} \right]^{1/\beta}. \tag{2.43}$$

where $g \equiv D(a)/a$. The fitting function f_{NL} tends to $f_{NL}(x) = x$ in the linear, $x \ll 1$, limit and $f_{NL}(x) = Vg^3(\Omega_m)x^{3/2}$ in the small scale limit with stable clustering (for CDM in standard gravity, the linear correlation function evolves $\propto \delta^2 \sim a^2$, whereas the nonlinear correlation is decoupled from the expansion and hence evolves $\sim a^3$ relative to the mean density). There are five free parameters fit from N-body simulations in standard gravity as functions of the linear spectral index $n_{eff} = d\ln P_\delta / d\ln k (k = k_L/2)$: A and α parameterize the power law in the quasi-linear, large scale regime, V parameterizes the amplitude of the $f_{NL}(x)$ in the stable clustering limit, $x \gg 1$, B describes the second order deviation from linear growth and β softens the transition between the linear and fully virialized regimes. The cosmological model only enters into the fit through g, consistent with the Zel'dovic approximation in which the final positions of particles are obtained by extrapolating their initial comoving displacements, q, using the linear growth factor, $x(a,t) = a(t)\,[q + D(a)\nabla\psi(q)]$.

The quality of the PD fit is founded on the broad applicability of the Zel'dovic approximation. However, with a scale dependent modification of gravity, or the introduction of a difference between ϕ and ψ it is not clear *a priori* how well the

Zel'dovic approximation will apply, and if applicable, whether the numerical values of the coefficients will remain the same as those for standard gravity. That is, with scale dependent modifications the possibility for shell crossings arises which causes a break down of the Zel'dovic approximation, while in the case of anisotropic stress there is a deviation from the normal evolution of particles in the modified peculiar accelerations that might well move away from a case well described by the Zel'dovic approximation.

Looking at the functional form of the fit in particular, we can consider three regimes to make predictions, namely the large and small scale limits and a transition regime. Large scales which remain linear or quasi linear should be well described. On these scales the Zel'dovic approximation should hold and using a ΛCDM growth factor for g is acceptable as we expect deviations on smaller scales. Similarly α and β might be expected to adapt to the changed input power via their spectral index dependence as in linear scales essentially all the information is contained in the amplitude and spectral index of the power spectrum.

In the small scale case not directly probed in our simulations, one can immediately argue for changes to the correlation function of the collapsed structures, in particular, for changes to the value of the virialized normalization V. One can also expect increased sensitivity to deviations from a simple ΛCDM $g(a)$, especially if the modification is such that the real growth factor is scale dependent, e.g. $g(a) \to g(k, a)$

The mildly non linear or transition regime, where we directly compare results, is equally rich in opportunities for failures. Modifications to gravity, especially scale dependent ones, which effectively add a degree of freedom to the fits, could also be expected to affect the shape and scale of the smoothing function interpo-

lating between the linear and non-linear asymptotic behaviors essentially requiring corrections to β. For example, a scale or time-dependent modification to Poisson's equation could alter the critical over-density required for non-linear collapse, thus altering the details of the transition from linear to non-linear regimes.

The SP fit arises from a different approach based on the 'halo model' [202, 203] in which the continuous accretion of matter and merging of halos is accounted for, deviating away from the stable clustering approximation. In this scenario, the power spectrum of matter $\Delta^2_{NL} = \Delta^2_Q + \Delta^2_H$, is described on large scales by the correlations between different halos represented by a quasi-linear term, $\Delta^2_Q(k)$, and on small scales by a halo term, $\Delta^2_H(k)$, that accounts for power from the self-correlation of halos. In the fit, the two terms are phenomenologically selected functions of $y \equiv k/k_\sigma$, where the scale $k_\sigma(a)$ becomes non-linear at scale factor $a(t)$,

$$\Delta^2_Q(k) = \Delta^2_L(k) \left[\frac{(1+\Delta^2_L(k))^{\beta_n}}{1+\alpha_n \Delta^2_L(k)} \right] \exp\left(-\frac{y}{4} + \frac{y^2}{8} \right) \tag{2.44}$$

$$\Delta^2_H(k) = \frac{a_n y^{3f_1(\Omega_m)}}{1 + b_n y^{f_2(\Omega_m)} + (c_n f_3(\Omega_m) y)^{3-\gamma_n}} \times \tag{2.45}$$

$$\frac{1}{1+\mu_n y^{-1} + \nu_n y^{-2}}. \tag{2.46}$$

k_σ is determined by the standard error of the linear density field,

$$\sigma(k_\sigma^{-1}, a) \equiv 1, \tag{2.47}$$

$$\sigma(R, a) \equiv \int \Delta^2_L(k, a) \exp(-k^2 R^2) d\ln k. \tag{2.48}$$

The eight coefficients $\{\alpha_n, \beta_n, \gamma_n, \mu_n, \nu_n, a_n, b_n, c_n\}$, fit with spectral index dependent functions, and three Ω_m-dependent functions, f_1, f_2 ,and f_3 are empirically matched to standard gravity simulations.

In a general sense, we can expect issues to arise from the inclusion of the specific small scale information in the self correlation term. In particular, the

interpolation between the quasi-linear and halo regimes seems likely to be effected. An anisotropic stress might well be allowed via the spectral dependence of the parameters, but a scale dependent modification could potentially dramatically alter the nature of the transition from one regime into the other.

To discuss this fit in more detail in terms of how it might fail in modified gravity scenarios, we again consider the two limiting cases of large and small scales and the intermediate transition region. In the large scale limit the quasi-linear term dominates and the use of the spectral index dependent α and β suggests the fit will adapt well to a modification that does have significance on linear scales such as those considered here.

On small scales, just as in the PD case, there are obvious issues with using a halo self-correlation term. The functions f_1, f_2, and f_3 and the spectral dependent parameters a_n, b_n, c_n, μ_n and ν_n could well be expected to change with a change in gravity, essentially representing that the correlation coefficient in a virialized halo is expected to be different for various gravity scenarios.

Also as in the PD case, the interpolation from linear to non-linear regimes , from large to small scales, is expected to be significantly altered as the modifications can alter the critical over density required for non-linear collapse. In particular the form of a_n and to some extent β_n may be expected to require changes as these serve to determine the relative importance of the halo-halo and self correlation terms.

It is in light of these considerations that we study whether these analytic fits can readily describe modified gravity scenarios, with scale dependent or independent modifications to the Poisson equation, and or scale independent anisotropic shear.

2.3 Obtaining Weak Lensing Spectra

Modified gravity theories can impact weak lensing convergence power spectrum in addition to the matter power spectrum, thus we study the impact of our models on both. In standard gravity, the power spectrum of the convergence is given by:

$$P_\kappa(l) = \frac{9\Omega_{m,o}^2 H_0^4}{4c^4}\frac{1}{4}\int_0^{\chi_s}\frac{g^2(\chi)}{a^2\chi^2}P_\delta\left(\frac{l}{\chi}\right)d\chi$$

Where P_δ is the matter power spectrum and $g(\chi)$ is a weighting function that can be related to the comoving distance χ and the distribution of background or source galaxies $W_s(\chi)$.

$$g(\chi) = 2\chi\int_\chi^{\chi_s}\frac{\chi'-\chi}{\chi'}W_s(\chi')d\chi' \tag{2.49}$$

We assume a a simple delta function distribution of sources at $z_s = 1$, so,

$$g(\chi) = 2\chi\frac{\chi_s-\chi}{\chi_s}. \tag{2.50}$$

The convergence power spectrum is then

$$P_\kappa(l) = \frac{9\Omega_{m,o}^2 H_0^4}{4c^3}\int_{a_s}^1\frac{W^2(\chi,\chi_s)}{a^4H(a)\chi(a)^2}P_\delta\left(\frac{l}{\chi(a)}\right)da \tag{2.51}$$

with

$$W(\chi,\chi_s) \equiv \chi\left(\frac{\chi_s-\chi}{\chi_s}\right) \tag{2.52}$$

Where we have used the fact that the comoving distance, χ, is equal to the (comoving) angular diameter distance for a flat Universe so that

$$\chi(a) = \int_a^1\frac{cda'}{a'^2H(a')} \tag{2.53}$$

Gravitational modifications $Q \neq 1$ and/or $\eta \neq 0$, will act to modify $P_\delta(k,a)$. In addition, $Q \neq 1$ and/or $\eta \neq 0$ will modify how the convergence spectrum is related

to P_δ, (see for example [14]), resulting in

$$P_\kappa(l) = \frac{9\Omega_{m,o}^2 H_0^4}{4c^3} \times \int_{a_s}^1 \frac{W^2(\chi,\chi_s)(1+\eta/2)^2 Q^2}{a^4 H(a)\chi(a)^2} P_\delta\left(\frac{l}{\chi(a)}\right) da \quad (2.54)$$

where the evolution of P_δ is also affected by Q and η.

P_δ can be obtained from either the PM simulations or the analytic fits described in 2.2.3. To actually evaluate the integral we discretize it, binning by expansion factor.

When considering the N-body code derived P_δ, we have to account for the fact that the simulation only probes a range of k, yet for any given l, $k = l/\chi(a)$ can can lie outside this range at some redshift, $z_s > z > 0$. For the l range we consider, the range of k needed is virtually all given by the N-body simulation. Outside this range, on large scales the power spectrum is well approximated by the linear spectrum, at smaller scales we find that the analytic SP and PD predictions for the modified gravity spectra are within the 1σ errors at the edges of the range of k provided by the simulations so we pad the simulated spectra with the non-linear analytic fits to modified gravity linear power spectrum.

2.4 Results

2.4.1 Parameters for Simulations

For the PM code parameters we take $N = 256,\ N_P = 128,\ L = 100h^{-1}Mpc,\ \epsilon = 0.1,\ z_i = 50,\ a_{step} = 0.002$ and for our cosmological model we take $n_s = 1,\ \sigma_8 =$

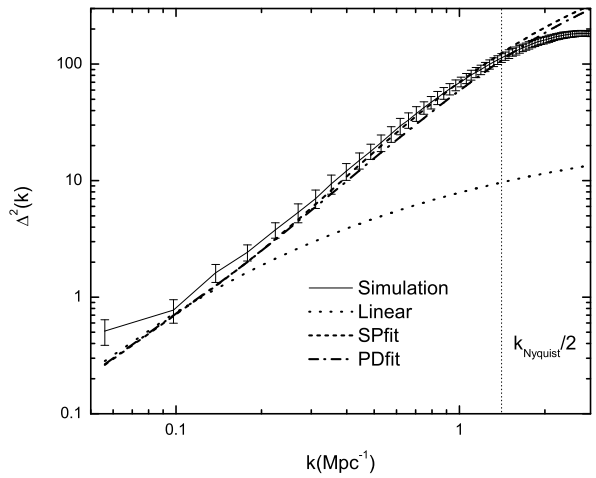

Figure 2.3: Dimensionless matter power spectrum, $\Delta^2(k) \equiv k^3 P_\delta(k)/2\pi^2$, for standard gravity. The full line and errors bars show the average power spectrum and standard deviation for 24 simulations. The vertical dotted line represents $k_{Nyquist}/2$, which is a conservative estimate for the largest k at which we can believe the simulation results as in [1]. The Peacock and Dodds (PD) (dot-dashed) and Smith and Peacock (SP) (dashed) analytical fits are also shown.

1, $\Omega_K = 0$, $\Omega_m = 0.3$, $\Omega_b = 0.026$, $\Omega_{cdm} = 0.274$, and $h = 0.7$. The resulting simulations measure scales $0.1 \lesssim k \lesssim 1 Mpc^{-1}$.

The box size and number of cells play into spatial resolution of the simulation, and are chosen to allow us to effectively probe the decade of k in which the mildly non-linear effects manifest themselves and from which we can extract a reasonable weak lensing spectrum for $l \sim 200 - 1000$, a range relevant to upcoming experiments. The number of particles are chosen to ensure a sufficient particle resolution for the box size and number of cells used. The initial redshift is chosen to be the same as used in the linear evolution, and is based on the same requirement that the modification scale be large compared to the box size at the initial redshift.

The initial positions of the particles at z_i, are assigned by means of a random number generator consistent with the initial power spectrum. Depending on the seed used to initialize the random number generator, the resultant spectra may agree well with standard ΛCDM analytic fits with the same parameters or might over- or under-produce power, even in the original unaltered code of [197]. We therefore run the simulations with 24 random seeds to get a good sample size and a more robust average. In order to weight the behavior of each simulation equally, we consider the modifications in terms of the "average of the ratios" of the modified power spectrum to the standard gravity spectrum for the same seed, rather than the "ratio of the averages" that would preferentially weight those simulations that over-produce power.

For scale dependent modified gravity we find the Numerical Recipes routine [204] for the Fourier transform, though slightly more time consuming, is more stable than the one provided in the original code. In the case of scale independent modifications and standard gravity, both algorithms produce identical results. The softening parameter value used for the scale dependent modification is much smaller than the smallest separation in the code and provides agreement with standard gravity from analytic predictions and standard gravity simulations with the code at least at the level or better than the unmodified Klypin code.

In Figure 2.3 we show the results of the 24 simulations of standard gravity against the SP and PD fits, in order to demonstrate the fiducial model against which the modified gravity simulations are compared. The simulations are consistent with the analytical fits in the range $0.1 Mpc^{-1} \lesssim k \lesssim 1 Mpc^{-1}$. A conservative estimate for the largest k at which we can believe the simulation results are reasonable is $k_{Nyquist}/2$ [1], which for our simulations is $1.41 Mpc^{-1}$. We consider the

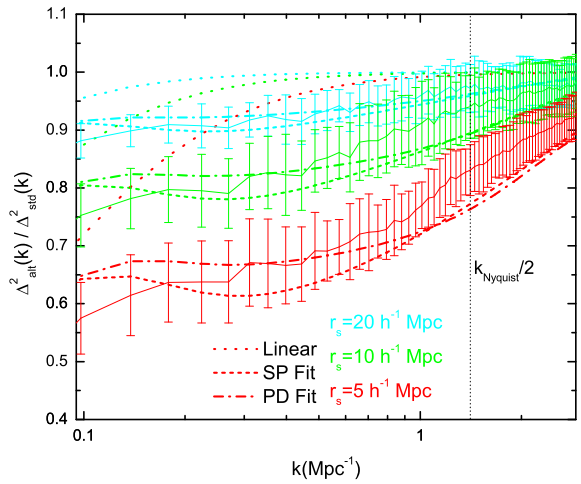

Figure 2.4: Ratios of the $z = 0$ dimensionless matter power spectrum in the modified gravity model to that for standard gravity, for the 5D gravity model described in 2.1.1 for $r_s = 20h^{-1}Mpc$ (top, blue), $10h^{-1}Mpc$ (middle, green) and $5h^{-1}Mpc$ (bottom, red). The full line and errors bars show the average of the ratios and standard deviation for 24 simulations. The vertical dotted line represents $k_{Nyquist}/2$, which is a conservative estimate for the largest k at which we can believe the simulation results as in [1]. The Peacock and Dodds (PD) (dot-dashed) and Smith and Peacock (SP) (dashed) analytical fits agree with simulations at within 1σ for each r_s, in the region of interest, $k = 0.1$ to 1 Mpc^{-1}.

simulations to be valid only up to $k_{Nyquist}/2$, rather than up to $k_{Nyquist}$ as this more conservative limit represents a regime in which standard gravity simulations and fits agree to within 1.5 times the standard error in the simulation, in comparison to 10 (for the PD fit) and 13 (for the SP fit) times the standard error at $k_{Nyquist}$. For the model parameterizations we consider, we find that the linear scales used to generate the nonlinear k in the range $0.1Mpc^{-1} - k_{Nyquist}/2$ lie in the range $k \sim 0.07 - 0.5Mpc^{-1}$.

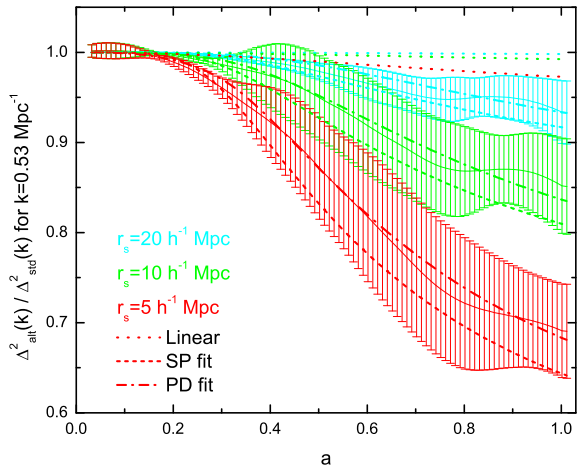

Figure 2.5: The ratios of the dimensionless matter power spectrum in modified to standard gravity, $\Delta^2_{alt}(k)/\Delta^2_{std}(k)$ as a function of redshift $50 \leq z \leq 0$ for $k = 0.53 Mpc^{-1}$. The color coding and lines styles are as in Figure 2.4. The dotted lines show the ratios of the associated linear spectra. Note that, the evolution is well tracked by the analytical fits, with both lying within 1σ for the simulations. At late times the SP fit drifts to around, or just over, the 1σ error.

2.4.2 Simulation and Analytic Fit Results

5D Gravity Model

The ratio of the dimensionless power spectrum today for the 5D gravity model discussed in 2.1.1 to standard gravity, is shown in figure 2.4. We find that the simulations are consistent with the PD [7] fit at the 1σ level for modified gravity to standard gravity. This is consistent with the results of [1] for a Yukawa type modification (that, like the modification we consider here, is a scale dependent modification). The SP fits are slightly less consistent with the numerical predictions however still lie within 1σ of the simulation mean. We, therefore, find no

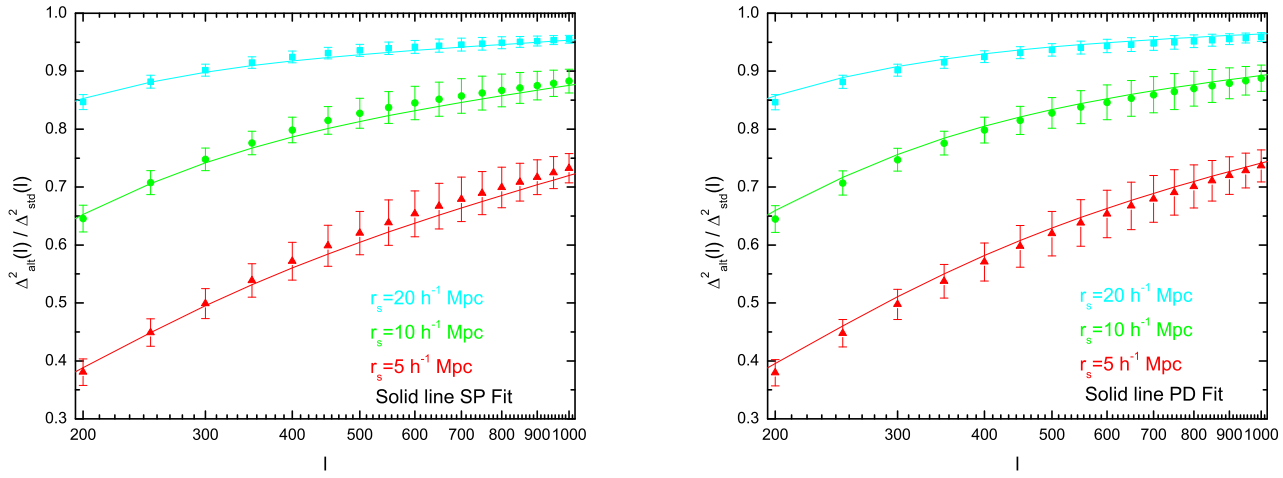

Figure 2.6: The ratio of the weak lensing dimensionless convergence power spectrum, $\Delta^2(l) \equiv l^2 P_\kappa(l)/2\pi$, for a δ function lensing source at $z_s = 1$, as a function of multipole, l, for the 5D gravity model in 2.1.1 to that in standard gravity in comparison to the SP fit (left hand panel) and PD fit (right hand panel). The points and errors are the average and standard deviation of the ratios the 24 simulations. The predicted spectra from the analytical fits (full lines) are wholly consistent with the simulations for all 3 modified gravity models with $r_s = 20h^{-1}Mpc$ (top, blue), $10h^{-1}Mpc$ (middle, green) and $5h^{-1}Mpc$ (bottom, red).

statistical basis for preferring PD over the SP [8] fit of $P_\delta(z = 0)$.

To consider the suitability of the analytic fitting functions when applied to weak lensing it is insufficient to purely consider their agreement with predictions today, the entire evolution must be tracked between the redshift of the lensed source and today, as weak lensing integrates $P(k, a)$ over the expansion factor a, c.f. (2.54). We, therefore, track the redshift history of the non-linear evolution, and the comparison with the analytical fits, as shown in Figure 2.5. We find both fits lie within 1σ though after $a \sim 0.75$ the SP results are just encompassed by the 1σ errors.

The ratios of the modified gravity weak lensing spectra to those of standard gravity are well recovered by the PD and SP fits, as shown in Figure 2.6. The ratios of the weak lensing convergence spectra are slightly less sensitive to the exact form of the modification than the matter power spectra, for two reasons. Firstly, the integral in (2.51) is mostly weighted towards integrand values at early times when the analytical fits are in very strong agreement with the simulations. Thus, for instance the late-time transition of the SP fit to the outer regions of the 1 sigma level is not so significant to the convergence power as it is to the final matter power spectrum. Secondly, we 'pad' the spectrum at k values outside the simulated range with the analytical fit, in order to evaluate $l = k\chi(a)$ in (2.51). This is mitigated (as discussed in 2.3) by the similarity of the fits and the code spectra at the edges of our range of k and the fact that the contribution from padded k values is small in comparison to those drawn from the simulated range: for $l = 200$, P_κ is padded with the non-linear analytical spectrum at $a > 0.955$, which corresponds to 1.3% of P_κ for standard gravity; for $l = 1000$ the padding is required for $0.8 < a < 1.0$ which contributes to 14% of the value of P_κ.

DGP

The effects of non-linear growth in DGP models are of great interest in establishing observational distinctions between this model and standard ΛCDM at cosmological scales, in [14] the non-linear power spectrum was estimated using the Smith and Peacock analytical fit, while in [15] an analytical ansatz is applied. Both the DGP model and the model in 2.1.1 are motivated by 5D modifications to gravity. The difference between DGP and that model is that DGP not only modifies the Poisson equation but also the peculiar acceleration through the presence of an anisotropic stress.

For the arguably more complex DGP model, the SP and PD fits are both still in good agreement with the N-body simulations at a=1, at the 1σ level over the simulated scales, as shown in Figure 2.7. This is also true over the course of the evolution as the modification from ΛCDM switches on, as shown in Figure 2.8.

Note that we do not provide a weak lensing analysis in this model, as due to the change in H (and hence in $\chi(a)$) evaluating $k = l/\chi(a)$ consistently results in a need for much smaller scales, i.e. $k \gtrsim 4.6 Mpc^{-1}$ for the range of l's we have considered. We thus restrict our discussion of DGP to matter power spectra and their evolution.

Even though r_c is chosen to be in close agreement with the background evolution of our fiducial cosmological model, and has essentially degenerate evolution at early times, the DGP model shows marked deviation from standard gravity at late times. We note that the suppression of the non-linear power spectrum shown with respect to standard gravity for the PD and SP fits and N-body simulations is qualitatively similar to that shown with the ansatz of [15], although we leave a quantitative assessment of the ansatz to future work.

Twin Toy Models

In order to investigate the abilities of the two analytical fits to predict non-linear behavior in the two types of modifications, we consider a set of twin toy models, described in 2.1.3. TM1 has a modified Poisson equation $\{Q = 1 + \Sigma_0 a, \eta = 1\}$ while TM2 has anisotropic stress $\{Q = 1, \eta = 2\Sigma_0 a\}$. Both models have the same form of relationship of the weak lensing potential to the over density, characterized by the function $\Sigma(k, a) = Q(1 + \eta/2)$. As shown in figure 2.11, despite the degenerate background evolutions, the different modifications in each

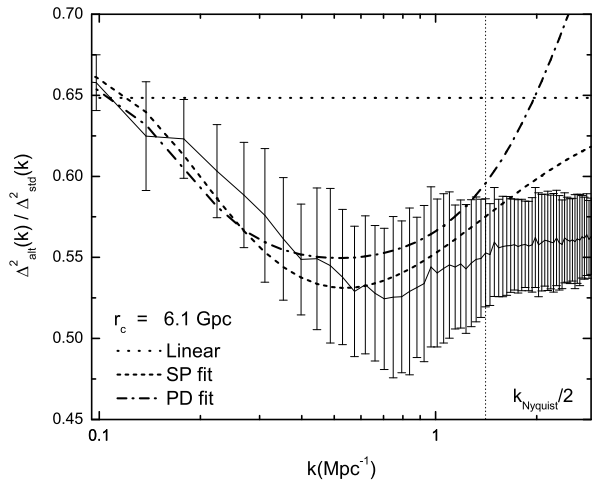

Figure 2.7: Ratios of the matter power spectrum in the DGP model with $r_c = 6.1 Gpc^{-1}$ to that in standard gravity, both models have $H_0 = 70 kms^{-1} Mpc^{-1}$ and $\Omega_m = 0.3$. The full line is the average of the 24 realizations and errors represent the standard deviation of the simulations. The SP (dashed) and PD (dot-dash) analytic fits are in good agreement over the scales measured by the simulation, $k = 0.1$ to 1 Mpc^{-1}. The linear power spectrum ratio is shown by the dotted line.

model lead to different linear scale independent growth factors. For both models, the SP and PD analytical fits track both the scale dependent behavior and time evolution of non-linearities in both types of scenario, as shown in Figures 2.9 and 2.10. The weak lensing correlations for PD and SP fits are virtually identical for each model so we only show the results for SP fits in Figure 2.11, the difference between the simulations and analytical fits is negligible for both models.

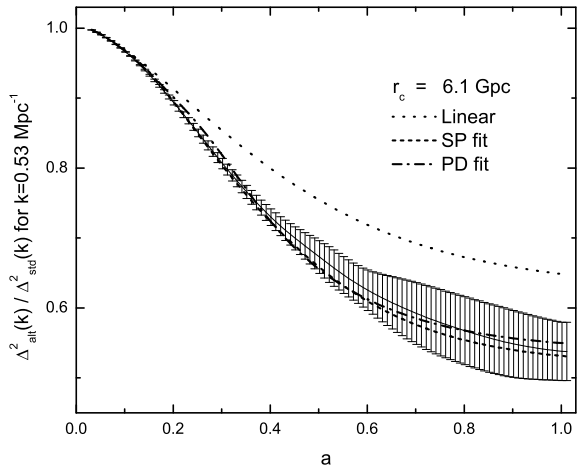

Figure 2.8: The evolution of the ratio of the DGP matter power spectrum to standard gravity for $k = 0.53\ Mpc^{-1}$ in the DGP model as a function of scale factor, a. The full line is the average of the 24 realizations and errors represent the standard deviation of the simulations. The SP (dotted) and PD (dot-dash) analytic fits are good at predicting the transition and development of non-linear growth at all epochs.

2.4.3 Discussion

The non-linear fits of Peacock and Dodds and Smith and Peacock have been shown to work across broad cosmological models, with different fractional mass densities, curvature and initial power spectrum spectral indices. The utility of these fits derives from the wide applicability of the Zel'dovic approximation and a common fractional over-density level on which non-linear structures start to decouple from the background expansion. In both fits there is the conjecture that the statistics of the gravitational clustering obey a similarity transform $P_NL(k/a) = \tilde{P}(k/k_{NL})$ for which no proof is given, but instead is tested by simulation. In this chapter we assess whether such a similarity transform similarly exists in modified gravity theories, and moreover that the existing quantitative values for the fit coefficients

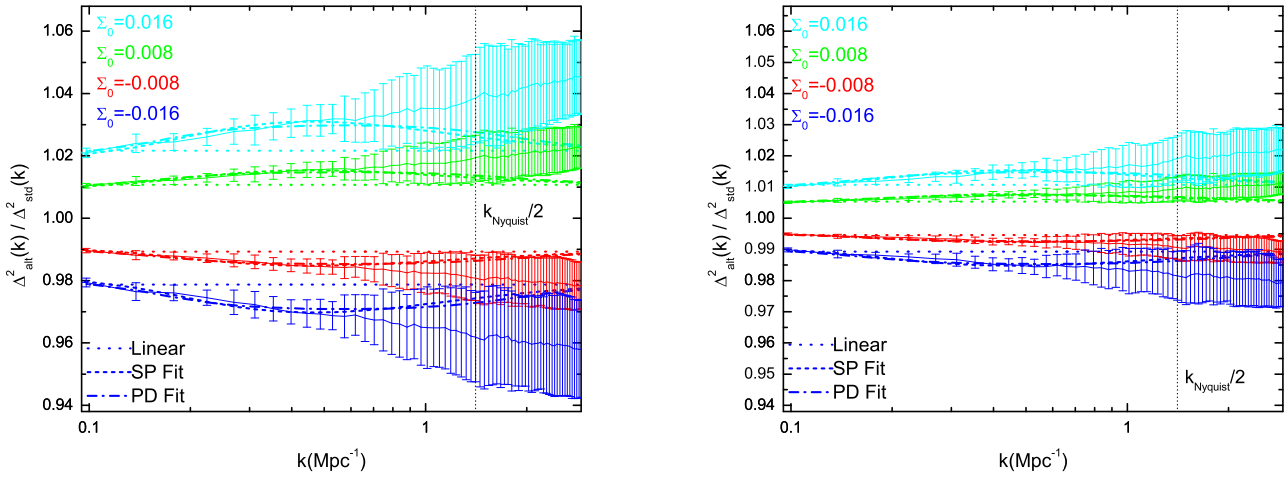

Figure 2.9: The ratios of matter power spectra at a=1 for modified gravity to standard gravity in the TM1(left panel) and TM2 (right panel) models for $\Sigma_0 = -0.016$ (dark blue, bottom), -0.008 (red) ,0.008 (green) and 0.016 (light blue, top) as a function of scale, k. As in earlier figures, full line represents the average of the 24 simulations, error bars represent one standard deviation, and $k_{Nyquist}/2$ is indicated by the vertical dotted line. The predictions of the SP (dashed) and PD (dot-dash) fits are nearly identical, and are in excellent agreement with the simulations for both the weaker modifications with $\Sigma_0 = \pm 0.008$ and the strong ones with $\Sigma_0 = \pm 0.016$. The linear power spectra, showing the differences in linear growth factor arising from the modifications are shown by the dotted lines.

can be used. This is not necessarily the case *a priori*.

To test the fits we have performed non-linear simulations of models in which modifications to Poisson and the peculiar acceleration occur exactly in this mildly non-linear, transition regime. We have found that both the SP and PD analytical fits give reasonably good agreement with the simulations, in spite of the scale and time dependent modifications.

This implies that applicability the Zel'dovic approximation extends even to

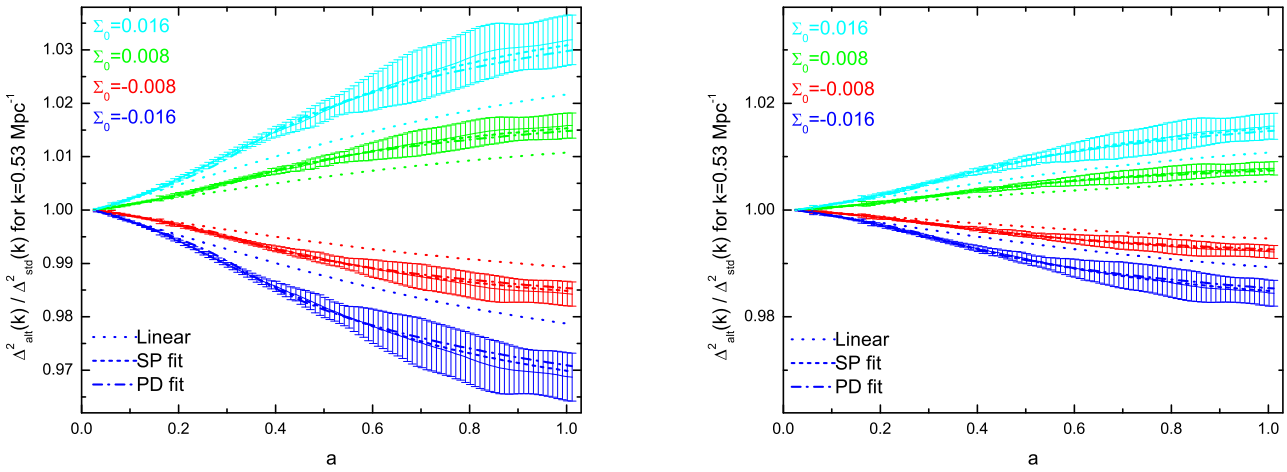

Figure 2.10: The evolution of the power spectrum over time for TM1 (left panel), and TM2 (right panel). Throughout the entire simulation the fits track the simulation results results extremely well. The color coding and line styles are the same as in Figure 2.9.

scenarios in which anisotropic stress and scale dependent modifications to gravity are present in the mildly non-linear regime. This suggests that such modifications have a significant role in reducing the linear growth factor which is well matched by the spectral index dependency of the fitting functions. Since our simulations focus on the ability of the fits to accurately match the transition from linear to non-linear, they don't tell us if modifications on small scales, in which the sub-halo correlations are key, are well described, for example if r_s in 2.20 were significantly smaller, e.g. less than $1Mpc$. This is an area of interest for further analysis, especially in recently discussed theories in which galactic scale modifications could be present (e.g. [205]).

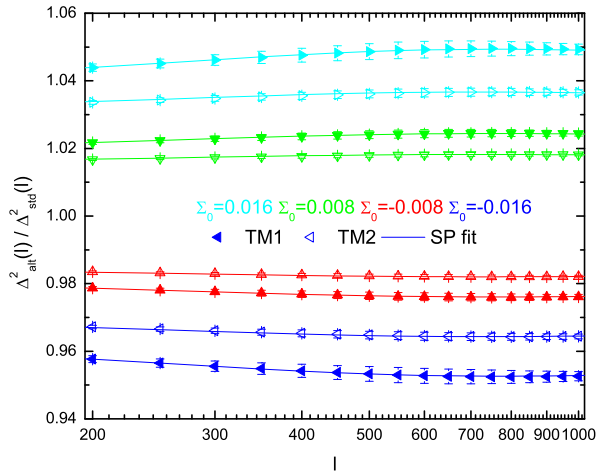

Figure 2.11: The ratios of modified convergence power to standard convergence power in the twin models TM1 (full triangles) and TM2 (empty triangles) for $\Sigma_0 = 0.016$ ($\triangleleft$, blue), -0.008 ($\triangle$,red) ,0.008 ($\triangledown$, green) and 0.016 ($\triangleright$, light blue) shown against the predicted spectrum using the SP fit (full line), as the predictions of SP and PD are virtually identical. As is to be expected, given the strong agreement between the fits and simulations of the matter power spectrum, the weak lensing spectra from the simulations are predicted well by the analytical fits.

2.5 Conclusions

The use of complementary cosmological observations to probe the properties of dark energy has proved extremely powerful. Observations sensitive to the background evolution, e.g. supernovae, or the wholly linear regime, e.g. the Cosmic Microwave Background, have been the major observational tools to constrain dark energy to date. There is now significant interest, however, in applying a broader range of observations including those sensitive to large scale structure including large scale galaxy surveys, such as the Sloan Digital Sky Survey, and current and prospective weak lensing surveys. For each of these, in order to make precise in-

ferences about dark energy theoretical systematic errors about the modeling of non-linear corrections must be addressed.

We considered the ability of the commonly used non-linear analytical fits of Peacock and Dodds [7] and Smith and Peacock [8] to predict non-linear growth in a variety of theories beyond standard gravity. We consider models in which the Poisson equation is modified, based on 5D gravity, [192, 193, 188] and also those in which peculiar acceleration response to the gravitational potential is altered, including the DGP model [121].

We find that the two fitting functions provide robust predictions for theories with both type of modification, in terms of accurately predicting the matter power spectrum today, and also, vitally for calculating the weak lensing convergence spectrum, they predict the development of non-linearities over time. Both consistently give predictions within 1σ of 24 simulated N-body realizations of the theory. Our results imply that the similarity conjecture for mapping linear to non-linear power empirically found to be satisfied in standard gravity simulations is also applicable to scenarios in which gravity has scale and time dependent modifications. This suggests that the spectral index dependence of the fitting function and the linear growth factor effectively describe alterations in the non-linear collapse due to scale dependent modifications to gravity and anisotropic stress at the scales studied in the models here.

We conclude that current analytic fits using the linear power spectrum in modified gravity theories can be used to accurately predict the non-linear growth in theories with scale independent or dependent modifications, and in those with or without anisotropic stress in the mildly non-linear regime. We find no statistical evidence for a preference, on the basis of overall performance, for one analytical fit

over the other.

Many modified gravity models, for example DGP and $f(R)$ models, exhibit gravitational modifications on sub-halo scales. Whether such modifications are well described by the halo term in the SP fit or the stable clustering approximation in the PD fit necessitates smaller scale simulations in the substantially non-linear regime, which lies outside the scope of this thesis.

We have limited our investigation of anisotropic stress to scale independent modifications, and indeed further work is warranted in investigating whether the conclusions found for those are applicable to scale dependent anisotropic stress, as found in $f(R)$ theories. It will also be interesting to investigate the agreement between simulations and the recently proposed non-linear ansatz [15] for modified gravity models.

CHAPTER 3

CONSTRAINING INTERACTIONS IN COSMOLOGY'S DARK SECTOR

(Excerpted from work published as

Rachel Bean, Eanna Flannagan, Istvan Laszlo, and Mark Trodden [206])

This chapter deals with establishing constraints on dark sector interactions using recent supernovae, large scale structure and cosmic microwave background observations. Cosmological constraints are presented for a dark matter-dark matter interaction. It is shown that long range interactions between fermionic dark matter particles mediated by a light scalar with a Yukawa coupling are constrained to be less than 5% of the strength of gravity at a distance scale of 10 Mpc.

The chapter proceeds as follows: section 3.1 describes an example of dark sector interactions a Yukawa dark matter interaction that can have astrophysically observable consequences. 3.1.1 summarizes the theoretical and observational constraints on dark sector interactions. Constraints from cosmological data on the Yukawa dark matter interaction are presented in 3.2.

3.1 Yukawa Interaction Between Dark Matter Particles

Rather than coupling dark matter to some other field, we can modify the coupling of dark matter particles with themselves. One class of models of this type involve an interaction between fermionic dark matter, ψ, and an ultra-light pseudo scalar boson, ϕ, that interacts with the dark matter through a Yukawa coupling with

strength g, described by the Lagrangian [73],

$$\begin{aligned}\mathcal{L} &= i\bar{\psi}\gamma_\mu\nabla^\mu\psi - m_\psi\bar{\psi}\psi - \frac{1}{2}\nabla_\mu\phi\nabla^\mu\phi - \frac{1}{2}m_\phi^2\phi^2 \\ &\quad + g\phi\bar{\psi}\psi. \end{aligned} \tag{3.1}$$

For $g \neq 0$, on scales smaller than $r_s = m_\phi^{-1}$, the Yukawa interaction acts like a long-range 'fifth' force in addition to gravity. The effective potential felt between two dark matter particles is

$$V(r) = -\frac{Gm_\psi^2}{r}\left[1 + \alpha_{\rm Yuk}\exp\left(-\frac{r}{r_s}\right)\right], \tag{3.2}$$

with

$$\alpha_{\rm Yuk} \equiv 2g^2\frac{M_p^2}{m_\psi^2}. \tag{3.3}$$

In our investigations of this model in Sec. 3.2 we will neglect the cosmological effects of the scalar field ϕ, and assume that dark energy is a cosmological constant . The cosmological implications of Yukawa-like interactions of dark matter particles have previously been considered across a range of astrophysical scales, including dark matter halos [207, 61, 208], tidal tails [71, 72], cluster dynamics [76], and large scale structure surveys [209].

3.1.1 Theoretical and Observational Constraints

Models such as the ones described above face a range of theoretical and observational constraints arising from both particle physics and gravity. We will focus on a subclass of these in this chapter, but it is worth mentioning the general web of desiderata and constraints. These include:

- *Disagreement with the required background cosmology.* Obviously, a successful model must be able to reproduce the correct expansion history of the

universe, preferably without excessive fine tuning of initial conditions. This can be a real problem for some models, for example some $f(R)$ modified gravity models [210]. In sections 3.2 we investigate cosmological evolution in coupled models.

- *Problems with linear perturbations around the FRW solution.* Here the possibilities include disagreements with solar system tests of gravity [211], or incorrect predictions for the linear power spectrum of matter perturbations. In addition instabilities causing catastrophic collapse of over-densities can be present in some regimes for coupled theories [146, 147, 148, 149, 150, 151].
- *Problems in the nonlinear regime* There is the also possibility of interesting phenomena in the nonlinear regime. Some may be positive; for example the Chameleon effect [137, 138] can ameliorate problems with Solar System tests [212, 213]. Some other phenomena can be problematic, for example in some models the spatially averaged metric is not a solution of the field equations that one obtains by assuming homogeneity and isotropy (i.e. the "microscopic" and "macroscopic" field equations differ) [214, 215].

In this chapter we will focus on the constraints obtained from the background cosmological evolution and linearized cosmological perturbations.

3.2 Cosmological Constraints on a Yukawa-type Dark Matter Interaction

The astrophysical implications of Yukawa-like interactions have been considered across a range of scales: in the context of dark matter halos [207, 61, 208]; tidal

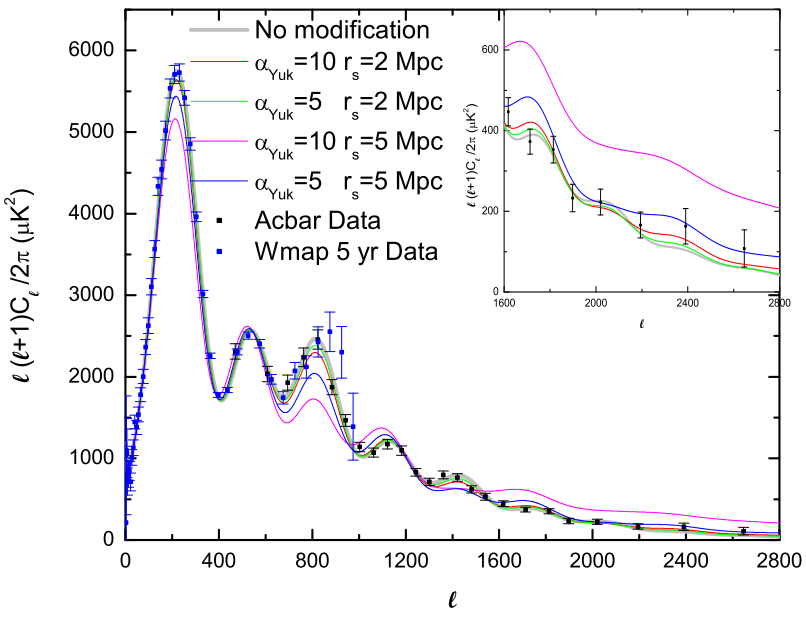

Figure 3.1: CMB temperature power spectrum comparing a fiducial minimally coupled ΛCDM model (grey) with four models with the Yukawa interaction with $\alpha_{\rm Yuk} = 10, r_s$=2Mpc (red), $\alpha_{\rm Yuk} = 5, r_s = 2$ Mpc (green) $\alpha_{\rm Yuk} = 10, r_s$=5Mpc (magenta), $\alpha_{\rm Yuk} = 5, r_s$=5Mpc (blue). Data from WMAP 5 year (blue points) and ACBAR (black points) experiments are also shown. The inset plot shows a blow up of the small scale anisotropies measured by ACBAR.

tails [71, 72]; cluster dynamics [76]; and large scale structure surveys [209]. In our analysis we consider large scale cosmological constraints on a Yukawa coupling described in section 3.1. We modify the publicly available CAMB code [216] to include this modified force between dark matter particles. This alters the growth of matter perturbations. For example, the dark matter density fluctuations evolve according to

$$\ddot{\delta}_c \quad + \quad \mathcal{H}\dot{\delta}_c - 4\pi G a^2 \left[\frac{G_c(k)}{G} \rho_c \delta_c + \rho_b \delta_b + 2\rho_\gamma \delta_\gamma \right] = 0. \tag{3.4}$$

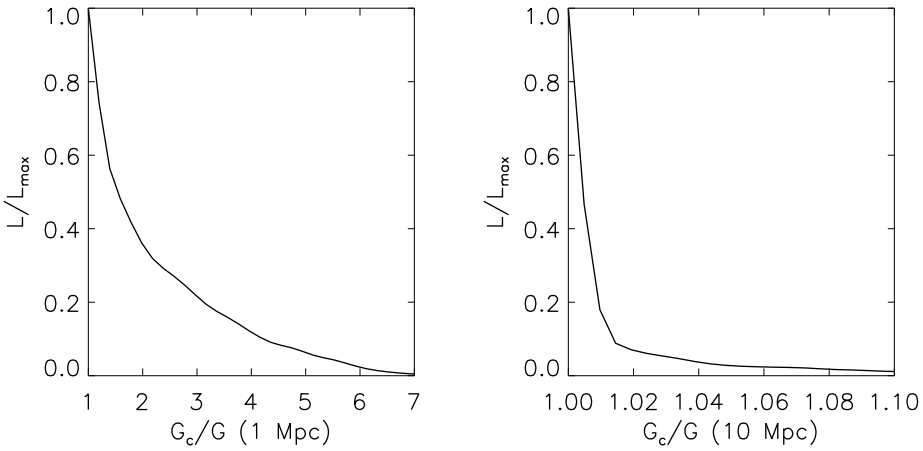

Figure 3.2: 1D likelihood constraints on G_c/G at 1Mpc (left panel) and 10Mpc (right panel) for the Yukawa dark matter interaction, in light of WMAP 5 year and ACBAR CMB anisotropy, and SDSS LRG matter power spectrum observations.

Here $G_c(k)$ is the effective gravitational constant governing the interaction between dark matter particles, given from Eq. (3.2) by

$$G_c(k) \;=\; G\left[1+\frac{\alpha_{\rm Yuk}}{1+(kr_s)^{-2}}\right]. \tag{3.5}$$

We use the CosmoMC code [199] to obtain cosmological constraints on the ratio G_c/G from the 5 year WMAP CMB temperature and polarization data [114, 217], small scale CMB temperature data from ACBAR [110, 113] and the SDSS LRG matter power spectrum [5]. We include CMB lensing, and marginalize over the amplitude of the secondary Sunayev-Zel'dovich anisotropies.

In Figure 3.1 we show the effect of the Yukawa coupling on the CMB temperature anisotropies. With the addition of small scale anisotropy measurements from ACBAR, constraints on the interaction are able to be made.

In Figure 3.2 we show the constraints on G_c/G at two scales, 1 Mpc and

10 Mpc with $G_c/G(1Mpc) \leq 2.7$ and $G_c/G(10Mpc) \leq 1.05$ at the 68% confidence limit. The improvement in the fit to the data obtained by introducing the Yukawa interaction is not statistically significant however, the best fit effective $\chi^2 = -2\ln\mathcal{L} = 1354.0$ in comparison to 1354.1 for a ΛCDM model.

Yukawa interactions on the levels allowed by large scale constraints could well have interesting implications for gravitational dynamics on cluster, galactic and sub-galactic scales [73, 74, 71, 72]. Frieman and Gradwohl [73] argue that the intracluster gas distribution could constrain $-0.5 \lesssim \alpha_{\rm Yuk} \lesssim 1.3$ for r_s of a few hundred kpc, which would translate to $-0.5 \lesssim G_c/G(1\,{\rm Mpc}) \lesssim 2.2$, comparable with our constraints from large scale data. Kesden and Kamionkowski [71, 72] demonstrate that couplings of strength $G_c/G \gtrsim 1.04$ on $\lesssim 100$ kpc scales could well have observable implications for baryonic and dark matter distributions in tidal disruptions of dwarf galaxies, although a comparison with data is yet to be performed. We leave a detailed analysis of the joint constraints on Yukawa interactions from combined astrophysical and cosmological scales to future work.

We note that the observational constraints on the Yukawa coupling $\alpha_{\rm Yuk}$ also yield constraints on the more general class of models parameterized by a baryonic coupling function $\alpha_b(\phi)$ and a dark matter coupling function $\alpha_c(\phi)$. In these models the effective Newton's constant G_{ij} for coupling between sector i and sector j is given by $G_{ij} = G(1+\gamma_i\gamma_j)$ with $\gamma_i = \sqrt{2}M_p\alpha_i'(\phi_0)$ [150]. Now dark matter is observed only through its gravitational interactions. Therefore the observations cannot distinguish between a situation with baryonic and dark matter densities ρ_b, ρ_c and Newton's constants G_{cc}, G_{cb} and G_{bb}, and a situation with densities ρ_b, $e^{\nu}\rho_c$ and coupling constants $e^{-2\nu}G_{cc}$, $e^{-\nu}G_{cb}$ and G_{bb}, where ν is an arbitrary constant

[1]. If we define the parameter

$$\begin{aligned} \alpha &\equiv \frac{G_{cc}G_{bb}}{G_{cb}^2} - 1 \\ &= \frac{(1+\gamma_c^2)(1+\gamma_b^2)}{(1+\gamma_c\gamma_b)^2} - 1, \end{aligned} \tag{3.6}$$

then we see that α is invariant under the above symmetry, and also α reduces to $\alpha_{\rm Yuk}$ for the models discussed in this section for which $\alpha_b = 0$, at short lengthscales $r \ll r_s$. It follows that the arguments of Ref. [73] give the constraint

$$-0.5 \lesssim \alpha \lesssim 1.3. \tag{3.7}$$

This constraint already significantly limits some models, especially together with the Solar System constraints.

3.3 Conclusions

The cosmological observations of the past few decades have provided firm evidence for significant physics beyond the standard model of particle physics. It now seems clear that the successful formation of structure in the universe demands a new particulate component of the cosmic energy budget - dark matter - and that cosmic acceleration may require some kind of dark energy, or a significant infrared modification of general relativity.

While these phenomena have been revealed through their gravitational effects, their microphysical properties remain undetermined although, of course, there exist many complementary bounds on what those properties may eventually prove to be. A priori, there is no reason that dark matter and the physics responsible for

[1]Note that G_{cc} is denoted G_c in the rest of this chapter.

cosmic acceleration should find themselves in entirely disconnected sectors of our underlying fundamental theory. Indeed, that small portion of the energy budget about which we know a great deal - visible matter - comprises a richly detailed spectrum with multiple interactions and a beautiful underlying symmetry structure - the standard model. It thus seems reasonable, in light of our current ignorance regarding the nature of cosmology's dark sector, to explore possible interactions between dark matter, cosmic acceleration and visible matter.

In this chapter we have studied a model of possible astrophysical interest, in which long range interactions between fermionic dark matter is mediated by a light scalar with a Yukawa coupling. We have shown that large scale cosmological measurements constrain such interactions to be less than 5% of gravity at a distance scale of 10 Mpc.

It is a testament to the many diverse sources of data in modern cosmology that the simple possibility of couplings between, say, dark sector components, can be constrained in so many different ways. The web of constraints that we have delineated in this thesis sets strict limits on allowed interactions in the dark sector, and may have important ramifications both for phenomenological models, and for fundamental theory.

CHAPTER 4

DISENTANGLING DARK ENERGY AND COSMIC TESTS OF GRAVITY FROM WEAK LENSING SYSTEMATICS

(Accepted to MNRAS as
Istvan Laszlo, Rachel Bean, Donnacha Kirk and Sarah Bridle [218]
Closely related work submitted to MNRAS as
Donnacha Kirk, Istvan Laszlo, Sarah Bridle, Rachel Bean [219])

This chapter considers the impact of key astrophysical and measurement systematics and their interactions with cosmological parameters of interest, in particular the different redshift dependencies of gravity modifications compared to intrinsic alignments, the main astrophysical systematic. In this chapter, we characterize and quantify the degeneracies between dark energy parameter measurements and weak lensing systematics, and assess how they affect the ability of upcoming photometric "Stage III" and "Stage IV" large scale structure surveys such as the Dark Energy Survey (DES), the Subaru Measurement of Images and Redshifts survey, *Euclid*, the Large Synoptic Survey Telescope(LSST) and the Wide Field Infra-Red Space Telescope(WFIRST) to obtain bounds on the nature of cosmic acceleration and gravity on cosmic scales. An extension of this, not reproduced in this work, involves how surveys can be optimized in light of intrinsic alignment and galaxy bias systematics ([219]).

4.1 Intrinsic Alignments and Weak Lensing

As weak lensing data increases in quality, systematics become key, and indeed a large observational systematic must be considered. When weak lensing measurements are made, they are based on the assumption that, prior to lensing, galaxy

shapes and orientations are uncorrelated. However, galaxies are in fact intrinsically aligned. As structure is assembled, galaxies forming in a common potential will acquire an intrinsic correlated ellipticity. This intrinsic alignment (IA) of galaxy shapes results in two effects, firstly the obvious fact that nearby galaxies will be preferentially aligned, this is called the Intrinsic-Intrinsic (II) correlation and would appear as a spurious indication of lensing. The second effect is more subtle, a galaxy near a lens will be aligned with the lens, while a background galaxy lensed will appear anti-correlated, giving rise to the Gravitational-Intrinsic (GI) correlation, and lessens the weak lensing signal([220]).

Such intrinsic alignment is real, comparing simulations to observations reveals a need for these effects ([221, 222, 223, 224, 225, 226, 227, 228, 229, 230]) and alignments have been directly observed in existing large scale structure surveys ([231, 232, 233, 234, 235, 226, 236, 237, 238, 229, 239, 240, 239, 241, 242]). In fact, at relevant redshifts, IA can be as much as 10% of the observed shear signal. This is unacceptable when seeking percent level constraints on cosmological parameters, for instance to measure the dark energy equation of state to some within 1% requires a weak lensing measurement of the similar precision. Thus, ignoring IA can bias the dark energy equation of state by as much as 10% ([243]).

Fortunately, the II term can be removed from data with relatively little loss in weak lensing information, by avoiding inclusion of physically close galaxy pairs as in [244, 245, 246, 247]. However, since the GI contribution depends on line of sight interactions between background lensed galaxies and foreground lensing galaxies, it cannot be removed, since the line of sight distortion introduced by lensing is the observable of interest. Thus, for weak lensing measurements to truly improve constraints as instrumental errors are reduced requires that IA be accounted for

([226]).

One way to account for IA is to remove both II and GI terms, or at least down weight them by "nulling" ([248, 249]). While this technique does treat both IA signals, it removes a significant amount of data, thus reducing constraints obtainable. In order to retain the full information one must understand IA contributions.

As a result, much work has focused on attempting to produce a viable model for IA formation and evolution, with at least some physical motivation, primarily derived from the Linear Alignment (LA) model ([250, 251, 220, 243, 252]). The reasonable assumption, underlying the models is that galaxies take on shapes that are aligned with those of the common dark matter halo in which they form, which in turn responds to the background gravitational tidal field. It should be noted that in particular this holds for elliptical galaxies, and not for spirals, which instead respond to torques acting on their angular momentum axes, and so do not produce a significant IA contribution. This model reproduces GI measurements([253, 254]), and so serves as a suitable starting point. However, a variety of factors influence alignment after formation, such as mergers and other accretion events as structure is assembled as well as other baryonic processes, as discussed in detail in [255, 256]. In addition (or perhaps as a result of these process) IAs seem to depend on additional factors such as color, redshift, galaxy type, and luminosity dependence and one-halo corrections ([226, 229, 236, 242, 239, 257, 258, 253]).

The LA model can be made to allow for such effects to a degree by simply introducing a gridded bias scheme, gridded in scale and redshift space, and marginalizing over the additional parameters. Such a scheme can account for uncertainties in the IA amplitude, variation with galaxy type and evolution effects, but necessarily degrades constraints as it introduces additional parameters [259, 243, 260, 253].

While, analyses have considered the impact of IA [261, 262] on constraints they have not considered them jointly with MG parameters. For instance [263, 258, 264] have shown that IA effects can be mitigated by using cross correlations of position and shear data (proposed and effectively used to boost constraints without IA or MG by [265] and [259] respectively). However, these same cross correlations are utilized by [157, 266], for instance, to enhance the constraints on modified gravity. Thus, the correlations are used to determine both IA and MG information, and so when both are considered simultaneously one might expect degeneracies to arise between IA and MG parameters, resulting in loss of constraining power.

The IA signal therefore is a contaminant in weak lensing signals and if included reduces constraining power when considering MG theories. In this chapter, the effects of the inclusion of IAs and uncertainties in modeling them on constraining power is examined, furthering studies of this important systematic by [261, 262] and introducing in particular the joint consideration of IA and MG theories. Another work ([219]), not discussed here, extends this extends this and assesses how, in light of the interplay between IA and MG, upcoming surveys might best be designed to obtain maximum constraining power, extending [267, 268, 262, 269, 270, 271] to once again include MG considerations simultaneously with the IA systematics.

The way in which systematic uncertainties, such as galaxy bias and intrinsic alignments, are modeled can change dark energy equation of state parameter and modified gravity figures of merit by a factor of four. The inclusion of cross-correlations of cosmic shear and galaxy position measurements helps reduce the loss of constraining power from the lensing shear surveys. When forecasts for Planck CMB and Stage IV surveys are combined, constraints on the dark energy equation of state parameter and modified gravity model are recovered, relative to

those from shear data with no systematic uncertainties, provided fewer than 36 free parameters in total are used to describe the galaxy bias and intrinsic alignment models as a function of scale and redshift, thus while some uncertainty in the IA model is tolerated, it is important to be able to parameterize IAs well. To facilitate future investigations, we also provide a fitting function for the matter power spectrum arising from the phenomenological modified gravity model we consider.

The chapter proceeds as follows: in section 4.2 we outline the formalism used to describe the cosmological model, including dark energy parameters to describe modifications to ΛCDM in how the homogeneous expansion and growth of inhomogeneities evolve. We describe how the large scale structure and CMB surveys are modeled and how we treat uncertainties in galaxy bias and intrinsic alignments. In section 4.3 we present the results of the Fisher matrix investigation. In an Appendix we introduce a fitting function that allows others to generate weak lensing and galaxy position correlations for the modified gravity model we consider here.

4.2 Formalism

In this section we describe the details of our analytical approach: the cosmological model we use to parameterize dark energy and modifications to gravity is outlined in section 4.2.1, sections 4.2.2 and 4.2.3 respectively describe the statistical correlations for large scale structure and CMB observables and the survey specifications we assume. In 4.2.4 and 4.2.5 we describe how systematic uncertainties in the galaxy bias model and intrinsic alignments are included in the analysis. Throughout this work we assume a flat universe, this assumption was relaxed and found to have no significant impact on results, hence we do not discuss it further.

4.2.1 Cosmological Model

Theories that suggest a cosmic scale modification to gravity can produce deviations from ΛCDM in both the homogeneous expansion history and the growth of inhomogeneities. We model alterations from ΛCDM in the expansion history using an effective equation of state parameter for the additional physics producing the cosmic acceleration ([272])

$$w = w_0 + w_a(1 - a), \tag{4.1}$$

where a is the expansion factor, with $a = 1$ today, and w_0 and w_a describe the effective equation of state today and its derivative with respect to a respectively ($w_0 = -1$ and $w_a = 0$ recover a cosmological constant, Λ.).

The Friedmann equation relates the Hubble expansion rate, $H(a)$, to the cosmic energy density, $\rho(a)$

$$H^2(a) = \frac{8\pi G}{3c^2}\sum_i \rho_i(a) \tag{4.2}$$

$$= H_0^2\left[\frac{\Omega_m}{a^3} + \frac{\Omega_\gamma}{a^4} + \Omega_\Lambda a^{-3(1+w_0+w_a)}e^{3w_a(1-a)}\right] \tag{4.3}$$

where ρ_i is the homogeneous (background) density of component i, H_0 is Hubble's constant, Ω_m and Ω_γ are the fractional energy densities today in non-relativistic and relativistic matter respectively.

To describe the growth of inhomogeneities we use the conformal Newtonian gauge using the notation of [2]

$$ds^2 = -a^2(\tau)[1 + 2\psi(x,\tau)]d\tau^2 + a^2(\tau)[1 - 2\phi(x,\tau)]dx^2 \tag{4.4}$$

where τ is conformal time, x_i are comoving coordinates and ψ and ϕ are the Newtonian potentials.

We consider a phenomenological parameterization for cosmic scale deviations from GR that employs two functions to modify the perturbed Einstein equations. Such modifications have been widely discussed in the literature, both because they are phenomenologically simple, and also because they can be mapped onto predictions for modifications derived from scalar tensor and higher dimensional theories of gravity.

Unlike with the equation of state parameter, notation for these modifications varies widely. Here we write the modified Einstein equations as

$$k^2\phi = -4\pi G Q a^2 \sum_i \rho_i \Delta_i \tag{4.5}$$

$$\psi - R\phi = -12\pi G Q a^2 \sum_i \rho_i (1+w)\frac{\sigma_i}{k^2}. \tag{4.6}$$

where the first, the Poisson equation, comes from a combination of the time-time and time-space Einstein equations, and the second is the anisotropic space-space equation. Here k is the comoving wave number, Δ_i is the perturbation of component i in the component's rest-frame (the frame in which it has zero peculiar velocity) and σ_i is its anisotropic stress. Δ_i is a gauge invariant perturbation, related to a perturbation in a general frame, δ_i, in which the component's peculiar velocity is, v_i, by $\Delta_i = \delta_i + 3\mathcal{H}(1+w_i)v_i/k$. In the discussion below, we focus on density perturbations in CDM, denoted by Δ_c.

In General Relativity the two functions $Q = R = 1$. The function $Q(k,a)$ describes the relation between space-space gravitational potential perturbation and a matter over density through the Poisson equation, creating an effective gravitational constant $G_{eff}(k,a) = Q(k,a)G$. The second function $R(k,a)$ modifies the relationship between the two Newtonian potentials. In GR, an inequality between these can only be generated by the presence of relativistic matter, through the presence of anisotropic shear stress. Shear stresses are rapidly suppressed in

non-relativistic matter, and would be extraordinarily difficult to sustain in a fluid with a negative equation of state parameter. As such, $R \neq 1$ could be viewed as a potential smoking gun signal of a modification to GR being present. We assume that the fluid equations for normal matter are unaltered and assume that dark energy, as a modification of gravity rather than a fluid, does not cluster.

The growth of over densities on large and small scales have different dependencies on Q and R [176]. On small scales, they are purely determined by the peculiar motion during infall, ψ, proportional to QR,

$$\ddot{\Delta}_c + \mathcal{H}\dot{\Delta}_c - \frac{3\mathcal{H}^2}{2}\Omega_m(a)QR\Delta_c \approx 0, \tag{4.7}$$

where $\mathcal{H} = d\ln a/d\tau = aH$. For late-time, large scale behavior the degeneracy between Q and R is not present and CDM density perturbation evolution is governed by

$$\ddot{\Delta}_c + \mathcal{H}\dot{\Delta}_c - 3(\ddot{\phi} + \mathcal{H}(2\dot{\phi} + \dot{\psi}) + (2\dot{\mathcal{H}} + \mathcal{H}^2)\psi) \approx 0. \tag{4.8}$$

We assume that time evolution of the effects of modifications to GR on the growth of inhomogeneities would vary in concert with alterations to the background expansion, and consider modifications of the form,

$$Q(a) = 1 + (Q_0 - 1)a^s \tag{4.9}$$

$$R(a) = 1 + (R_0 - 1)a^s. \tag{4.10}$$

For our analysis we fix $s = 3$ to allow modifications to the growth of structure to evolve at a comparable rate to the onset of an accelerative component in the homogeneous expansion history. We omit any scale dependence in our modifications. Two conditions, $Q(a) > 0$ and $R(a) > -1$ are imposed to ensure that over densities remain gravitationally attractive and that light is bent towards the lens.

4.2.2 Observables

We are interested in how well measurements of weak lensing shear distortions and galaxy counts, from future surveys, will be able to constrain deviations from ΛCDM. Combining these observables is key to detecting changes in the growth history of the universe as they depend differently on the Newtonian potentials.

We characterize each observable by their 2D angular power spectrum, C_ℓ, for auto- and cross-correlations between each observable in a given redshift bin. For two fields X and Y, C_ℓ, under the Limber approximation, is given by

$$C_\ell^{XY} = \int_0^{\chi_\infty} \frac{d\chi}{\chi^2} W_X(\chi) W_Y(\chi) S_X(k_\ell, \chi) S_Y(k_\ell, \chi) \tag{4.11}$$

where $k_\ell = \ell/\chi$, and $X, Y = \{\delta, G\}$ for mass and lensing shear fields respectively. W_X and S_X are the window function and source function associated with the field X, respectively.

The source functions for the mass distribution and weak lensing shear are

$$S_\delta = \Delta_c, \tag{4.12}$$

$$S_G = -\frac{k^2}{2}(\phi + \psi). \tag{4.13}$$

where we have assumed that the density perturbation for matter is equivalent to that for CDM

The power spectrum for the correlation between fields X and Y is related to the source functions by, $P_{XY} \equiv \langle S_X S_Y \rangle$, allowing one to rewrite the angular correlation in a common form:

$$C_\ell^{XY} = \int_0^{\chi_\infty} \frac{d\chi}{\chi^2} W_X(\chi) W_Y(\chi) P_{XY}(k_\ell, \chi). \tag{4.14}$$

The galaxy and lensing window functions are dependent on the normalized distribution of galaxy number density in each redshift bin i for the relevant survey, $n_i(\chi)$. We assume the galaxies are distributed according to ([273]) with

$$n(z) \propto z^2 \exp\left[-\left(\frac{z}{z_0}\right)^{3/2}\right]. \tag{4.15}$$

We break up the galaxy distribution into N_{ph} photometric redshift bins, divided so that they each contain an equal number of galaxies. The photometric redshifts are measured with accuracy $\sigma(z) = \sigma_{z0}(1+z)$ and could have a potential systematic offset, which we model as a constant within each redshift bin, Δz_i. The observed distribution of galaxies in bin i is given by

$$n_i(z) = \frac{n(z)}{2}\left[\mathrm{erf}(z_i - z + \Delta z_i) - \mathrm{erf}(z_{i-1} - z + \Delta z_{i-1})\right] \tag{4.16}$$

The galaxy and lensing window functions are then given by

$$W_m^i(\chi) = \hat{n}_i(z) \tag{4.17}$$

$$W_G^i(\chi) = \int_\chi^{\chi\infty} d\chi' \hat{n}_i(\chi') \frac{r(\chi) r(\chi' - \chi)}{r(\chi')}, \tag{4.18}$$

where $r(\chi)$ is the comoving angular diameter distance to comoving distance χ, and $\hat{n}_i$ is the normalized number density,

$$\hat{n}_i(z) = \frac{n_i(z)}{\int_{z'=0}^{\infty} n_i(z') dz'}. \tag{4.19}$$

In relating the observed correlations of galaxies to the dark matter correlation functions above, we must account for a bias between dark and luminous matter. This bias is dependent on the galaxy type, redshift and environment in a way that is poorly understood. We allow for this uncertainty by introducing a redshift and scale dependent bias parameter, b_g, to relate the auto-correlation of the galaxies to the autocorrelation of the mass and an independent, correlation parameter, r_g, to describe the bias in the cross-correlation of luminous matter and the mass. The

correlation parameter, r_g, would be equal to unity if the galaxies trace the mass, and less than unity if there is some stochasticity in the galaxy formation process e.g. see [274] for a review.

The galaxy position auto-correlation and galaxy position-shear cross-correlation are then related to the underlying mass and shear observables by

$$P_{gg}(k,\chi) = b_g^2(k,\chi)P_{\delta\delta}(k,\chi), \tag{4.20}$$

$$P_{gG}(k,\chi) = b_g(k,\chi)r_g(k,\chi)P_{\delta G}(k,\chi). \tag{4.21}$$

where g and δ, denote galaxy and underlying mass observables respectively.

Note that in modified gravity models the lensing source term and the mass source term must be different

$$P_{\delta G}(k,\chi) = \left[\frac{Q(\chi)(R(\chi)+1)}{2}\right] P_{\delta\delta}(k,\chi), \tag{4.22}$$

$$P_{GG}(k,\chi) = \left[\frac{Q(\chi)(R(\chi)+1)}{2}\right]^2 P_{\delta\delta}(k,\chi). \tag{4.23}$$

The growth of the dimensionless power spectrum $P_{\delta\delta}$ is itself dependent on modified gravity parameters Q and R, as summarized by (4.7) and (4.8).

To obtain the lensing and galaxy position correlations in the modified gravity scenarios we integrate the full equations of motion using a modified version of CAMB ([275]).

To support other researchers investigating the role of modified gravity models on large scale structure observations, without having to integrate the full perturbation equations, we provide a fitting function in the Appendix for the ratio, $r_{fit}(k,z)$, between a fiducial ΛCDM linear matter power spectrum, $P_{\delta\delta,\Lambda CDM}(k,z)$ and the one for a modified gravity model described in 4.2.1, parameterized by

Survey Parameters	Stage III	Stage IV
Area(sq. deg.)	5000	20000
$\sqrt{2}z_0$	0.8	0.9
z_{min}	0.001	0.001
z_{max}	3	3
N_g	10	35
N_{ph}	5	10
σ_{z0}	0.07	0.05
γ_{rms}	0.23	0.35

Table 4.1: Summary of the photometric large scale structure survey specifications assumed for the Stage III and Stage IV survey: survey area; median survey redshift, $\sqrt{2}z_0$; minimum and maximum redshifts observed, z_{min} and z_{max}; number of galaxies, per square arcminute, N_g; number of photometric redshift bins, N_{ph}; standard photometric redshift measurement error at $z = 0$, σ_{z0}, and the r.m.s. shear measurement error, γ_{rms}.

ν(GHz)	100	143	217
f_{sky}	0.8	0.8	0.8
θ_{FWHM}(arc min)	10.7	8.0	5.5
$\sigma_T(\mu\text{K})$	5.4	6.0	13.1
$\sigma_E(\mu\text{K})$	-	11.4	26.7

Table 4.2: CMB survey specifications for a Planck-like survey. We model this on the temperature, T, and E-mode polarization specifications from three lowest frequency bands for the Planck HFI instrument.

Q_0, R_0 and s:

$$r_{fit}(k, z; Q_0, R_0, s) \equiv \frac{P_{\delta\delta,fit}(k, z; Q_0, R_0, s)}{P_{\delta\delta,\Lambda CDM}(k, z)}. \tag{4.24}$$

4.2.3 Survey specifications

We consider the impact of including IAs on cosmological constraints for a near-term Dark Energy Task Force (DETF) [21] Stage III survey, such as DES or HSC, and a longer-term Stage IV survey, such as Euclid, LSST or WFIRST.

The noise for each survey is modeled as statistical errors given by

$$N_\ell^{\epsilon_i\epsilon_j} = \delta_{ij}\frac{\gamma_{rms}^2}{2n_j}, \tag{4.25}$$

$$N_\ell^{n_i n_j} = \delta_{ij}\frac{1}{n_j}, \tag{4.26}$$

$$N_\ell^{n_i\epsilon_j} = 0, \tag{4.27}$$

where γ_{rms} is the root mean square uncertainty in the shear measurement of the galaxies and n_j is number of galaxies per steradian in j^{th} photometric redshift bin so $\sum_i n_i = N_g$.

The survey specifications assumed in our analysis for the Stage III and IV surveys are given in Table 4.1.

We include complementary constraints from temperature (T) and E-mode polarization (E) measurements from a Planck-like CMB survey up to $l = 3000$. As summarized in Table 4.2, we model this by considering the three lowest frequency bands of the *Planck* HFI instrument, three channels for temperature data and 2 for E mode polarization, as described in the Planck Bluebook [1]. We assume each frequency channel has Gaussian beams of width θ_{FWHM} and error in $X = T, E$ of σ_X, so that the noise in channel c is given by

$$N_\ell^{XX,c} = (\sigma_{X,c}\theta_{FWHM,c})^2\, e^{\ell(\ell+1)\theta^2_{FWHM,c}/8\ln(2)}, \tag{4.28}$$

and over all channels,

$$N_\ell^{XX} = \left[\sum_c \left(N_{\ell,c}^{XX}\right)^{-1}\right]^{-1}. \tag{4.29}$$

[1] *www.rssd.esa.int/SA/PLANCK/docs/Bluebook − ESA − SCI*(2005)1_*V*2.*pdf*

4.2.4 Intrinsic Alignments

Cosmic shear describes the distortion of the image of a distant galaxy due to the bending of light from that galaxy by gravity as it passes massive large-scale structure. For a galaxy in the i^{th} photo-z bin, the observed ellipticity, ϵ, of the galaxy can be written as a sum of three independent contributions: the cosmic shear γ_G, the intrinsic, non-lensed shape of the galaxy, γ_I, and apparent ellipticity introduced through instrumental and foreground noise, ϵ_{rnd},

$$\epsilon^i(\theta) \quad = \quad \gamma^i_G(\theta) + \gamma^i_I(\theta) + \epsilon^i_{rnd}(\theta). \tag{4.30}$$

The cosmic shear signal γ_G is very small, and we cannot measure directly the intrinsic shear of any individual galaxy. To recover the cosmic shear, therefore, one averages over a number of galaxies on a small patch on a sky. Assuming that their intrinsic ellipticities are distributed randomly, and that their light passes by similar large scale structure, the intrinsic ellipticities cancel in the two-point function, and we are left with the cosmic shear signal.

In reality, the assumption that intrinsic ellipticities are randomly distributed on the sky is inaccurate. There are two strains of intrinsic alignment of galaxy ellipticities, both arising from the same physics of galaxy formation.

The measured weak lensing signal reflects a correlation in shapes arising from distant galaxies passing near the same foreground gravitational lens. However, if the background images are already correlated, this boosts the measured signal and gives rise to a systematic deviation in the observed shear.

In section 4.2.4, we describe the linear alignment model ([250, 220]) we use as our basis to describe intrinsic alignment contributions. In this model, galaxies

quickly align along the curvature of the gravitational potential. While this model does provide a reasonable starting point for an overall agreement with observations, and thus a suitable baseline for use in our statistical analysis, it neglects known complicating factors of dependency on galaxy luminosity, galaxy type and redshift, and the effect of post-processing of IA in mergers and accretion events ([226, 229, 236, 242, 257, 253, 239, 254]). In section 4.2.4 we therefore extend beyond the LA model, in an attempt to allow for these effects, through the inclusion of additional non-linear corrections, and scale and redshift dependent bias terms.

The Linear Alignment Model

The Linear Alignment (LA) model introduced in [250, 220] assumes that galaxies would align with the stretching axis of the potential in which they form, so that the intrinsic shear is assumed to be

$$\gamma_I^{(1,2)} = -\frac{C_f}{4\pi G}(\nabla_x^2 - \nabla_y^2, \nabla_x \nabla_y)\psi(z_f). \tag{4.31}$$

$\psi(z_f)$ is the smoothed gravitational potential field sourcing the shear alignments at a primordial redshift, z_f, when galaxy formation occurred and C_f is a normalization determined by matching the model to observations. We take $z_f = 50$ here, however we expect z_f to be well within the matter dominated era, when the potential ψ remains roughly constant in time and gravity can be well-described by GR, so that the analysis should be largely insensitive to the precise value of z_f assumed.

The presence of intrinsic alignments alters the observed shear correlations. We denote the *measured* galaxy shear and position observables by ϵ and n, to distinguish them from the underlying theoretical IA-free shear and position variables, G and g respectively. The observed angular correlation functions for galaxy shear

and position, when intrinsic alignments are included, are given by

$$C_\ell^{\epsilon\epsilon} = C_\ell^{GG} + C_\ell^{GI} + C_\ell^{II}, \tag{4.32}$$

$$C_\ell^{n\epsilon} = C_\ell^{gG} + C_\ell^{gI} \tag{4.33}$$

ignoring magnification terms ([263]).

The Intrinsic-Intrinsic (II) alignment correlation applies to physically close galaxies. These form in the same large-scale gravitational potential and their intrinsic ellipticities tend to align with the field lines of that potential. When these galaxies are observed on the sky they will tend to point in the same direction. This alignment produces a spurious correlation which adds to the observed cosmic shear signal.

Since the II correlation is greatest for closely positioned galaxies, there is a related correlation between the position and the intrinsic alignment of a pair of physically close galaxies, this is the galaxy position-intrinsic alignment (gI) correlation.

Somewhat more subtle is the Gravitational-Intrinsic alignment (GI) correlation which applies to galaxies close on the sky but separated in redshift. The intrinsic ellipticity of the foreground galaxy will tend to align with the nearby gravitational potential which, in turn, is responsible for gravitationally lensing the background galaxy. This tends to produce an anti-correlation which subtracts from the observed cosmic shear signal as we observe the galaxies oriented orthogonally.

We can write angular correlation functions involving intrinsic alignments using the formalism in (4.11), defining a source term, S_I, and window function, W_I, for

the intrinsic alignments

$$S_I(k,\chi) = -\frac{C_f}{4\pi G}k^2\psi(k,z_f), \tag{4.34}$$

$$W_I^i(\chi) = W_m^i(\chi) = \hat{n}_i(\chi). \tag{4.35}$$

The angular correlation is often written in terms of the linear power spectra, $P_{XY} = \langle S_X S_Y \rangle$,

$$\begin{aligned} C_{ij}^{GI}(l) &= \int_0^{\chi_\infty} \frac{d\chi}{\chi^2} W_{G,i}(\chi)\hat{n}_j(\chi)P_{GI}(k,\chi), \\ C_{ij}^{II}(l) &= \int_0^{\chi_\infty} \frac{d\chi}{\chi^2} \hat{n}_i(\chi)\hat{n}_j(\chi)P_{II}(k,\chi), \\ C_{ij}^{gI}(l) &= \int_0^{\chi_\infty} \frac{d\chi}{\chi^2} \hat{n}_i(\chi)\hat{n}_j(\chi)P_{gI}(k,\chi). \end{aligned} \tag{4.36}$$

One can write the correlations in (4.36) in terms of the matter power spectrum at z_f,

$$\begin{aligned} P_{GI}(k,z) &= \frac{Q(k,z)[1+R(k,z)]}{2}\frac{D(k,z)}{D(k,z_f)}C_f\bar{\rho}_m(1+z_f)P_{\delta\delta}(k,z_f), \\ P_{II}(k,z) &= C_f^2\bar{\rho}_m^2(1+z_f)^2P_{\delta\delta}(k,z_f), \\ P_{gI}(k,z) &= b_g(k,z)\frac{D(k,z)}{D(k,z_f)}C_f\bar{\rho}_m(1+z_f)P_{\delta\delta}(k,z_f), \end{aligned} \tag{4.37}$$

where $\bar{\rho}_m$ is the mean matter density today and $D(k,z)$ is the linear growth factor for CDM perturbations,

$$\Delta_c(k,z) = \frac{D(k,z)}{D(k,z_f)}\Delta_c(k,z_f). \tag{4.38}$$

In GR the linear growth factor is scale independent. If gravity is modified on cosmic scales, however, it can be scale dependent, and sensitive to the functions Q and R.

How does one normalize the IA correlations, and the constant C_f? [243] provide a numerical value for C_ℓ^{II}, by comparing with [220] who used observations of low

redshift galaxies today. Rather than normalizing the IA source function at z_f, they normalize it, with constant C_1, relative to the gravitational potential today assuming a ΛCDM cosmology, ψ_Λ,

$$S_I(k,z) = -\frac{C_1}{4\pi G}k^2\psi_\Lambda(k,0). \tag{4.39}$$

They find $C_1 = 5\times10^{-14}(h^2 M_{sun}/Mpc^{-3})^{-1} = 8.25h^{-2}\times10^4 Mpc^2$. We extrapolate the normalization of ([243]) at $z = 0$ to $z = z_f$ by assuming a ΛCDM growth factor, $D_\Lambda(z)$ ([276]). The early and late time normalizations, C_f from C_1, are then related by

$$C_f = C_1\frac{D_\Lambda(0)}{D_\Lambda(z_f)(1+z_f)}. \tag{4.40}$$

Generalizing the IA model

Though the correlations in galaxy orientation might be formed in the era of galaxy formation, the intrinsic alignments we observe will invariably be sensitive to the evolution of those galaxies, and the galaxy environment.

One factor that is not included in the LA model is the impact of non-linear clustering of galaxies on the distribution of the galaxies sourcing the intrinsic alignments. A non-linear alignment (NLA) model was introduced as an ad-hoc way to incorporate non-linear clustering into the LA model ([226, 243]). This replaces the linear power spectrum in the intrinsic alignment angular correlation expression (4.37) with the non-linear power spectrum based on the fitting function derived from the halo model of [277].

While this is somewhat adhoc, it was found to give a qualitatively similar result to the more motivated halo model of intrinsic alignments in [257] and it has been

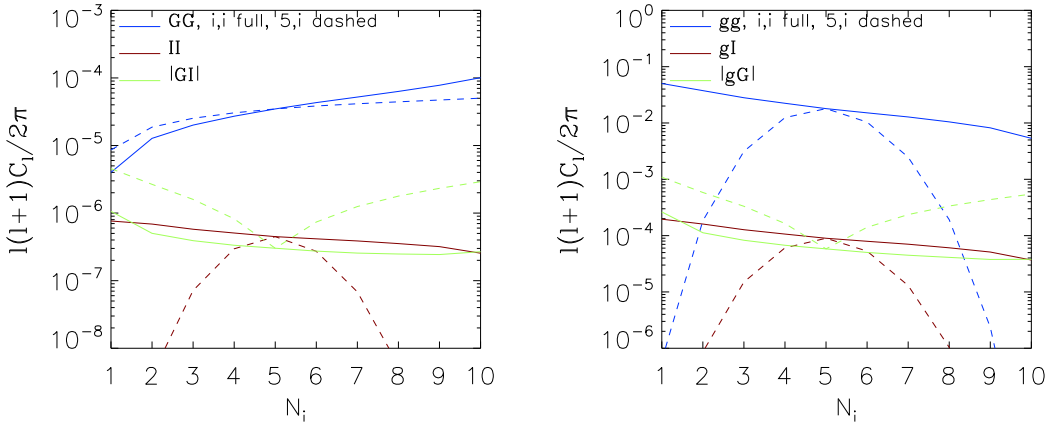

Figure 4.1: A comparison of the intrinsic alignment and cosmological contributions, assuming a fiducial ΛCDM cosmology, to the shear-shear [left panel] and position-shear correlations [right panel] as a function of photometric redshift bin, N_i, for the Stage IV survey specification for a single multipole, $\ell = 1000$. Same-bin 'ii' [full lines] and cross-bin correlations with the 5^{th}, central, redshift bin '$5i$' [dashed] are shown for the cosmological correlations GG, gg and gG, and the intrinsic alignment correlations II, GI, and gI. For the gG, gI and GI correlations we plot the larger of i5 and 5i correlations in each case.

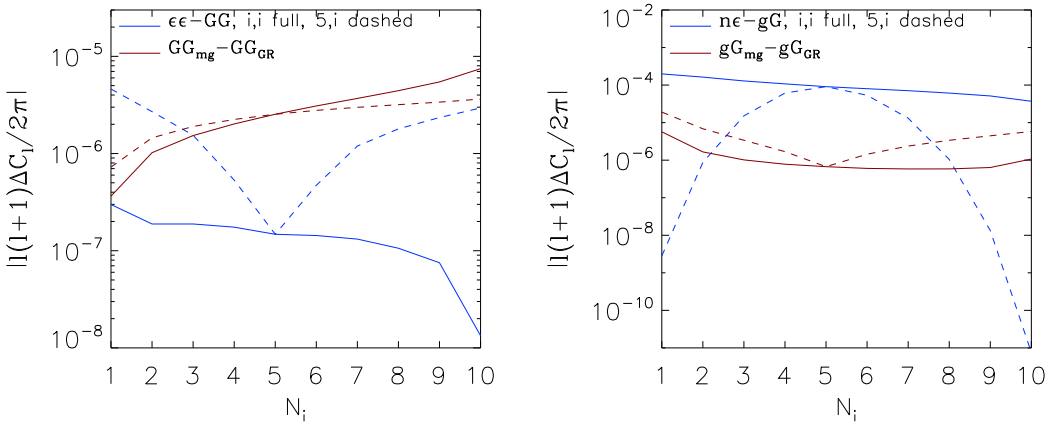

Figure 4.2: The difference in shear-shear [left panel] and position-shear correlations [right panel] in which IAs are included [blue lines] or using a modified gravity model (with no IAs) [red lines] in comparison to a fiducial model, in which no IAs are included and GR is assumed. The modified gravity model shown has $Q_0 = 1.05$ and $R_0 = 1$. As in figure 4.1, we show correlations for $\ell = 1000$ in each photometric redshift bin, N_i, for the Stage IV specification.

shown, in for example [226, 254], that it gives a more consistent fit to the data than the linear alignment model.

We extend this approach to take into account the modified growth history, if gravity deviates from GR. We model the effect of non-linear clustering by boosting the IA source function, S_I^{NLA} relative to that predicted by linear alignments,

$$S_I^{NLA}(k,\chi) = S_I^{LA}(k,\chi)\sqrt{\frac{P_{\delta\delta}(k,\chi)^{nonlin}}{P_{\delta\delta}(k,\chi)^{lin}}}. \tag{4.41}$$

here $P_{\delta\delta}^{lin}$ is the linear matter power spectrum predicted modified gravity model, and $P_{\delta\delta}^{nonlin}$ is the non-linear spectrum after a correction is applied to the power spectrum using the Smith et. al. halo fitting function ([277]). The use of the Smith et al. fitting function, for a modified expansion history, is equivalent to assuming that non-linear collapse in the modified gravity theories follows the Zel'dovich approximation; this was shown to be reasonable if the phenomenological modifications in (4.5) and (4.6) hold to nonlinear scales ([1, 156]). We briefly discuss the motivation and possible impact of deviations from this assumption later in the analysis.

In figure 4.1 we show how each intrinsic alignment contribution to the observed correlations varies as a function of redshift for a fixed multipole, $\ell = 1000$. We refer the interested reader to [263] for a figure detailing the variation in lensing, galaxy and IA correlations across all multipoles and redshift bins. The same-bin correlations vary monotonically as a function of redshift (denoted by the index of the photometric redshift bin), while the cross-bin correlations involving galaxy positions dramatically fall off as the photometric redshift bins become more separated. By contrast, the cross-bin correlations for GG and GI, can remain significant even in cross-correlations between widely separated bins because of the broad redshift kernel for the lensing window function.

Figure 4.2 compares the amplitude and variation in shear and galaxy correlations when, separately, IAs are added and when the modified gravity theory is allowed. While the two effects can be of comparable amplitude, their distinct redshift dependencies, if the intrinsic alignment model is perfectly known, could assist in disentangling them.

Intrinsic alignments are unlikely, however, to be described fully by the linear alignment model; they will depend on the details of galaxy formation within dark matter halos, and baryonic physics within galaxies, with complexity beyond this model. For example, it is known that the IA signal depends strongly on galaxy type and color, ([239, 254]); spirals are supported by angular momentum, and so more likely subject to tidal torquing of the angular momentum vector, while elliptical galaxies are better described by linear alignments. This bifurcation translates into color dependence, as spirals are blue while ellipticals are older and redder, and is noted in surveys which split samples by color ([226, 229, 236]). Redshift and luminosity dependences, and one-halo corrections at smaller scales also exist, as in ([226, 229, 236, 242, 257, 253]).

Rather than attempt to incorporate these numerous effects by direct modeling, we choose to allow a scale and redshift dependent bias factor to parameterize our ignorance and marginalize over the bias parameter in a redshift and scale gridding. We introduce two additional bias parameters into the IA correlations, b_I and r_I, analogous to the galaxy bias b_g and r_g, to reflect our uncertainty in the bias model:

$$P_{II} = b_I^2 P_{II}^{(fid)} \tag{4.42}$$

$$P_{GI} = b_I r_I P_{GI}^{(fid)} \tag{4.43}$$

where the fiducial functions are given by the LA or NLA mode.

4.2.5 Modeling Galaxy Bias and IA Amplitudes

We consider two scenarios for galaxy and IA bias. In our simple model all bias parameters are k and z independent, i.e. b_g, b_I, r_g and r_I are each a single constant free parameter determining the amplitude of the bias. In the more realistic scenario, motivated by [263] each bias coefficient, $B_X \in \{b_g, r_g, b_I, r_I\}$, is interpolated from a $N_k \times N_z$ grid of values logarithmically spaced in k and z, B_X^{ij}, respectively,

$$\begin{aligned} B_X(k,a) &= (1-\Delta_k)\left[(1-\Delta_z)B_X^{ij} + \Delta_z B_X^{ij+1}\right] \\ &\quad +\Delta_k\left[(1-\Delta_z)B_X^{i+1j} + \Delta_z B_X^{i+1j+1}\right] \end{aligned} \tag{4.44}$$

for $k_i < k < k_{i+1}$ and $z_j < z < z_{j+1}$, with

$$\Delta_k \equiv \frac{\ln(k/k_i)}{\ln(k_{i+1}/k_i)} \tag{4.45}$$

$$\Delta_z \equiv \frac{\ln[(1+z)/(1+z_j)]}{\ln[(1+z_{j+1})/(1+z_j)]} \tag{4.46}$$

and modulated by a free constant amplitude parameter. We choose $k_{min} = 10^{-3} Mpc^{-1}$ and $k_{max} = 30 Mpc^{-1}$ for the gridding, and assume $B_X(k < k_{min}) = 1$ and $B_X(k > k_{max}) = B_X^{N_k N_z}$ at all times. We consider scenarios in which $1 \leq N_k = N_z \leq 5$. Each of the $N_k \times N_z$ grid nodes is a freely varying parameter. This means that, in our more sophisticated model, there are $4N_kN_z$ nuisance parameters when all correlations and cross-correlations are included.

A multi-bin marginalization over bias parameters is arguably conservative, however we believe it reasonably reflects the current uncertainties in the bias and IA models. It was inspired by the work of [259] which was used in [278] who bin the biases in redshift and multipole bins, rather than redshift and wave number as we do here.

For observables involving the galaxy position correlations we truncate the max-

imum ℓ used as a function of redshift bin, as per [279, 263] to remove poorly understood biasing on non-linear scales from the likelihood calculation. We introduce a maximum wave number k_{max} for a photometric redshift bin i, and neglect all $\ell_i > k_{max}\chi(z_i)$.

Our analysis spans from the optimistic to conservative scenarios. Optimistically one might assume one can extract, and therefore exclude, IAs with perfect precision and can model the galaxy bias as scale and redshift independent. A conservative perspective would be to represent our ignorance in IA and galaxy bias modeling with 100 marginalized parameters ($N_k = N_z = 5$). Where, within this range, the realistic range will finally fall will depend on progress in understanding IAs potentially through the use of complementary spectroscopic redshift surveys and the development of galaxy training sets, or preferential selection of galaxy subgroups in which intrinsic alignments are less pronounced, and galaxy bias is well-understood.

4.3 Analysis

For our analysis of the impact of systematics on dark energy constraints, we consider constraints on 10 cosmological parameters:

$$\begin{aligned} \mathbf{p} &= \{\Omega_\Lambda, w_0, w_a, Q_0, \frac{Q_0(1+R_0)}{2}, \Omega_b h^2, \Omega_m h^2, \tau_{reion}, \\ &\quad n_s, \ln(10^{10} A_s)\} \end{aligned} \tag{4.47}$$

where τ_{reion} is the optical depth to the epoch of reionization, and n_s and A_s are the spectral index and normalization of the primordial spectrum of curvature perturbations, with pivot scale $k = 0.05 Mpc^{-1}$. We choose fiducial values for these

parameters assuming ΛCDM, and consistent with a *7-year Wilkinson Microwave Anisotropy Probe*$WMAP7$ best-fit cosmology ([34]).

As can be seen in 4.2.2, a primary constraint on modified gravity parameters from weak lensing is the combination from $Q_0(1+R_0)/2$, rather than R_0. We therefore use Q_0 and $Q_0(1+R_0)/2$ as variables in the Fisher analysis, and take GR with $Q = R = 1$ as the fiducial model.

Unless stated otherwise, we consider a conservative scenario for astrophysical systematics, and marginalize over the galaxy and intrinsic alignment biases b_g, r_g, b_I, r_I with $N_k = N_z = 5$ bins. We assume $b_g = r_g = b_I = r_I = 1$ for the fiducial model.

Our fiducial scenario involves a 5×5 grid of 4 auto-correlation and cross-correlation galaxy and IA bias parameters and 10 cosmological parameters, giving a total of 110 parameters.

The large number of parameters, especially when using the full bias model, favors the use of a Fisher matrix approach. For N parameters, only $N+1$ samples are required to estimate the parameter covariance matrix, $C_{ij} = F_{ij}^{-1}$, with,

$$F_{ij} = \sum_{ab} \sum_{\ell} \frac{\partial \mathscr{D}_a(\ell)}{\partial p_i} Cov_{ab}^{-1} \frac{\partial \mathscr{D}_b(\ell)}{\partial p_j}, \tag{4.48}$$

where $\mathscr{D}(\ell) = \{C_\ell^{CMB}, C_\ell^{n_i n_j}, C_\ell^{n_i \epsilon_j}, C_\ell^{\epsilon_i \epsilon_j}\}$ are the set of observables across all multipole bins, and redshift bin combinations. We consider correlations for $10 \leq \ell \leq 3000$ in 50 logarithmically spaced bins in ℓ space.

To calculate the partial derivatives,$\partial \mathscr{D}(\ell)/\partial p$, we take a 2% reduction in each parameter with non-zero fiducial value, and an absolute step of -0.02 for all parameters whose fiducial value is zero. We checked that the results are insensitive

to the exact size of the step size, obtaining consistent results with 1% and 3% step sizes.

The covariance matrix Cov_{ab}^{-1} between two observables, in multipole bin with mid-value ℓ and spanning $\ell_{min}(\ell) \leq \ell' \leq \ell_{max}(\ell)$, is given by

$$\begin{aligned} Cov[C_\ell^{W_i X_j}, C_\ell^{Y_m Z_n}] &= \frac{\hat{C}_\ell^{W_i Y_m}\hat{C}_\ell^{X_j Z_n} + \hat{C}_\ell^{W_i Z_n}\hat{C}_\ell^{Y_m X_j}}{f(\ell) f_{sky}} \\ \hat{C}_\ell^{W_i X_j} &\equiv C_\ell^{W_i X_j} + N_\ell^{W_i X_j} \\ f(\ell) &\equiv \sum_{\ell'=\ell_{min}(\ell)}^{\ell_{max}(\ell)} (2\ell'+1). \end{aligned} \tag{4.49}$$

We have modified the publicly available CosmoMC ([199]) and CAMB [275] codes to calculate the Fisher matrix and the correlation functions for the future survey specifications, in light of the IA and modified gravity models.

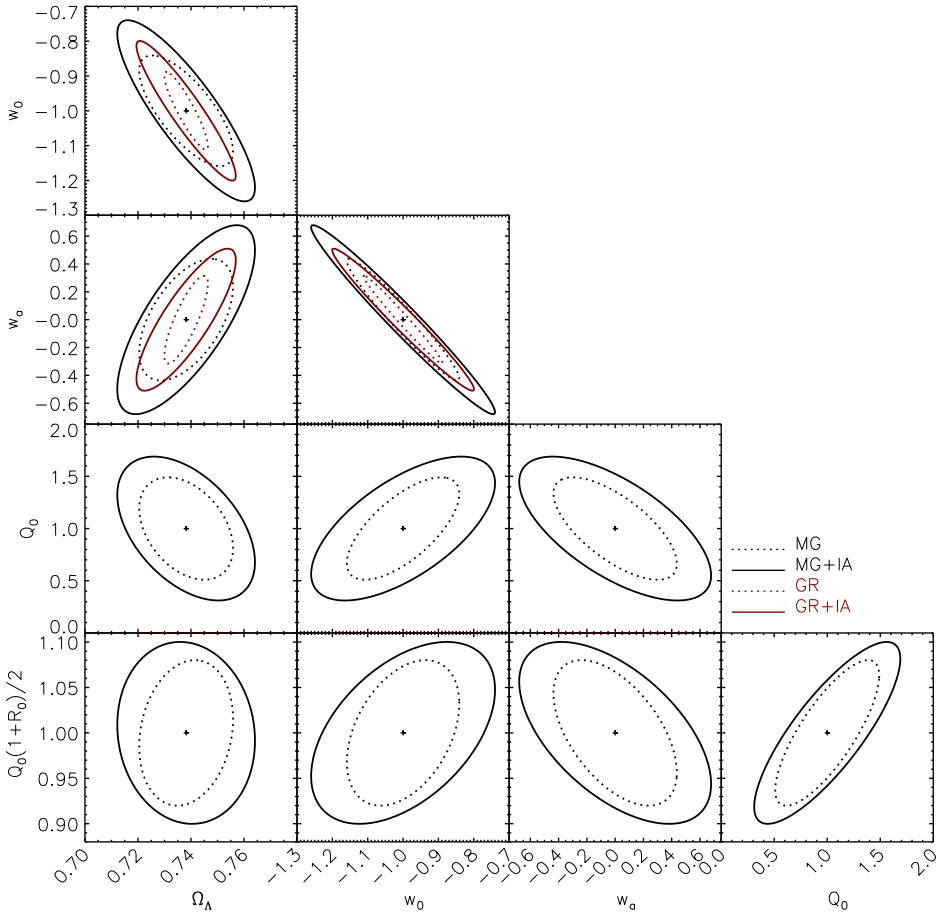

Figure 4.3: A comparison of dark energy constraints in the 2D marginalized parameter planes when intrinsic alignments are included using the LA model [full lines], in comparison to when it is assumed that IA's are perfectly understood and can be extracted to reveal the underlying cosmological shear and galaxy position correlations [dotted lines]. 95% confidence level constraints are shown when both GR is assumed [red] and when large scale modifications to gravity "MG" are allowed [black]. These results combine Planck-like CMB data with a Stage IV survey's galaxy position and shear auto and cross correlations.

Survey	Scenario	$\sigma(\Omega_\Lambda)$	$\sigma(w_0)$	$\sigma(w_a)$	$\sigma(w_p)$	FoM_{EoS}	$\sigma(Q_0)$	$\sigma\left(\frac{Q_0(1+R_0)}{2}\right)$	FoM_{MG}	FoM_{comb}	$\lvert r_{corr}\rvert$
Assuming GR											
Stage III	no IA	0.014	0.169	0.451	0.029	76.1					
	LA	0.025	0.272	0.677	0.042	35.2					
	NLA	0.027	0.294	0.728	0.043	32.3					
Stage IV	no IA	0.003	0.045	0.127	0.008	1041.1					
	LA	0.008	0.081	0.207	0.017	287.3					
	NLA	0.008	0.086	0.217	0.017	268.7					
Allowing an alternate modified gravity model											
Stage III	no IA	0.019	0.226	0.605	0.034	48.8	0.666	0.091	40.1	54.9	0.59
	LA	0.030	0.363	0.923	0.043	25.3	0.894	0.118	25.0	29.6	0.53
	NLA	0.032	0.383	0.971	0.043	23.8	0.897	0.118	23.7	27.7	0.51
Stage IV	no IA	0.007	0.064	0.176	0.017	334.5	0.198	0.032	253.6	469.8	0.79
	LA	0.010	0.105	0.274	0.022	166.1	0.280	0.041	151.6	202.1	0.62
	NLA	0.011	0.106	0.276	0.022	164.0	0.292	0.041	143.7	190.8	0.60
Stage IV	no IA	0.008	0.072	0.204	0.024	200.5	0.226	0.039	196.3	327.9	0.78
	LA	0.012	0.111	0.295	0.031	109.9	0.290	0.045	129.8	162.7	0.64
+sys. offsets	NLA	0.012	0.112	0.296	0.031	108.4	0.301	0.046	123.8	153.9	0.61

Table 4.3: Comparison of figures of merit and marginalized 1-σ errors for dark energy equation of state (EoS) parameters $\{w_0, w_a\}$ and modified gravity (MG) parameters $\{Q_0, Q_0(1+R_0)/2\}$. A combined figure of merit including covariances between all 4 parameters, $FoM(comb)$, and a correlation coefficient, r_{corr}, between the EoS and MG parameters are also included. The table shows prospective constraints from galaxy position and weak lensing auto- and cross-correlations from Stage III and Stage IV surveys in combination with temperature and polarization data from a Planck-like CMB survey. We assume a conservative model for galaxy and IA bias parameters, with $N_k = N_z = 5$. The results with "+sys. offsets" include marginalization over weak lensing calibration and photometric redshift offset parameters meant to reflect possible instrumental systematic errors.

Both relaxing the assumption that gravity is described by GR on cosmic scales and adding in systematic uncertainties increase the degrees of freedom fit by the prospective data and hence can degrade the quality of the cosmological information obtained. In figure 4.3 we show these dual effects on the 2D marginalized constraints for the dark energy parameters. The constraints shown are for all data combined: CMB, galaxy position, lensing shear and cross-correlations, with the conservative bias marginalization model using an $N_k = N_z = 5$ grid. Either including IAs, or allowing a modification to gravity, separately has a roughly comparable effect on reducing the constraining power on w_0 and w_a, with IAs having a slightly larger impact. The inclusion of intrinsic alignments, while not significantly changing the degeneracy direction, does noticeably weaken the modified gravity parameter constraints.

We quantify the constraining power of the surveys using the covariance matrix for the parameters , $C_{ij} = F_{ij}^{-1}$. The diagonal elements of the covariance matrix give the 1-σ measurement uncertainty in each parameter, $\sigma_i = \sqrt{C_{ii}}$. A 2×2 submatrix of a pair of parameters, $\tilde{C}(p_i, p_j)$, then gives the figure of merit (FoM) that includes the covariances between the parameters,

$$FoM(p_i, p_j) \equiv det[\tilde{C}(p_i, p_j)]^{-1/2}. \tag{4.50}$$

With this definition $FoM = 1/\sigma_{eff}^2$, where σ_{eff} is the geometric mean of the principal axes of the 2-dimensional error ellipsoid. Note this differs by a factor of $1/6.17\pi$, from another commonly quoted FoM, the area of the 95% confidence ellipsoid in the 2D marginalized space. Using a FoM that varies as the determinant of the covariance matrix was first presented in [280], along with ones based on the area or volume of the error ellipses in two or multidimensional parameter spaces, and has been widely adopted throughout the literature. We consider the Dark Energy Task Force figure of merit on the equation of state (EoS) parameter,

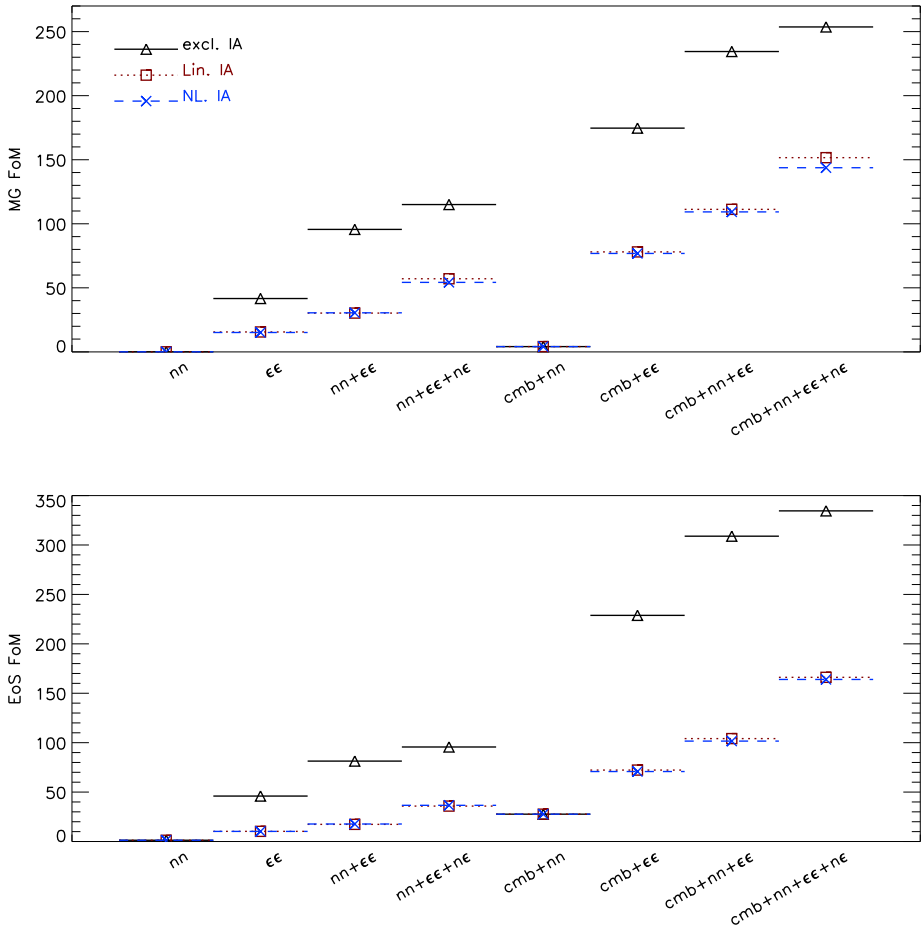

Figure 4.4: How figures of merit (FoM) are affected by intrinsic alignments and the choice of data sets utilized in the analysis for equations of state parameters (w_0 vs w_a) and modified gravity parameters (Q_0 vs. $Q_0(1+R_0)/2$). We compare analyses in which IAs are ignored [black full, triangle], where they are included using the linear alignment model [red dotted lines, square] and the non-linear alignment model [blue dashed, cross]. Datasets include a Planck-like CMB survey, denoted 'cmb', and Stage IV galaxy position-position 'nn', shear-shear '$\epsilon\epsilon$' and shear-galaxy position cross-correlations '$n\epsilon$'. Results are shown for a 5 by 5 grid bias model and no priors.

$FoM(w_0, w_a)$ both in the absence of modifications to gravity, and also when the modified gravity parameters are included and marginalized over. We quantify constraints on the modified gravity parameters by considering an equivalent 2×2 FoM, $FoM(Q_0, Q_0(1 + R_0)/2)$.

An alternative way to measure dark energy constraints is to consider the combined constraints from equation of state parameter and modified gravity together, through considering the FoM from a 4×4 covariance submatrix,

$$FoM(comb) \equiv det[\tilde{C}(w_0, w_a, Q_0, Q_0(1 + R_0)/2)]^{-1/4}. \tag{4.51}$$

[281] applied an analogous statistic to compare constraints on a multi-parameter, model-independent dark energy figure of merit. This FoM accounts for all covariances between the equation of state and modified gravity parameters, but at the same time entangles the EoS and MG constraints, with their different dependencies on measurements of the expansion history and growth of structure. With this definition, for n parameters, our FoM gives a measure of $1/{\sigma_{eff}}^2$, the mean error in the n-dimensional confidence ellipsoid. We note that [281] define a slightly different $FoM = 1/{\sigma_{eff}}^n$, giving a figure of merit that scales with the volume of the n-dimensional space.

For a 2×2 covariance matrix, M, for parameters x and y, one can calculate a correlation coefficient $r_{corr} = \sigma_{xy}/\sigma_x\sigma_y = \sqrt{1 - det(M)/\sigma_x^2\sigma_y^2}$. By dividing the 4×4 covariance matrix for all 4 parameters, $\{w_0, w_a, Q_0, Q_0(1 + R_0)/2\}$, into 2×2 submatrices, we can define an equivalent correlation coefficient between the equation of state parameters and modified gravity parameters,

$$|r_{corr}| \equiv \sqrt{1 - \frac{FoM(w_0, w_a)FoM(Q_0, \frac{Q_0(1+R_0)}{2})}{FoM(comb)^2}}. \tag{4.52}$$

Table 4.3 summarizes the 1-σ, figure of merit (FoM) and correlation coefficient,

r_{corr} results for constraints coming from prospective Stage III and Stage IV surveys. We compare the different IA treatments, and the effect of lensing calibration and photometric redshift offsets.

In the absence of modifications to gravity, IAs still have a significant impact, as was, for example, pointed out in ([263]). If IAs are assumed to be perfectly understood then one can achieve a $\sim$ 14 fold improvement in the dark energy FoM from the Stage IV survey relative to Stage III. However when astrophysical uncertainties about IAs are included, and marginalized over, we find that the relative improvement of the photometric Stage IV survey, is reduced to 9.

When the modification to gravity described in 4.2.1 is included, measurements of the growth of structure no longer purely constrain w_0 and w_a. With IAs excluded, the EoS figure of merit with modified gravity allowed is weakened by 50% relative to GR for a stage III survey, and by 70% for stage IV.

The inclusion of IA uncertainties reduces both the EoS and MG figures of merit by roughly a factor of 2 relative to those when IAs are excluded from the analysis. Both with and without IAs included, the modified gravity FoM for a Stage IV survey is roughly a factor 6 improvement over that for Stage III.

Overall, when both modified gravity and dark energy parameters are considered together, the FoM improves by a factor 8.5 between Stage III and Stage IV in the absence of IAs, and this is reduced to just under 7 with the conservative modeling of IAs. The similarities in the adjustments in DE and MG FoM between Stage III and Stage IV suggest a high degree of correlation between the two parameter pairs. This is quantitatively reinforced by the correlation coefficient r_{corr}; the correlations are higher for Stage IV than for Stage III and are degraded by $\sim$15

and 25%, respectively, with the inclusion of intrinsic alignments.

There is only a small difference between the figures of merit when the linear alignment and nonlinear alignment models are included; with the NLA model giving slightly poorer constraints. The small difference suggests that the differences between the LA and NLA models are to a large extent drowned out by the uncertainties in the IA bias model. Small scale galaxy position correlations, which would be sensitive to differences in LA vs NLA through the gI term, are typically excluded since the multipoles exceed ℓ_{max}.

For the analysis shown in the table alone, we also consider the impact of two additional instrumental systematics: photometric redshift offsets and lensing shear calibration offsets , on the figures of merit. Photometric redshift offsets, Δz_i alter the galaxy distribution inferred from observations as in (4.16). When systematic offsets are considered, we model them following [278]: we allow independent offsets in each photometric redshift bins and impose a prior on these offsets of $\sigma(\Delta z_i) = 0.002$. We model shear calibration offsets by altering the measured shear correlations

$$C_\ell^{\epsilon_i\epsilon_j,offset} = (1+\Delta m_i)(1+\Delta m_j)C_\ell^{\epsilon_i\epsilon_j} \quad (4.53)$$

$$C_\ell^{n_i\epsilon_j,offset} = (1+\Delta m_j)C_\ell^{n_i\epsilon_j} \quad (4.54)$$

and impose a prior of $\sigma(\Delta m_i) = 0.001\sqrt{N_{ph}}$ in each bin. This approach to the shear calibration offsets, and in particular that the errors in each bin contribute as multiplicative errors as above was first shown in [270]. Shear and redshift calibration offsets introduce an additional 10 parameters. Shear calibration offsets are qualitatively degenerate with the inclusion of IA correlations of unknown amplitude in the $\epsilon\epsilon$ correlation, and both cause a reduction in the figures of merit. While the systematic shear offsets in $\epsilon\epsilon$ and $n\epsilon$ are wholly correlated, the IA con-

tributions can differ through the inclusion of the r_I degree of freedom in the GI cross-correlations. As such, the degradation in the constraints from including the instrumental systematic offsets, as we model them here, are not as severe as those from marginalizing over the uncertainties in the IA model.

In figure 4.4, we breakdown the impact of including IAs on the figures of merit derived as one combines CMB plus galaxy, lensing and galaxy lensing cross correlations in a piece-wise fashion. The inclusion of intrinsic alignments significantly deteriorates the expected dark energy constraints coming from weak lensing on its own, while the use of a grid bias model leads to the galaxy-galaxy correlations providing little constraining power on the non-bias parameters in the model. When lensing and galaxy position data are added in tandem, however, they are able to provide improved constraints, over and above the lensing data alone. When IAs are included, the combined constraints are noticeably weaker than the constraints predicted by pure shear-shear measurements when IAs are neglected. The effects are mitigated to a good degree by gaining complementary information about the underlying cosmological potentials, and isolating out the IAs, by adding in galaxy position data. In particular, the inclusion of cross-correlations, between galaxies and lensing, allow the correlated effects of the II and GI IA contributions to reduce the uncertainties in the IA model.

Our findings for constraints on equation of state parameters are consistent with those of [263]; in the absence of CMB data, figures of merit with all galaxy position and weak lensing correlations and IAs included are comparable with those predicted by weak lensing alone in the absence of IAs. We do find, however that when we include CMB data the FoM with IAs never becomes comparable with those when IAs are excluded, even when all cross-correlation information is in-

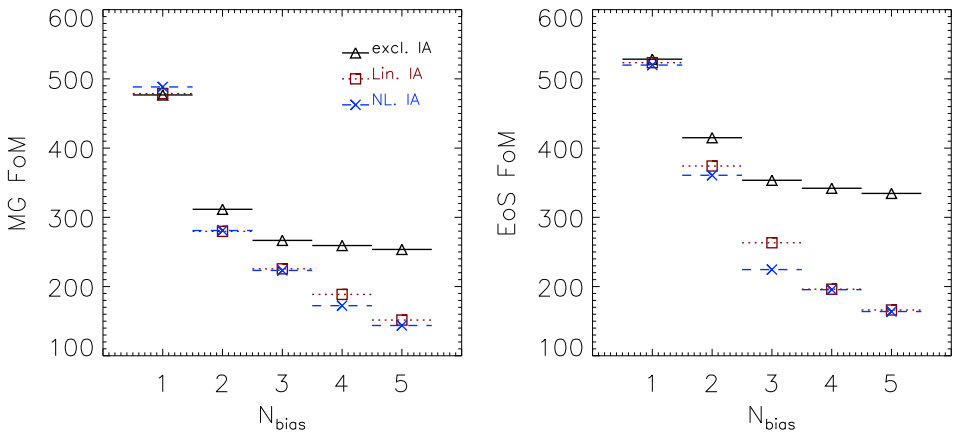

Figure 4.5: The impact of the number of k and z bins, $N_k = N_z = N_{bias}$, in the bias model on the equation of state (EoS) parameter and modified gravity (MG) figures of merit (FoM). Scenarios are shown in which IAs are excluded [black ,triangle], and in which linear alignment (LA) [red, square] and nonlinear alignment (NLA) [blue, cross] models for intrinsic alignments are used. If IAs are excluded one sees a plateauing of the figure of merit as the number of bias marginalization parameters in increased. With the addition of parameters to describe uncertainties in the IA amplitude no such plateauing is seen. The inclusion of IA, with an assumption that they are well understood, and can be described by scale and redshift independent nuisance parameters ($N_{bias} = 1$) actually improves the dark energy constraints because the IAs provide additional cosmological information about the high redshift potential $\phi(z_f)$. If uncertainties in the IA model are allowed however, there is a significant deterioration in the constraints on both FoM. The results presented here are for prospective CMB and Stage IV large scale structure survey utilising all galaxy position and shear auto- and cross- correlations.

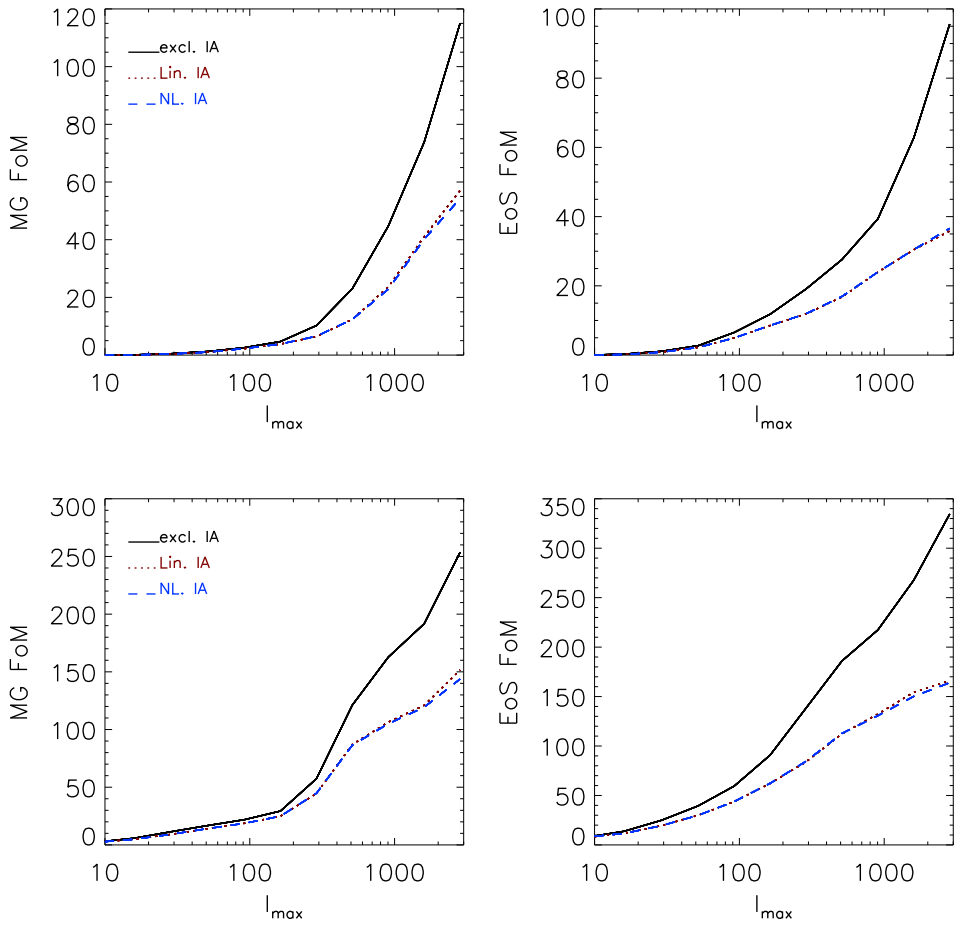

Figure 4.6: The impact of including observations on small scales, denoted by the maximum multipole, l_{max}, up to which correlations are considered, on the equation of state (EoS) parameter and modified gravity (MG) figures of merit (FoM) . Results are shown for a Stage IV photometric survey alone [upper panel] and [lower panel] including complementary constraints from a Planck-like CMB survey when IAs are excluded [black full line] and included using the LA [red,dotted] and NLA [blue,dashed] models. While including smaller-scale observations would appear to improve both figures of merit, one has to consider the theoretical uncertainties present in modeling these small scales, especially in the context of modifications to gravity, therefore it is worthwhile assessing how a conservative approach of neglecting such scales might impact the projected cosmological constraints.

cluded.

In a number of recent analyses of dark energy constraints from prospective surveys, the uncertainties in the galaxy bias model are treated by a single, scale and redshift independent, factor. In figure 4.5 we highlight that this assumption can have a dramatic effect on the predicted constraining power of the survey. Allowing a gridded galaxy bias model, while excluding IA uncertainties, reduces the EoS figure of merit by roughly a third, and MG figure of merit by almost a half.

Including intrinsic alignments in the analysis, while assuming single, scale and redshift independent, amplitude has a marginal impact on the EoS and MG FoMs. In fact, interestingly, assuming that you know how IAs are formed and evolve provides additional information, actually improving the constraints.

One can understand this by noting that the GG, II and GI components all depend on the underlying matter distribution but each exhibit a different evolution with redshift. Assuming a single-parameter normalization, but multiply-binned measurements (from tomography) for the IAs, enables us to obtain an independent measurement of $\psi(z_f)$ from the GG and both IAs. When uncertainties in the IA model are introduced, however, by using the grid bias model, they markedly degrade the dark energy constraints. One doesn't see the plateauing of the FoM that one would see with intrinsic alignments excluded from the analysis.

We rationalize the plateau with no intrinsic alignments as follows: the contributions from shear-shear, shear-position and position-position power spectra have different dependencies on redshift resolution. We expect the constraining power of position-position alone to be weak given the multipole cuts, and to be badly

affected by even a small number of free bias parameters. Therefore we should be dominated by shear-shear and shear-position information which are much more resilient to a lack of redshift information because, when IAs are not included, each is modulated by the broad lensing weight function.

We can combine the information in figures 4.4 and 4.5 to identify how many free parameters can be accommodated before constraints degrade relative to conventional constraints from CMB plus shear-shear correlations alone when IAs are ignored. CMB plus shear-shear data alone give a modified gravity figure of merit of 170 (figure 4.4), which is roughly the same value obtained when including all two-point cross-correlations and including a bias grid with $N_{\rm bias} = 4$ (figure 4.5). For the equation of state parameter figure of merit we can use a bias grid with $N_{\rm bias} = 3$ before we reach the same figure of merit using all two-point functions as we would obtain from the traditional approach. A bias grid with $N_{\rm bias} = 3$ has $3 \times 3 \times 4 = 36$ free parameters in total, 18 for galaxy bias and a further 18 for the intrinsic alignment model. We therefore need astrophysics to be sufficiently kind that the bias functions are sufficiently smooth in both scale and redshift, or to have sufficient information from simulations to be able to parameterize the functions with roughly this number of free parameters.

The inclusion of information in the mildly nonlinear regime can have a potentially significant effect on improving constraints on dark energy parameters, purely as a result of the large number of modes available to include in the analysis. If modifications to gravity are included however then one has to make an assessment of how well large scale structure growth in the non-linear regime is understood. Recent analyses show that in some specific modified gravity theories there can be subtleties in the non-linear behavior that might have to be included

([282, 283, 284, 285, 286, 287, 288, 289]). In figure 4.6 we highlight the sensitivity of the figure of merit to the assumptions about the smallest scales to be included in the analysis, parameterized here by l_{max}.

When CMB data is included, the pressure to go to high multipoles is reduced. There is only a 50% increase in FoM on increasing the maximum multipole from 1000 to 3000, compared to over a factor of two when CMB data is not used.

4.4 Conclusions

Using tests of the expansion history of space-time and the growth of large scale structure, in tandem, gives the best prospects for testing gravity on cosmic scales. Weak lensing, galaxy position, CMB ISW and potential peculiar velocity observations provide very complementary constraints on the gravitational potentials, through measuring both their sum, $\phi + \psi$ and ψ on its own.

Fundamental to realizing the full potential of these complementary observations is a requirement to minimize both instrumental and astrophysical systematic uncertainties that can dilute the cosmological constraining power of upcoming surveys. Weak lensing observations could potentially offer a direct way to measure the gravitational potentials without the bias uncertainty in relating galaxy positions to the underlying CDM matter distribution. On the other hand, intrinsic alignments provide a significant systematic signal. Uncertainties about IA formation, evolution, and variation amongst galaxy-type, have to be factored into a realistic assessment of how well weak lensing shear measurements can constrain a cosmological model.

In this chapter, we have shown that how systematic uncertainties are modeled can have a profound impact on the predicted dark energy and modified gravity constraints from future large scale structure imaging surveys.

By utilizing a grid-based approach to marginalize over uncertainties in both galaxy bias and intrinsic alignment contributions to lensing shear and galaxy position correlations, we have provided conservative and optimistic bounds for constraints on both dark energy equation of state parameters and a useful phenomenological modified gravity model.

We considered three figures of merit to quantitatively compare constraints on the dark energy equation of state and modified gravity parameters both separately and in combination. Quoting separate figures of merit for EoS and MG parameters can be used to show their different dependences on data sets and assumptions. They can also contrast the equation of state parameter dependence on expansion history measurements, and modified gravity parameter dependence on the growth history. We have found, however, that there is a high degree of correlation between these two sets of parameters so that treating them independently ignores an important association. We proposed, and quantified, a combined figure of merit and related correlation coefficient as a way to address this.

We have found that the constraints have a significant sensitivity to how galaxy bias and intrinsic alignments are incorporated into the analysis. The equation of state parameter and modified gravity figures of merit are a factor of 4 smaller when a conservative scale and redshift dependent grid model is used, than when bias and IAs uncertainties are assumed to be redshift and scale independent. Marginalizing over systematic uncertainties in the IA model led to a factor of two reduction in the figures of merit.

Whether a linear alignment or nonlinear alignment model underpinned the IA model had only a small effect in comparison to our assumptions about the evolution of bias and IAs in redshift and scale. Understanding the astrophysical evolution and population dependence of intrinsic alignments, therefore, could dramatically improve the cosmological information that comes out of future photometric large scale structure surveys, such as DES, HSC, Euclid, LSST and WFIRST. The implications of weak lensing systematics for optimizing cosmic shear surveys to measure dark energy are discussed in a related work([219]).

In addition to uncertainties in bias and IAs, an understanding of evolution in the nonlinear regime could also have a profound impact on constraints, through increasing the maximum multipole to which analyses can proceed. If GR governs cosmic evolution this may be achievable, while the model dependence of the non-linear regime in modified gravity models could make this far more challenging.

Combining information from the photometric surveys we have considered here with that from spectroscopic galaxy data, such as might come from BigBOSS, EUCLID and WFIRST, might allow closely situated galaxies to be isolated, and their intrinsic alignments to be studied. We will consider in future work how this could provide an important avenue to improve our understanding of intrinsic alignments and in turn maximize the cosmological constraining power of future wide and deep photometric surveys.

We finally note that, as part of this work, we have provided a fitting function to allow other researchers to generate weak lensing and galaxy position correlations for modified gravity theories of the form we consider here.

CHAPTER 5

CONCLUSIONS

This work has explored how cosmologists study the dark sector, from modeling dark components, to generating simulated observables, to comparing them against real observables to constrain theories, and finally to predict future constraints and guide survey design. A framework in which to broadly test for deviations from general relativity and with which to constrain families of modified gravity theories is adopted and explained, and a key systematic in weak lensing is explored. These last sections review these findings and end with a discussion of possible ways to improve upon these works and the next steps to take.

In chapter 2 the common approach of using non-linear analytical fits developed for ΛCDM to predict non-linear growth in modified theories was tested. It was shown that in fact these fits are applicable, at least up to the mildly nonlinear scales for modifications of the peculiar acceleration equation and Poisson equation. This suggests the similarity conjecture for mapping linear to non-linear power (the empirical result on which the fits are based) holds also in cases with scale and time dependent modifications of gravity.

Chapter 3 investigated whether a dark matter self-interaction could be used to explain the ACBAR CMB excess power. Motivated also in part by explaining the general class of problems with dark matter leading to excess structure on small scales (missing satellites and cuspiness problems), a Yukawa type coupling between dark matter particles was considered. Despite allowing the coupling to vary, no improved fit was found to the data over ΛCDM. Though an interaction was not ruled out, it was not favored. The work was an excerpt of a more general exploration of possible dark sector interactions [206].

Finally chapter 4 returned to modified gravity theories as dark energy candidates and examined how upcoming surveys might be able to constrain them in light of the large astrophysical systematic of intrinsic alignments. Constraints were found for Planck like CMB data combined with a Stage III or Stage IV survey with and without IA, modeling IA both as linear and nonlinear. Other survey forecasts which neglect to include this astrophysical systematic are reproduced and compared to our IA cases. For the GR case, IA reduce figures of merit by a factor of 2 for a stage 3 survey and factor of roughly 4 for a stage IV survey. When MG is included, the factor is again around 2 for Stage III and also around 2 for stage IV. It is worth noting that the seemingly lesser reduction in figure of merit is due to a dramatic reduction in starting point when considering MG compared to IA (the no IA Stage IV GR FoM is 1041, while the no IA stage IV MG FoM is only 334.5). Thus, neglecting IA result in quite an overly optimistic characterization of the survey, even when using all data sets considered. In fact, it is found that because a sound IA model is lacking and its parameters are somewhat degenerate with those of the MG model, constraints are reduced to the level that essentially a full suite of complimentary observables are required to achieve the same level of constraining power when IAs are modeled as quoted in forecasts that neglected a direct treatment of IAs. The modeling of bias in the IA scheme was shown to be the most important, though changing between a linear and a nonlinear model also had some impact. Ultimately, for weak lensing surveys to truly improve constraining power, a motivated, or understood, or at the very least constrained model of IAs will be required.

5.1 Future Directions

Despite the work contained herein spanning the last 5 years, it remains an accurate depiction of the current state of our understanding of the dark sector, modified gravity theories and IAs. Thus, much of the suggestions presented in each chapter remain relevant, however there are a few new developments and quite a few other things to highlight in light of the combined studies.

5.1.1 Non-linearities and MG Theories

Additional work regarding the applicability of the nonlinear fitting formulae has discovered problems when truly pressing to smaller scales (beyond the mildly non-linear regime) and finds that the formulae fail to capture full non linear effects and chameleon effects (e.g. [283]). Thus, it would be interesting to develop formulae for capturing such effects utilizing only few parameters. To that end it becomes important to also discuss modified gravity theories and their add-ons, like the chameleon effect, in terms of a generalized model.

5.1.2 Intrinsic Alignments

IA play a large part in the signal we measure for weak lensing observations, and the linear alignment model does serve as suitable starting point, however many complexities are known and only included in the bias terms, which results in many nuisance parameters that greatly reduce constraining power of observations, whether considered separately or jointly. The effect becomes even more severe when MG parameters, degenerate with IA parameters, enter the mix. Thus, an improved

understanding and modeling of IAs is needed whether physically motivated and analytical, or simply determined as a fit to simulations or observations. This task is crucial, and indeed could in time lead to IAs becoming a new cosmological probe rather than a systematic.

There are many paths available to accomplishing this goal. Simulations can track the evolution of galaxies, and test to what degree alignments freeze in, and to what degree the alignments are altered and perhaps can at least provide a fitting function for this aspect of IAs.

Observationally already much is known, for instance red galaxies are the ones that show strong alignments, while blue galaxies do not, further the strength of the alignments seems tied to the magnitudes of the galaxies (e.g. [241]). So already modeling of IAs can be improved by considering these facts. Further observations are now available to better test IAs. Using for instance WiggleZ spectroscopic data and redshifts and RCS2 imaging and WL data, it becomes possible to probe IAs as together these surveys provide good deep data imaging and spectroscopic data on the same fields. From this data the possibility exists to obtain the observed weak lensing signal, identify the lenses and lensing geometry using the spectroscopic data to identify clusters, further supported by use of the red sequence method RCS2 employs, and thus recreate the true weak lensing.

In addition this same data set will, by providing both galaxy position and cosmic shear data on overlapping fields, give a powerful probe of the mass to light bias (b_g) mentioned in chapter 4.

It is of interest also to consider the implications IA considerations have on survey design. This work has been carried out by the same collaboration as carried

out the work of chapter 4. In [219], it was found that surveys with finite time should go deep rather than wide when IAs are included, as IAs strongly contaminate low redshift data. Further, it is shown that IA analysis demands more accurate redshift determination, in order to recapture same constraints as forecast which does not consider IA. It would be interesting to consider what effects a corrected IA signal (accounting for the color and luminosity dependence of IA, or based on a model or fit) would have on these conclusions, and other design characteristics.

5.1.3 Other Observables

Redshift space distortions as a probe of velocity information provide a new window on LSS, enabling a probe of cluster dynamics and assembly of structure, beyond the mere snapshot afforded by noting galaxy positions or galaxy counts, or even galaxy shear. Utilization of this information, as given by WiggleZ or by other velocity surveys such as BOSS, will further constraining power, though by what degree remains to be seen. Theoretically this should provide insight on both potentials in a distinct way to that of weak lensing measurements, as the velocity probes how matter is in fact moving in response to the potential it creates.

In some sense, these distortions were a contaminant to obtaining galaxy counts (distorting their redshift location, thus distorting perceived distributions) but have become an observable. In the same way, once an understanding of how IAs really occur is established it too will become a probe in its own right.

Further one could hope there will be new distance measures opening up new scales on the distance ladder or providing complimentary measures. One prospect is gravitational wave observations which might serve as standard candles (e.g.

[290]).

5.1.4 Outlook

Data is pouring in and rapidly improving, simulations are becoming more sophisticated and combined with precision measurements are demanding a lot of theorists to create viable models that can match the new data on LSS. This is an exciting time as observational windows continue to open, offering new insights and tests with which to differentiate between the many theories that till recently had in some sense outpaced observations. Now the shoe is on the other foot, and observations are demanding a full understanding of the theory behind what it is we are observing in terms of IAs or modeling in terms of now requiring matches not only to background expansion but also to LSS, in terms of power today, but also in terms of velocity, and many other subtleties. It is an exciting time and in deed the golden age of cosmology.

APPENDIX A

FITTING FUNCTION USED IN CHAPTER 4

A.1 Fitting Function Form

Some modified gravity (MG) models, such as $f(R)$ theories, can be tailored to reproduce a selected expansion history. However their predictions for the growth of structure can then differ from that predicted by that expansion history assuming GR. Here we consider a fitting function for a modified gravity model in which the expansion history is described by ΛCDM, but the growth history is modified through a deviation from GR described by two parameters, Q_0 and R_0, and a third parameter s which encapsulates the time dependence of the deviation:

$$\begin{aligned} Q(a) &= 1 + (Q_0 - 1)a^s \\ R(a) &= 1 + (R_0 - 1)a^s. \end{aligned} \tag{A.1}$$

In the main analysis in this thesis we have assumed $s = 3$.

The key input into calculating the galaxy position and weak lensing shear observables is the matter power spectrum as a function of scale, k, and redshift, z. Here we obtain a analytical fit for the ratio of the matter power spectrum in the modified gravity model in (A.1), to that predicted by ΛCDM for the same cosmological parameters:

$$r_{fit}(Q_0, R_0, s) = \frac{P(k)_{lin,MG}}{P(k)_{lin,\Lambda CDM}}. \tag{A.2}$$

To motivate the form of the fit, we note that the behavior of growth in this model is described in [176] has two distinct regimes as given in (4.7) and (4.8). On

small scales the growth purely depends on the product $Q_0 R_0$, via (4.7). On large scales, the behavior involves various derivatives of the modified gravity parameters, and the equations depend uniquely on Q_0 and R_0. Our fit distinguishes between these two regimes in scale, and fits the evolution with redshift of the high wave number ('H') and low wave number ('L') regime separately. The two regimes are joined via a third function, $x(k)$, assuming a transition scale, k_c.

$$
\begin{aligned}
r_{fit}(k,z) &= [1-x(k)]\, r_L(z) + x(k) r_H(z) && \text{(A.3)}\\
r_L(z) &\equiv 1 + \left[L_1\,(1-R_0) + L_2\left(e^{L_3} - e^{L_3 Q_0}\right)\right] \\
&\quad \times \left(e^{L_4 z} + L_5\right) && \text{(A.4)}\\
r_H(z) &\equiv 1 + H_1(1-Q_0 R_0)\left(e^{H_2 z} + H_3\right) && \text{(A.5)}\\
x(k) &\equiv \tanh\left[\left(\frac{k}{k_c}\right)^p\right] && \text{(A.6)}
\end{aligned}
$$

The values for the 10 fitting parameters $\{L_1, L_2, L_3, L_4, L_5, H_1, H_2, H_3, k_c, p\}$, are obtained using OriginLab's Origin software to fit our custom function to the power spectra coming from the CAMB code. While $s = 1$ and $s = 3$ have been most commonly used choice in the literature, we obtain the fit for $s = 1 - 4$, using a grid of values in Q_0 and R_0 between 0.9 and 1.1. The spectra were calculated at 50 redshift steps in $0 \leq z \leq 3$ and for over a hundred values in k ranging from 7×10^{-6} to $40 Mpc^{-1}$. For $s = 3$, 23 different $\{Q_0$,$R_0\}$ pairs were used to obtain the fit, for $s = 1$ and $s = 2$ a subset of these was used, and found to be sufficient to achieve sub percent accuracy in the C_ℓs.

Table A.1 provides the values for the fits parameters for each value of s.

Fit Parameter	$s = 1$	$s = 2$	$s = 3$	$s = 4$
L_1	0.5293	0.4947	0.4268	0.3635
L_2	-4.733	-5.692	-6.300	-6.575
L_3	-1.610	-1.660	-1.764	-1.817
L_4	-0.8678	-1.610	-2.409	-3.263
L_5	0.2878	0.0867	0.0336	0.0156
H_1	-0.5655	-0.2023	-0.0984	-0.0557
H_2	-0.6144	-1.263	-1.935	-2.718
H_3	0.1803	0.0754	0.0317	0.0153
$k_c[Mpc^{-1}]$	1×10^{-3}	7×10^{-4}	6×10^{-4}	5×10^{-4}
p	0.9422	1.048	1.076	1.090

Table A.1: Summary of values for the 10 parameters used in the fitting function, given for each value of s, the power law exponent in the modified gravity function (A.1).

A.2 Performance

The fit given above reproduces the ratios of the matter power spectrum in (A.2), derived from CAMB, to better than 0.01% for $k > 10k_c$, within 0.6% around the transition scale, k_c, and within 0.8% at scales around the horizon scale today. This is sufficient to reproduce the C_ℓs in the modified gravity scenario to within sub percent ($\sim$0.1%) levels. The error is largest for low ℓs and increases as s decreases.

Figure A.1 shows the ratio of the matter power spectrum today for the modified gravity model to that for the fiducial ΛCDM model for both the fit and the full integration using CAMB. At $z = 0$, where the modifications are largest, as a function of k, the fit matches the simulations to within 0.8 % and remains accurate at this level for all z for 5% changes in Q_0 and R_0.

When calculating the angular correlation function, C_ℓ, the power spectrum fit is integrated over k, z. Applying the fit factor to a standard power spectrum, and using this fit power spectrum to compute C_ℓs for galaxy autocorrelations, galaxy-

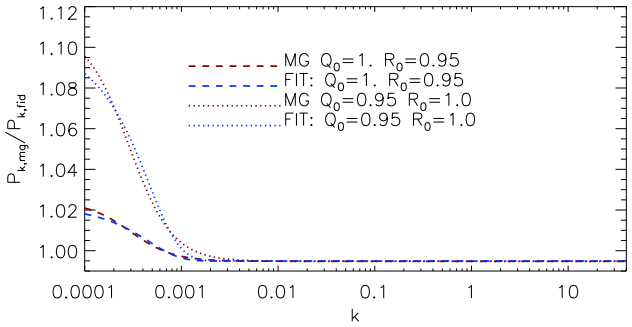

Figure A.1: Ratios of $z = 0$ matter power spectra in modified gravity model to the fiducial ΛCDM model obtained via simulation [red] compared with the ratios obtained using the fitting function [blue]. Two models shown are $Q_0 = 1, R_0 = 0.95$ [dashed lines] and $Q_0 = 0.95, R_0 = 1$ [dotted lines]. At small scales the two models are degenerate, since the evolution of the matter perturbations is only dependent on the product QR, while at large scales their behaviors are distinct. The fitting function provides agreement to within 0.01% for most scales. At the transition scale $k \sim k_c$ and on horizon scales the fit is a litter poorer, $\sim 0.8\%$, however this limited range of scales contributes only a small amount to the angular correlations C_ℓ used in the analysis.

weak lensing cross-correlations, and weak lensing auto-correlations results in sub percent(0.1%) level accuracy, as shown in figure A.2.

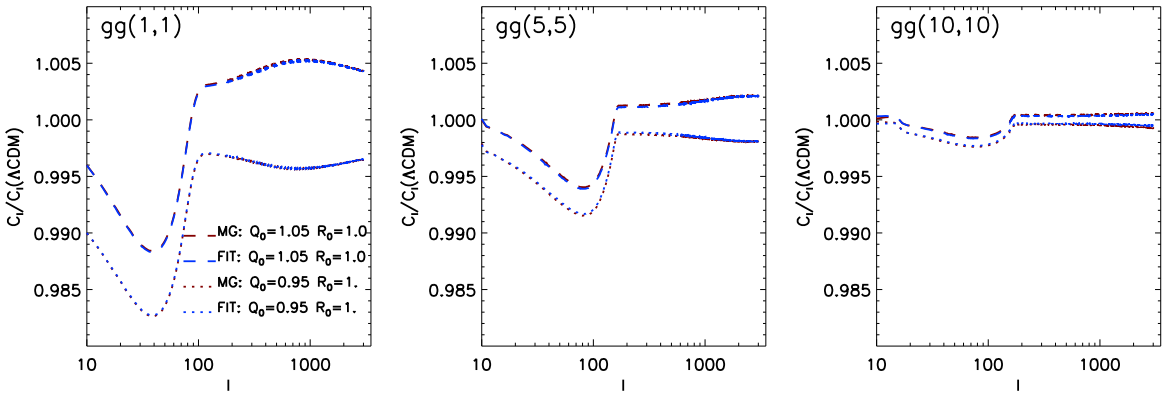

Figure A.2: A comparison of the ratios of the C_ℓs in the modified gravity model to the fiducial ones obtained via simulation [red] compared to the ratios obtained using the fitting function [blue]. Two models are shown Dashed lines are $Q_0 = 1.05, R_0 = 1.00$ [dashed lines] and for $Q_0 = 0.95, R_0 = 1$ [dotted lines] . Subpanels left to right indicate correlations in low to high tomographic redshift bins, $1-1$, $5-5$, and $10-10$ respectively. The agreement between fit and simulated C_ℓs is at the level of $\sim 0.1\%$.

BIBLIOGRAPHY

[1] H. F. Stabenau and B. Jain. N-body simulations of alternate gravity models. *Phys. Rev.*, D74:084007, 2006.

[2] Chung-Pei Ma and Edmund Bertschinger. Cosmological perturbation theory in the synchronous and conformal newtonian gauges. *Astrophys. J.*, 455:7–25, 1995.

[3] Hideo Kodama and Misao Sasaki. Cosmological perturbation theory. *Prog. Theor. Phys. Suppl.*, 78:1–166, 1984.

[4] Shaun Cole et al. The 2df galaxy redshift survey: Power-spectrum analysis of the final dataset and cosmological implications. *Mon. Not. Roy. Astron. Soc.*, 362:505–534, 2005.

[5] M. Tegmark et al. Cosmological constraints from the sdss luminous red galaxies. *Phys. Rev.*, D74:123507, 2006.

[6] Will J. Percival et al. The shape of the SDSS DR5 galaxy power spectrum. *Astrophys. J.*, 657:645–663, 2007.

[7] J. A. Peacock and S. J. Dodds. Nonlinear evolution of cosmological power spectra. *Mon. Not. Roy. Astron. Soc*, 280:L19, 1996.

[8] R.E. Smith et al. Stable clustering, the halo model and nonlinear cosmological power spectra. *Mon. Not. Roy. Astron. Soc*, 341:1311, 2003.

[9] Chung-Pei Ma, R. R. Caldwell, Paul Bode, and Li-Min Wang. The mass power spectrum in quintessence cosmological models. *Astrophys. J.*, 521:L1–L4, 1999.

[10] Patrick McDonald, Hy Trac, and Carlo Contaldi. Dependence of the nonlinear mass power spectrum on the equation of state of dark energy. *Mon. Not. Roy. Astron. Soc.*, 366:547–556, 2006.

[11] Eric V. Linder and Martin J. White. Going nonlinear with dark energy cosmologies. *Phys. Rev.*, D72:061304(R), 2005.

[12] Akihito Shirata, Yasushi Suto, Chiaki Hikage, Tetsuya Shiromizu, and Naoki Yoshida. Galaxy clustering constraints on deviations from newtonian gravity at cosmological scales ii: Perturbative and numerical analyses of power spectrum and bispectrum. *Phys. Rev.*, D76:044026, 2007.

[13] Akihito Shirata, Tetsuya Shiromizu, Naoki Yoshida, and Yasushi Suto. Constraining deviations from newton's law of gravity on cosmological scales: Confrontation to power spectrum of sdss galaxies. *Phys. Rev.*, D71:064030, 2005.

[14] Luca Amendola, Martin Kunz, and Domenico Sapone. Measuring the dark side (with weak lensing). 2007.

[15] Wayne Hu and Ignacy Sawicki. A parameterized post-friedmann framework for modified gravity. 2007.

[16] Masahiro Takada and Bhuvnesh Jain. Cosmological parameters from lensing power spectrum and bispectrum tomography. *Mon. Not. Roy. Astron. Soc.*, 348:897, 2004.

[17] Bhuvnesh Jain and Andy Taylor. Cross-correlation tomography: Measuring dark energy evolution with weak lensing. *Phys. Rev. Lett.*, 91:141302, 2003.

[18] Gary M. Bernstein and B. Jain. Dark energy constraints from weak lensing cross-correlation cosmography. *Astrophys. J.*, 600:17–25, 2004.

[19] Rachel Bean, David Bernat, Levon Pogosian, Alessandra Silvestri, and Mark Trodden. Dynamics of linear perturbations in f(r) gravity. *Phys. Rev.*, D75:064020, 2007.

[20] P. Zhang et al. A discriminating probe of gravity at cosmological scales. 2007.

[21] A. Albrecht, G. Bernstein, R. Cahn, W. L. Freedman, J. Hewitt, W. Hu, J. Huth, M. Kamionkowski, E. W. Kolb, L. Knox, J. C. Mather, S. Staggs, and N. B. Suntzeff. Report of the Dark Energy Task Force. *ArXiv Astrophysics e-prints*, September 2006.

[22] John A. Peacock et al. Report by the esa-eso working group on fundamental cosmology. 2006.

[23] Nick Kaiser, Gillian Wilson, and Gerard A. Luppino. Large-scale cosmic shear measurements. 2000.

[24] David M. Wittman, J. Anthony Tyson, David Kirkman, Ian Dell'Antonio, and Gary Bernstein. Detection of weak gravitational lensing distortions of distant galaxies by cosmic dark matter at large scales. *Nature*, 405:143–149, 2000.

[25] Ludovic van Waerbeke et al. Detection of correlated galaxy ellipticities on cfht data: first evidence for gravitational lensing by large-scale structures. *Astron. Astrophys.*, 358:30–44, 2000.

[26] David Bacon, Alexandre Refregier, and Richard Ellis. Detection of cosmic shear with the william herschel telescope. 2000.

[27] T. Schrabback et al. Evidence for the accelerated expansion of the Universe

from weak lensing tomography with COSMOS. *ArXiv e-prints*, November 2009.

[28] R. Massey et al. COSMOS: Three-dimensional Weak Lensing and the Growth of Structure. *ApJS*, 172:239–253, September 2007.

[29] L. Fu et al. Very weak lensing in the CFHTLS wide: cosmology from cosmic shear in the linear regime. *Astronomy and Astrophysics*, 479:9–25, February 2008.

[30] J. Benjamin, C. Heymans, E. Semboloni, L. Van Waerbeke, H. Hoekstra, T. Erben, M. D. Gladders, M. Hetterscheidt, Y. Mellier, and H. K. C. Yee. Cosmological constraints from the 100-deg^2 weak-lensing survey. *Monthly Notices of the Royal Astronomical Society*, 381:702–712, October 2007.

[31] H. Hoekstra, H. K. C. Yee, M. D. Gladders, L. F. Barrientos, P. B. Hall, and L. Infante. A Measurement of Weak Lensing by Large-Scale Structure in Red-Sequence Cluster Survey Fields. *Astrophysical Journal*, 572:55–65, June 2002.

[32] M. Hetterscheidt, P. Simon, M. Schirmer, H. Hildebrandt, T. Schrabback, T. Erben, and P. Schneider. GaBoDS: The Garching-Bonn deep survey. VII. Cosmic shear analysis. *Astronomy and Astrophysics*, 468:859–876, June 2007.

[33] O. Le Fèvre, Y. Mellier, H. J. McCracken, S. Foucaud, S. Gwyn, M. Radovich, M. Dantel-Fort, E. Bertin, C. Moreau, J.-C. Cuillandre, M. Pierre, V. Le Brun, A. Mazure, and L. Tresse. The VIRMOS deep imaging survey. I. Overview, survey strategy, and CFH12K observations. *Astronomy and Astrophysics*, 417:839–846, April 2004.

[34] D. Larson, J. Dunkley, G. Hinshaw, E. Komatsu, M.R. Nolta, et al. Seven-Year Wilkinson Microwave Anisotropy Probe (WMAP) Observations: Power Spectra and WMAP-Derived Parameters. *Astrophys.J.Suppl.*, 192:16, 2011.

[35] S. M. Carroll. The cosmological constant. *Living Rev. Rel.*, 4:1, 2001.

[36] A. Refregier et al. Dune: The dark universe explorer. 2006.

[37] J. Albert et al. Probing dark energy via weak gravitational lensing with the supernova acceleration probe (snap). 2005.

[38] J. Anthony Tyson. Precision studies of dark energy with lsst. *AIP Conf. Proc.*, 870:44–52, 2006.

[39] Massimo Persic and Paolo Salucci. Rotation curves of 967 spiral galaxies. *Astrophys.J.Suppl.*, 1995.

[40] Massimo Persic, Paolo Salucci, and Fulvio Stel. Rotation curves of 967 spiral galaxies: Implications for dark matter. 1995.

[41] D. Fabricant and P. Gorenstein. Further evidence for M87's massive, dark halo. *Astrophysical Journal*, 267:535–546, April 1983.

[42] G. Golse, J.P. Kneib, and G. Soucail. Constraints on (omega_m0, omega_lambda) from strong lensing in ac 114. 2002.

[43] R.D. Blandford and R. Narayan. Cosmological applications of gravitational lensing. *Ann.Rev.Astron.Astrophys.*, 30:311–358, 1992.

[44] Yannick Mellier. Probing the universe with weak lensing. *Ann.Rev.Astron.Astrophys.*, 37:127–189, 1999.

[45] Douglas Clowe, S.W. Randall, and M. Markevitch. Catching a bullet: Direct evidence for the existence of dark matter. *Nucl.Phys.Proc.Suppl.*, 173:28–31, 2007.

[46] M.J. Jee, A. Mahdavi, H. Hoekstra, A. Babul, J.J. Dalcanton, et al. A Study of the Dark Core in A520 with Hubble Space Telescope: The Mystery Deepens. *Astrophys.J.*, 747:96, 2012.

[47] Benjamin D. Wandelt et al. Self-interacting dark matter. 2000.

[48] Lars Bergstrom. Non-baryonic dark matter: Observational evidence and detection methods. *Rept. Prog. Phys.*, 63:793, 2000.

[49] B. Moore et al. Dark matter substructure within galactic halos. *Astrophys. J.*, 524:L19–L22, 1999.

[50] Anatoly A. Klypin, Andrey V. Kravtsov, Octavio Valenzuela, and Francisco Prada. Where are the missing galactic satellites? *Astrophys. J.*, 522:82–92, 1999.

[51] H. J. Mo and Shude Mao. Tully-Fisher Relation and its Implications for Halo Density Profile and Self-interacting Dark Matter. *Mon. Not. Roy. Astron. Soc.*, 318:163, 2000.

[52] Romeel Dave, David N. Spergel, Paul J. Steinhardt, and Benjamin D. Wandelt. Halo Properties in Cosmological Simulations of Self- Interacting Cold Dark Matter. *Astrophys. J.*, 547:574–589, 2001.

[53] Gianfranco Bertone, Dan Hooper, and Joseph Silk. Particle dark matter: Evidence, candidates and constraints. *Phys.Rept.*, 405:279–390, 2005.

[54] Christian Weinheimer. The Neutrino mass direct measurements. pages 335–344, 2003.

[55] L.J. Rosenberg and K.A. van Bibber. Searches for invisible axions. *Phys.Rept.*, 325:1–39, 2000.

[56] Benoit Famaey and Stacy McGaugh. Modified Newtonian Dynamics: A Review. 2011.

[57] J. A. Casas, J. Garcia-Bellido, and M. Quiros. Scalar - tensor theories of gravity with phi dependent masses. *Class. Quant. Grav.*, 9:1371–1384, 1992.

[58] Damien J. Holden and David Wands. Self-similar cosmological solutions with a non-minimally coupled scalar field. *Phys. Rev.*, D61:043506, 2000.

[59] Sean M. Carroll. Quintessence and the rest of the world. *Phys. Rev. Lett.*, 81:3067–3070, 1998.

[60] T. Damour, G. W. Gibbons, and C. Gundlach. DARK MATTER, TIME VARYING G, AND A DILATON FIELD. *Phys. Rev. Lett.*, 64:123–126, 1990.

[61] Steven S. Gubser and P. J. E. Peebles. Cosmology with a dynamically screened scalar interaction in the dark sector. *Phys. Rev.*, D70:123511, 2004.

[62] Glennys R. Farrar and P. James E. Peebles. Interacting dark matter and dark energy. *Astrophys. J.*, 604:1–11, 2004.

[63] Saul Barshay and Georg Kreyerhoff. Long-range interactions between dark-matter particles in a model with a cosmological, spontaneously-broken chiral symmetry. *Mod. Phys. Lett.*, A20:1155–1160, 2005.

[64] Orfeu Bertolami, Francisco Gil Pedro, and Morgan Le Delliou. Dark Energy-Dark Matter Interaction from the Abell Cluster A586. 2008.

[65] Morgan Le Delliou, Orfeu Bertolami, and Francisco Gil Pedro. Dark Energy-Dark Matter Interaction from the Abell Cluster A586 and violation of the Equivalence Principle. *AIP Conf. Proc.*, 957:421–424, 2007.

[66] Sean M. Carroll, Sonny Mantry, Michael J. Ramsey-Musolf, and Christopher W. Stubbs. Dark-Matter-Induced Weak Equivalence Principle Violation. 2008.

[67] Douglas P. Finkbeiner and Neal Weiner. Exciting Dark Matter and the INTEGRAL/SPI 511 keV signal. *Phys. Rev.*, D76:083519, 2007.

[68] Douglas P. Finkbeiner. WMAP microwave emission interpreted as dark matter annihilation in the inner Galaxy. 2004.

[69] Dan Hooper, Douglas P. Finkbeiner, and Gregory Dobler. Evidence Of Dark Matter Annihilations In The WMAP Haze. *Phys. Rev.*, D76:083012, 2007.

[70] Dan Hooper, Gabrijela Zaharijas, Douglas P. Finkbeiner, and Gregory Dobler. Prospects For Detecting Dark Matter With GLAST In Light Of The WMAP Haze. *Phys. Rev.*, D77:043511, 2008.

[71] Michael Kesden and Marc Kamionkowski. Galilean Equivalence for Galactic Dark Matter. *Phys. Rev. Lett.*, 97:131303, 2006.

[72] Michael Kesden and Marc Kamionkowski. Tidal Tails Test the Equivalence Principle in the Dark Sector. *Phys. Rev.*, D74:083007, 2006.

[73] Joshua A. Friedman and Ben-Ami Gradwohl. Dark matter and the equivalence principle. *Phys. Rev. Lett.*, 67:2926–2929, 1991.

[74] David N. Spergel and Paul J. Steinhardt. Observational evidence for self-interacting cold dark matter. *Phys. Rev. Lett.*, 84:3760–3763, 2000.

[75] P. M. Sutter and P. M. Ricker. Detecting dark matter-dark energy coupling with the halo mass function. 2008.

[76] Glennys R. Farrar and Rachel A. Rosen. A New Force in the Dark Sector? *Phys. Rev. Lett.*, 98:171302, 2007.

[77] John Ellis. Casting Light on Dark Matter. 2011.

[78] Laura Baudis and for the XENON Collaboration. Results from the XENON100 Dark Matter Search Experiment. 2012.

[79] D.S. Akerib et al. New results from the cryogenic dark matter search experiment. *Phys.Rev.*, D68:082002, 2003.

[80] A. Benoit et al. First results of the EDELWEISS WIMP search using a 320-g heat-and-ionization Ge detector. *Phys.Lett.*, B513:15–22, 2001.

[81] A. Benoit, L. Berge, A. Broniatowski, L. Chabert, B. Chambon, et al. Improved exclusion limits from the edelweiss wimp search. *Phys.Lett.*, B545:43–49, 2002.

[82] D. Yu. Akimov et al. Limits on inelastic dark matter from ZEPLIN-III. *Phys.Lett.*, B692:180–183, 2010.

[83] R. Bernabei et al. Search for WIMP annual modulation signature: Results from DAMA / NaI-3 and DAMA / NaI-4 and the global combined analysis. *Phys.Lett.*, B480:23–31, 2000.

[84] Francis Halzen et al. The AMANDA neutrino telescope and the indirect search for dark matter. *Phys.Rept.*, 307:243–252, 1998.

[85] Gordon Lim. Indirect search for Dark Matter with the ANTARES neutrino telescope. 2007.

[86] R. Abbasi et al. The IceCube Neutrino Observatory IV: Searches for Dark Matter and Exotic Particles. 2011.

[87] S.W. Barwick et al. Measurements of the cosmic ray positron fraction from 1-GeV to 50-GeV. *Astrophys.J.*, 482:L191–L194, 1997.

[88] T. Maeno et al. Successive measurements of cosmic ray anti-proton spectrum in a positive phase of the solar cycle. *Astropart.Phys.*, 16:121–128, 2001. 15 pages, 5 figures.

[89] S. Orito et al. Precision measurement of cosmic ray anti-proton spectrum. *Phys.Rev.Lett.*, 84:1078–1081, 2000.

[90] M. Boezio et al. The Cosmic ray anti-proton flux between 3-GeV and 49-GeV. *Astrophys.J.*, 561:787–799, 2001.

[91] S. Capozziello, M. De Laurentis, and G. Lambiase. f(R) Gravity and the PAMELA results for cosmic relic abundance. 2012.

[92] P. Sreekumar et al. EGRET observations of the extragalactic gamma-ray emission. *Astrophys.J.*, 494:523–534, 1998.

[93] Luigi Tibaldo and for the Fermi/LAT collaboration. Fermi LAT measurements of diffuse gamma-ray emission: results at the first-year milestone. *AIP Conf.Proc.*, 1223:89–98, 2010.

[94] D.A. Carter-Lewis, S. Biller, P.J. Boyle, J.H. Buckley, A. Burdett, et al. Spectrum of TeV gamma-rays from the Crab nebula. 1997.

[95] Rene A. Ong. The status of VHE astronomy. 2003.

[96] Miguel A. Sanchez-Conde and for the MAGIC collaboration. The search for DM in nearby dSph galaxies with MAGIC: candidates, results and prospects. *AIP Conf.Proc.*, 1166:191–196, 2009.

[97] R. Enomoto et al. Design study of CANGAROO-III, stereoscopic imaging atmospheric Cherenkov telescopes for sub-TeV gamma-ray. *Astropart.Phys.*, 16:235–244, 2002.

[98] A. Abramowski et al. Search for Dark Matter Annihilation Signals from the Fornax Galaxy Cluster with H.E.S.S. 2012.

[99] T.C. Weekes, C. Akerlof, S. Biller, A.C. Breslin, J.H. Buckley, et al. VERITAS: Very energetic radiation imaging telescope array system. 1997.

[100] Adam G. Riess et al. Observational evidence from supernovae for an accelerating universe and a cosmological constant. *Astron. J.*, 116:1009–1038, 1998.

[101] S. Perlmutter et al. Measurements of omega and lambda from 42 high-redshift supernovae. *Astrophys. J.*, 517:565–586, 1999.

[102] Adam G. Riess et al. Type ia supernova discoveries at z¿1 from the hubble space telescope: Evidence for past deceleration and constraints on dark energy evolution. *Astrophys. J.*, 607:665–687, 2004.

[103] Pierre Astier et al. The supernova legacy survey: Measurement of ω_m, ω_λ and w from the first year data set. *Astron. Astrophys.*, 447:31–48, 2006.

[104] Adam G. Riess et al. New hubble space telescope discoveries of type ia supernovae at $z > 1$: Narrowing constraints on the early behavior of dark energy. 2006.

[105] M. Kowalski et al. Improved Cosmological Constraints from New, Old and Combined Supernova Datasets. 2008.

[106] D. N. Spergel et al. First Year Wilkinson Microwave Anisotropy Probe (WMAP) Observations: Determination of Cosmological Parameters. *Astrophys. J. Suppl.*, 148:175, 2003.

[107] Jonathan L. Sievers et al. Implications of the Cosmic Background Imager Polarization Data. 2005.

[108] D. N. Spergel et al. Wilkinson microwave anisotropy probe (wmap) three year results: Implications for cosmology. 2006.

[109] G. Hinshaw et al. Three-year wilkinson microwave anisotropy probe (wmap) observations: Temperature analysis. 2006.

[110] Chao-Lin Kuo et al. Improved Measurements of the CMB Power Spectrum with ACBAR. 2006.

[111] N. Jarosik et al. Three-year wilkinson microwave anisotropy probe (wmap) observations: Beam profiles, data processing, radiometer characterization and systematic error limits. 2006.

[112] L. Page et al. Three year wilkinson microwave anisotropy probe (wmap) observations: Polarization analysis. 2006.

[113] C. L. Reichardt et al. High resolution CMB power spectrum from the complete ACBAR data set. 2008.

[114] M. R. Nolta et al. Five-Year Wilkinson Microwave Anisotropy Probe (WMAP) Observations: Angular Power Spectra. 2008.

[115] Daniel J. Eisenstein et al. Detection of the baryon acoustic peak in the large-scale correlation function of sdss luminous red galaxies. *Astrophys. J.*, 633:560–574, 2005.

[116] Will J. Percival et al. Measuring the Baryon Acoustic Oscillation scale using the SDSS and 2dFGRS. *Mon. Not. Roy. Astron. Soc.*, 381:1053–1066, 2007.

[117] Robert R. Caldwell and Marc Kamionkowski. The Physics of Cosmic Acceleration. *Ann.Rev.Nucl.Part.Sci.*, 59:397–429, 2009.

[118] Mark Trodden and Sean M. Carroll. TASI lectures: Introduction to cosmology. pages 703–793, 2004.

[119] E. G. Adelberger et al. Tests of the gravitational inverse-square law. *Ann. Rev. Nucl. Part. Sci.*, 53:77, 2003.

[120] B. Jain and J. Khoury. Cosmological tests of gravity. *Annals of Physics*, 325:1479–1516, July 2010.

[121] G. R. Dvali, Gregory Gabadadze, and Massimo Porrati. 4d gravity on a brane in 5d minkowski space. *Phys. Lett.*, B485:208–214, 2000.

[122] Ignacy Sawicki and Sean M. Carroll. Cosmological Structure Evolution and CMB Anisotropies in DGP Braneworlds. *arXiv e-prints: astro-ph/0510364*, 2005.

[123] Pengjie Zhang. Testing $f(R)$ gravity against the large scale structure of the universe. *Phys. Rev.*, D73:123504, 2006.

[124] Morad Amarzguioui, O. Elgaroy, D. F. Mota, and T. Multamaki. Cosmological constraints on $f(r)$ gravity theories within the palatini approach. *Astron. Astrophys.*, 454:707–714, 2006.

[125] Zong-Kuan Guo, Zong-Hong Zhu, J. S. Alcaniz, and Yuan-Zhong Zhang. Constraints on the DGP Model from Recent Supernova Observations and Baryon Acoustic Oscillations. *Astrophys. J.*, 646:1, 2006.

[126] M. Sadegh Movahed, Marzieh Farhang, and Sohrab Rahvar. Recent observational constraints on the DGP modified gravity. *Int. J. Theor. Phys.*, 48:1203–1230, 2009.

[127] Wenjuan Fang, Sheng Wang, Wayne Hu, Zoltan Haiman, Lam Hui, and Morgan May. Challenges to the DGP Model from Horizon-Scale Growth and Geometry. *Phys.Rev.*, D78:103509, 2008.

[128] Yong-Seon Song, Hiranya Peiris, and Wayne Hu. Cosmological Constraints on f(R) Acceleration Models. *Phys. Rev.*, D76:063517, 2007.

[129] F. C. Carvalho, E. M. Santos, J. S. Alcaniz, and J. Santos. Cosmological Constraints from Hubble Parameter on f(R) Cosmologies. *JCAP*, 0809:008, 2008.

[130] Fabian Schmidt, Alexey Vikhlinin, and Wayne Hu. Cluster Constraints on f(R) Gravity. *Phys.Rev.*, D80:083505, 2009.

[131] Jun-Qing Xia. Constraining DGP Gravity from Observational Data. *Phys. Rev.*, D79:103527, 2009.

[132] Lucas Lombriser, Wayne Hu, Wenjuan Fang, and Uros Seljak. Cosmological Constraints on DGP Braneworld Gravity with Brane Tension. *Phys. Rev.*, D80:063536, 2009.

[133] Edmund J. Copeland, M. Sami, and Shinji Tsujikawa. Dynamics of dark energy. *Int. J. Mod. Phys.*, D15:1753–1936, 2006.

[134] Bhuvnesh Jain and Justin Khoury. Cosmological Tests of Gravity. *Annals Phys.*, 325:1479–1516, 2010.

[135] Salvatore Capozziello, Nakia Carlevaro, Mariafelicia De Laurentis, Massimiliano Lattanzi, and Giovanni Montani. Cosmological implications of a viable non-analytical f(R)- gravity model. *arXiv e-prints: 1104.2169*, 2011.

[136] Tiberiu Harko, Francisco S.N. Lobo, Shin'ichi Nojiri, and Sergei D. Odintsov. $f(R,T)$ gravity. *Phys.Rev.*, D84:024020, 2011.

[137] Justin Khoury and Amanda Weltman. Chameleon fields: Awaiting surprises for tests of gravity in space. *Phys. Rev. Lett.*, 93:171104, 2004.

[138] Justin Khoury and Amanda Weltman. Chameleon cosmology. *Phys. Rev.*, D69:044026, 2004.

[139] Edmund J. Copeland, Andrew R Liddle, and David Wands. Exponential potentials and cosmological scaling solutions. *Phys. Rev.*, D57:4686–4690, 1998.

[140] Jean-Philippe Uzan. Cosmological scaling solutions of non-minimally coupled scalar fields. *Phys. Rev.*, D59:123510, 1999.

[141] Luca Amendola. Coupled quintessence. *Phys. Rev.*, D62:043511, 2000.

[142] Rachel Bean and Joao Magueijo. Dilaton-derived quintessence scenario leading naturally to the late-time acceleration of the universe. *Phys. Lett.*, B517:177–183, 2001.

[143] Rachel Bean. Perturbation evolution with a non-minimally coupled scalar field. *Phys. Rev.*, D64:123516, 2001.

[144] Subinoy Das, Pier Stefano Corasaniti, and Justin Khoury. Super-acceleration as signature of dark sector interaction. *Phys. Rev.*, D73:083509, 2006.

[145] Seokcheon Lee, Guo-Chin Liu, and Kin-Wang Ng. Constraints on the coupled quintessence from cosmic microwave background anisotropy and matter power spectrum. *Phys. Rev.*, D73:083516, 2006.

[146] Niayesh Afshordi, Matias Zaldarriaga, and Kazunori Kohri. On the stability of dark energy with mass-varying neutrinos. *Phys. Rev.*, D72:065024, 2005.

[147] Manoj Kaplinghat and Arvind Rajaraman. Stable Models of superacceleration. *Phys. Rev.*, D75:103504, 2007.

[148] Ole Eggers Bjaelde et al. Neutrino Dark Energy – Revisiting the Stability Issue. *JCAP*, 0801:026, 2008.

[149] Rachel Bean, Eanna E. Flanagan, and Mark Trodden. The Adiabatic Instability on Cosmology's Dark Side. *New J. Phys.*, 10:033006, 2008.

[150] Rachel Bean, Eanna E. Flanagan, and Mark Trodden. Adiabatic instability in coupled dark energy-dark matter models. *Phys. Rev.*, D78:023009, 2008.

[151] Luca Vergani, Loris P. L. Colombo, Giuseppe La Vacca, and Silvio A. Bonometto. Dark Matter - Dark Energy coupling biasing parameter estimates from CMB data. 2008.

[152] Mustapha Ishak, Amol Upadhye, and David N. Spergel. Probing cosmic acceleration beyond the equation of state: Distinguishing between dark energy and modified gravity models. *Phys.Rev.*, D74:043513, 2006.

[153] Lloyd Knox, Yong-Seon Song, and J. Anthony Tyson. Distance-redshift and

growth-redshift relations as two windows on acceleration and gravitation: Dark energy or new gravity? *Phys. Rev.*, D74:023512, 2006.

[154] Martin Kunz and Domenico Sapone. Dark energy versus modified gravity. *Phys. Rev. Lett.*, 98:121301, 2007.

[155] Yong-Seon Song. A Cosmological Test of Standard Gravity by Weak Lensing. *arXiv e-prints: astro-ph/0602598*, 2006.

[156] Istvan Laszlo and Rachel Bean. Nonlinear growth in modified gravity theories of dark energy. *Phys. Rev.*, D77:024048, 2008.

[157] Pengjie Zhang, Michele Liguori, Rachel Bean, and Scott Dodelson. Probing Gravity at Cosmological Scales by Measurements which Test the Relationship between Gravitational Lensing and Matter Overdensity. *Phys. Rev. Lett.*, 99:141302, 2007.

[158] Eric V. Linder. Redshift Distortions as a Probe of Gravity. *Astropart. Phys.*, 29:336–339, 2008.

[159] Bhuvnesh Jain and Pengjie Zhang. Observational Tests of Modified Gravity. *Phys. Rev.*, D78:063503, 2008.

[160] Edmund Bertschinger and Phillip Zukin. Distinguishing Modified Gravity from Dark Energy. *Phys. Rev.*, D78:024015, 2008.

[161] Gong-Bo Zhao, Levon Pogosian, Alessandra Silvestri, and Joel Zylberberg. Searching for modified growth patterns with tomographic surveys. *Phys. Rev.*, D79:083513, 2009.

[162] Yong-Seon Song and Kazuya Koyama. Consistency test of general relativity from large scale structure of the Universe. *JCAP*, 0901:048, 2009.

[163] Shaun A. Thomas, Filipe B. Abdalla, and Jochen Weller. Constraining Modified Gravity and Growth with Weak Lensing. *Mon. Not. Roy. Astron. Soc.*, 395:197–209, 2009.

[164] Yong-Seon Song and Olivier Dore. Testing gravity using weak gravitational lensing and redshift surveys. *JCAP*, 0903:025, 2009.

[165] Alessandra Silvestri and Mark Trodden. Approaches to Understanding Cosmic Acceleration. *Rept. Prog. Phys.*, 72:096901, 2009.

[166] Arthur Stril, Robert N. Cahn, and Eric V. Linder. Testing Standard Cosmology with Large Scale Structure. *Mon. Not. Roy. Astron. Soc.*, 404:239, 2010.

[167] Gong-Bo Zhao, Levon Pogosian, Alessandra Silvestri, and Joel Zylberberg. Cosmological tests of GR – a look at the principals. *Phys. Rev. Lett.*, 103:241301, 2009.

[168] Jacek Guzik, Bhuvnesh Jain, and Masahiro Takada. Tests of Gravity from Imaging and Spectroscopic Surveys. *Phys. Rev.*, D81:023503, 2010.

[169] Reinabelle Reyes et al. Confirmation of general relativity on large scales from weak lensing and galaxy velocities. *Nature*, 464:256–258, 2010.

[170] Levon Pogosian, Alessandra Silvestri, Kazuya Koyama, and Gong-Bo Zhao. How to optimally parametrize deviations from General Relativity in the evolution of cosmological perturbations? *Phys.Rev.*, D81:104023, 2010.

[171] Elise Jennings, Carlton M. Baugh, and Silvia Pascoli. Testing gravity using the growth of large scale structure in the Universe. *Astrophys. J.*, 727:L9, 2011.

[172] Matteo Martinelli et al. Constraining Modified Gravity with Euclid. *Phys. Rev.*, D83:023012, 2011.

[173] Jai-chan Hwang, Hyerim Noh, and Chan-Gyung Park. On cosmologically designed modified gravity theories. *arXiv e-prints: 1012.0885*, 2010.

[174] Yong-Seon Song, Gong-Bo Zhao, David Bacon, Kazuya Koyama, Robert C. Nichol, et al. Complementarity of Weak Lensing and Peculiar Velocity Measurements in Testing General Relativity. *Phys.Rev.*, D84:083523, 2011.

[175] Scott F. Daniel, Eric V. Linder, Tristan L. Smith, Robert R. Caldwell, Asantha Cooray, Alex Leauthaud, and Lombriser Lucas. Testing General Relativity with Current Cosmological Data. *Phys.Rev.*, D81:123508, 2010.

[176] Rachel Bean and Matipon Tangmatitham. Current constraints on the cosmic growth history. *Phys. Rev.*, D81:083534, 2010.

[177] Gong-Bo Zhao et al. Probing modifications of General Relativity using current cosmological observations. *Phys. Rev.*, D81:103510, 2010.

[178] Scott F. Daniel and Eric V. Linder. Confronting General Relativity with Further Cosmological Data. *Phys. Rev.*, D82:103523, 2010.

[179] Jason Dossett, Jacob Moldenhauer, and Mustapha Ishak. Figures of merit and constraints from testing General Relativity using the latest cosmological data sets including refined COSMOS 3D weak lensing. *Phys.Rev.*, D84:023012, 2011.

[180] Stefano Camera, Antonaldo Diaferio, and Vincenzo F. Cardone. Tomography from the Next Generation of Cosmic Shear Experiments for Viable f(R) Models. *JCAP*, 1107:016, 2011.

[181] Bhuvnesh Jain. Designing Surveys for Tests of Gravity. 2011.

[182] Timothy Clifton, Pedro G. Ferreira, Antonio Padilla, and Constantinos Skordis. Modified Gravity and Cosmology. *Phys.Rept.*, 513:1–189, 2012. 312 pages, 15 figures.

[183] Eric V. Linder. Model Independent Tests of Cosmic Gravity. *Phil.Trans.Roy.Soc.Lond.*, A369:4985–4997, 2011.

[184] Shinji Tsujikawa. Modified gravity models of dark energy. *Lect. Notes Phys.*, 800:99–145, 2010.

[185] Emma Beynon, David J. Bacon, and Kazuya Koyama. Weak lensing predictions for modified gravities at non- linear scales. 2009.

[186] Eric V. Linder and Robert N. Cahn. Parameterized beyond-einstein growth. 2007.

[187] Olivier Dore. 2007.

[188] J.-P. Uzan and F. Bernardeau. Lensing at cosmological scales: A test of higher dimensional gravity. *Phys. Rev.*, D64:083004, 2001.

[189] C. Sealfon, L. Verde, and R. Jimenez. Limits on deviations from the inverse-square law on megaparsec scales. *Phys. Rev.*, D71:083004, 2005.

[190] Shinji Tsujikawa. Matter density perturbations and effective gravitational constant in modified gravity models of dark energy. *Phys. Rev.*, D76:023514, 2007.

[191] Carlo Schimd, Jean-Philippe Uzan, and Alain Riazuelo. Weak lensing in scalar-tensor theories of gravity. *Phys. Rev.*, D71:083512, 2005.

[192] Ruth Gregory, V. A. Rubakov, and Sergei M. Sibiryakov. Opening up extra dimensions at ultra-large scales. *Phys. Rev. Lett.*, 84:5928–5931, 2000.

[193] Pierre Binetruy and Joseph Silk. Probing large-distance higher-dimensional gravity with cosmic microwave background measurements. *Phys. Rev. Lett.*, 87:031102, 2001.

[194] Arthur Lue, Roman Scoccimarro, and Glenn D. Starkman. Probing newton's constant on vast scales: Dgp gravity, cosmic acceleration and large scale structure. *Phys. Rev.*, D69:124015, 2004.

[195] Kazuya Koyama and Roy Maartens. Structure formation in the dgp cosmological model. *JCAP*, 0601:016, 2006.

[196] R. Maartens and E. Majerotto. Observational constraints on self-accelerating cosmology. *Phys. Rev.*, D74:023004, 2006.

[197] A. Klypin and J. Holtzman. Particle-mesh code for cosmological simulations. 1997.

[198] R. W. Hockney and J. W. Eastwood. *Computer Simulation Using Particles*. edited by Adam Hilger, IOP Publishing, Bristol, United Kingdom, 1989.

[199] Antony Lewis and Sarah Bridle. Cosmological parameters from cmb and other data: a monte- carlo approach. *Phys. Rev.*, D66:103511, 2002.

[200] M. Davis and P. J. E. Peebles. On the integration of the BBGKY equations for the development of strongly nonlinear clustering in an expanding universe. *Astrophys. J. Supplement Series*, 34:425–450, August 1977.

[201] A.J.S. Hamilton, P. Kumar, E. Lu, and A. Matthews. Detection of the

baryon acoustic peak in the large-scale correlation function of sdss luminous red galaxies. *Astrophys. J.*, 374:L1, 1991.

[202] U. Seljak. *Mon. Not. Roy. Astron. Soc.*, 318:203, 2000.

[203] J.A. Peacock and R.E. Smith. *Mon. Not. Roy. Astron. Soc.*, 318:1144, 2000.

[204] W. H. Press, S. A. Teukolsky, W. T. Vetterling, and B. P. Flannery. *Numerical Recipes : The Art of Scientific Computing*. Cambridge University Press, Cambridge, England, 2007.

[205] Wayne Hu and Ignacy Sawicki. Models of f(r) cosmic acceleration that evade solar-system tests. *Phys. Rev.*, D76:064004, 2007.

[206] Rachel Bean, Eanna E. Flanagan, Istvan Laszlo, and Mark Trodden. Constraining Interactions in Cosmology's Dark Sector. *Phys. Rev.*, D78:123514, 2008.

[207] Steven S. Gubser and P. J. E. Peebles. Structure formation in a string-inspired modification of the cold dark matter model. *Phys. Rev.*, D70:123510, 2004.

[208] Adi Nusser, Steven S. Gubser, and P. J. E. Peebles. Structure formation with a long-range scalar dark matter interaction. *Phys. Rev.*, D71:083505, 2005.

[209] Carolyn Sealfon, Licia Verde, and Raul Jimenez. Limits on deviations from the inverse-square law on megaparsec scales. *Phys. Rev.*, D71:083004, 2005.

[210] Luca Amendola, David Polarski, and Shinji Tsujikawa. Are f(r) dark energy models cosmologically viable ? *Phys. Rev. Lett.*, 98:131302, 2007.

[211] Takeshi Chiba. 1/r gravity and scalar-tensor gravity. *Phys. Lett.*, B575:1–3, 2003.

[212] Thomas Faulkner, Max Tegmark, Emory F. Bunn, and Yi Mao. Constraining f(R) gravity as a scalar tensor theory. *Phys. Rev.*, D76:063505, 2007.

[213] I. Navarro and K. Van Acoleyen. f(R) actions, cosmic acceleration and local tests of gravity. *JCAP*, 0702:022, 2007.

[214] Eanna E. Flanagan. Palatini form of 1/r gravity. *Phys. Rev. Lett.*, 92:071101, 2004.

[215] Baouji Li, David F. Mota, and Douglas J. Shaw. Microscopic and Macroscopic Behaviors of Palatini Modified Gravity Theories. 2008.

[216] Antony Lewis and Anthony Challinor. Evolution of cosmological dark matter perturbations. *Phys. Rev.*, D66:023531, 2002.

[217] J. Dunkley et al. Five-Year Wilkinson Microwave Anisotropy Probe (WMAP) Observations: Likelihoods and Parameters from the WMAP data. 2008.

[218] I. Laszlo, R. Bean, D. Kirk and S. Bridle. Modified gravity from cosmic shear with intrinsic alignments. 2011.

[219] D. Kirk, I. Laszlo, S. Bridle and R. Bean. Optimising cosmic shear surveys to measure modifications to gravity on cosmic scales. 2011.

[220] Christopher M. Hirata and Uros Seljak. Intrinsic alignment-lensing interference as a contaminant of cosmic shear. *Phys. Rev.*, D70:063526, 2004.

[221] Rupert A. C. Croft and Christopher A. Metzler. Weak lensing surveys and the intrinsic correlation of galaxy ellipticities. *Astrophys. J.*, 545:561–571, 2000.

[222] Robert G. Crittenden, Priyamvada Natarajan, Ue-Li Pen, and Tom Theuns. Spin induced galaxy alignments and their implications for weak lensing measurements. *Astrophys. J.*, 559:552–571, 2001.

[223] Alan Heavens, Alexandre Refregier, and Catherine Heymans. Intrinsic Correlation of Galaxy Shapes: Implications for Weak Lensing Measurements. *Mon. Not. Roy. Astron. Soc.*, 319:649, 2000.

[224] Catherine Heymans, 1 White, Martin J., Alan Heavens, Chris Vale, and Ludovic Van Waerbeke. Potential sources of contamination to weak lensing measurements: constraints from N-body simulations. *Mon.Not.Roy.Astron.Soc.*, 371:750–760, 2006.

[225] R. Mandelbaum, C. M. Hirata, M. Ishak, U. Seljak, and J. Brinkmann. Detection of large-scale intrinsic ellipticity-density correlation from the Sloan Digital Sky Survey and implications for weak lensing surveys. *Monthly Notices of the Royal Astronomical Society*, 367:611–626, April 2006.

[226] C. M. Hirata, R. Mandelbaum, M. Ishak, U. Seljak, R. Nichol, K. A. Pimbblet, N. P. Ross, and D. Wake. Intrinsic galaxy alignments from the 2SLAQ and SDSS surveys: luminosity and redshift scalings and implications for weak lensing surveys. *Monthly Notices of the Royal Astronomical Society*, 381:1197–1218, November 2007.

[227] Teppei Okumura, Y. P. Jing, and Cheng Li. Intrinsic Ellipticity Correlation

of SDSS Luminous Red Galaxies and Misalignment with their Host Dark Matter Halos. *Astrophys. J.*, 694:214–221, 2009.

[228] T. Okumura and Y. P. Jing. The Gravitational Shear-Intrinsic Ellipticity Correlation Functions of Luminous Red Galaxies in Observation and in the ΛCDM Model. *Astrophysical Journal Letters*, 694:L83–L86, March 2009.

[229] A. Faltenbacher, C. Li, S. D. M. White, Y.-P. Jing, Shu-DeMao, and J. Wang. Alignment between galaxies and large-scale structure. *Research in Astronomy and Astrophysics*, 9:41–58, January 2009.

[230] Maria J. Pereira and Greg L. Bryan. Tidal Torquing of Elliptical Galaxies in Cluster Environments. *Astrophys. J.*, 721:939–955, 2010.

[231] M. L. Brown, A. N. Taylor, N. C. Hambly, and S. Dye. Measurement of intrinsic alignments in galaxy ellipticities. *Mon. Not. Roy. Astron. Soc.*, 333:501, 2002.

[232] Christopher M. Hirata et al. Galaxy - galaxy weak lensing in SDSS: Intrinsic alignments and shear calibration errors. *Mon.Not.Roy.Astron.Soc.*, 353:529, 2004.

[233] M. J. Pereira and Jeffrey R. Kuhn. Dynamic Tidal Alignment of Cluster Galaxies. *arXiv e-prints: astro-ph/0411710*, 2004.

[234] Rachel Mandelbaum et al. Systematic errors in weak lensing: application to SDSS galaxy-galaxy weak lensing. *Mon. Not. Roy. Astron. Soc.*, 361:1287–1322, 2005.

[235] Ingolfur Agustsson and Tereasa G. Brainerd. The Orientation of Satellite Galaxies: Evidence of Elongation in the Direction of the Host. *Astrophys. J.*, 644:L25–L28, 2006.

[236] Rachel Mandelbaum et al. The WiggleZ Dark Energy Survey: Direct constraints on blue galaxy intrinsic alignments at intermediate redshifts. *arXiv e-prints: 0911.5347*, 2009.

[237] Tereasa G. Brainerd, Ingolfur Agustsson, Chad A. Madsen, and Jeffrey A. Edmonds. Large-Scale Intrinsic Alignment of Galaxy Images. 2009.

[238] R. J. Siverd, B. S. Ryden, and B. S. Gaudi. Galaxy Orientation and Alignment Effects in the SDSS DR6. *arXiv e-prints: 0903.2264*, 2009.

[239] Jounghun Lee. On the Intrinsic Alignments of the Late-Type Spiral Galaxies from the Sloan Digital Sky Survey Data Release 7. *Astrophys. J.*, 732:99, 2011.

[240] B. Joachimi, R. Mandelbaum, F.B. Abdalla, and S.L. Bridle. Constraints on intrinsic alignment contamination of weak lensing surveys using the MegaZ-LRG sample. *Astron.Astrophys.*, 527:A26, 2011.

[241] Jonathan Blazek, Matthew McQuinn, and Uros Seljak. Testing the tidal alignment model of galaxy intrinsic alignment. *JCAP*, 1105:010, 2011.

[242] Jiangang Hao, Jeffrey M. Kubo, Robert Feldmann, James Annis, David E. Johnston, Huan Lin, and Timothy A. McKay. Intrinsic Alignment of Cluster Galaxies: the Redshift Evolution. *Astrophys.J.*, 740:39, 2011.

[243] S. Bridle and L. King. Dark energy constraints from cosmic shear power spectra: impact of intrinsic alignments on photometric redshift requirements. *New Journal of Physics*, 9:444–+, December 2007.

[244] L. King and P. Schneider. Suppressing the contribution of intrinsic galaxy alignments to the shear two-point correlation function. *Astronomy and Astrophysics*, 396:411–418, December 2002.

[245] L. J. King and P. Schneider. Separating cosmic shear from intrinsic galaxy alignments: Correlation function tomography. *Astronomy and Astrophysics*, 398:23–30, January 2003.

[246] C. Heymans and A. Heavens. Weak gravitational lensing: reducing the contamination by intrinsic alignments. *Monthly Notices of the Royal Astronomical Society*, 339:711–720, March 2003.

[247] M. Takada and M. White. Tomography of Lensing Cross-Power Spectra. *Astrophysical Journal Letters*, 601:L1–L4, January 2004.

[248] B. Joachimi and P. Schneider. Controlling intrinsic alignments in weak lensing statistics: The nulling and boosting techniques. *arXiv e-prints: 1009.2024*, 2010.

[249] B. Joachimi and P. Schneider. Intrinsic alignment boosting: Direct measurement of intrinsic alignments in cosmic shear data. *Astron. Astrophys.*, 517:A4, 2010.

[250] P. Catelan, M. Kamionkowski, and R. D. Blandford. Intrinsic and extrinsic galaxy alignment. *Monthly Notices of the Royal Astronomical Society*, 320:L7–L13, January 2001.

[251] L. Hui and J. Zhang. Intrinsic/Extrinsic Density-Ellipticity Correlations and Galaxy-Galaxy Lensing. *arXiv e-prints: astro-ph/0205512*, May 2002.

[252] J. Lee, V. Springel, U.-L. Pen, and G. Lemson. Quantifying the cosmic web - I. The large-scale halo ellipticity-ellipticity and ellipticity-direction correlations. *Monthly Notices of the Royal Astronomical Society*, 389:1266–1274, September 2008.

[253] B. Joachimi, R. Mandelbaum, F. B. Abdalla, and S. L. Bridle. Constraints on intrinsic alignment contamination of weak lensing surveys using the MegaZ-LRG sample. *Astronomy and Astrophysics*, 527:A26+, March 2011.

[254] J. Blazek, M. McQuinn, and U. Seljak. Testing the tidal alignment model of galaxy intrinsic alignment. *ArXiv e-prints: 1101.4017*, January 2011.

[255] Marcel P. van Daalen, Joop Schaye, C. M. Booth, and Claudio Dalla Vecchia. The effects of galaxy formation on the matter power spectrum: A challenge for precision cosmology. *Mon. Not. Roy. Astron. Soc.*, 415:3649–3665, 2011.

[256] Elisabetta Semboloni, Henk Hoekstra, Joop Schaye, Marcel P. van Daalen, and Ian J. McCarthy. Quantifying the effect of baryon physics on weak lensing tomography. *arXiv e-prints: 1105.1075*, 2011.

[257] M. D. Schneider and S. Bridle. A halo model for intrinsic alignments of galaxy ellipticities. *Monthly Notices of the Royal Astronomical Society*, 402:2127–2139, March 2010.

[258] Donnacha Kirk, Sarah Bridle, and Michael Schneider. The Impact of Intrinsic Alignments: Cosmological Constraints from a Joint Analysis of Cosmic Shear and Galaxy Survey Data. *Mon. Not. Roy. Astron. Soc.*, 408:1502–1515, 2010.

[259] Gary M. Bernstein. Comprehensive Two-Point Analyses of Weak Gravitational Lensing Surveys. *Astrophys. J.*, 695:652–665, 2009.

[260] T. D. Kitching and A. N. Taylor. Path Integral Marginalization for Cosmology: Scale Dependent Galaxy Bias & Intrinsic Alignments. *arXiv e-prints: 1005.2063*, 2010.

[261] G. M. Bernstein. Comprehensive Two-Point Analyses of Weak Gravitational Lensing Surveys. *Astrophysical Journal*, 695:652–665, April 2009.

[262] B. Joachimi and S. L. Bridle. Simultaneous measurement of cosmology and intrinsic alignments using joint cosmic shear and galaxy number density correlations. *ArXiv e-prints*, November 2009.

[263] B. Joachimi and S.L. Bridle. Simultaneous measurement of cosmology and intrinsic alignments using joint cosmic shear and galaxy number density correlations. *Astron.Astrophys.*, 523:A1, 2010. * Brief entry *.

[264] Pengjie Zhang. A proposal on the galaxy intrinsic alignment self- calibration in weak lensing surveys. *Mon. Not. Roy. Astron. Soc.*, 406:L95, 2010.

[265] Wayne Hu and Bhuvnesh Jain. Joint Galaxy-Lensing Observables and the Dark Energy. *Phys. Rev.*, D70:043009, 2004.

[266] Pengjie Zhang, Rachel Bean, Michele Liguori, and Scott Dodelson. Weighing the spatial and temporal fluctuations of the dark universe. *arXiv e-prints: 0809.2836*, 2008.

[267] A. Amara and A. Refregier. Optimal Surveys for Weak Lensing Tomography. *ArXiv Astrophysics e-prints*, October 2006.

[268] S. Bridle and L. King. Dark energy constraints from cosmic shear power spectra: impact of intrinsic alignments on photometric redshift requirements. *New Journal of Physics*, 9:444–+, December 2007.

[269] Z. Ma, W. Hu, and D. Huterer. Effects of Photometric Redshift Uncertainties on Weak-Lensing Tomography. *Astrophysical Journal*, 636:21–29, January 2006.

[270] Dragan Huterer, Masahiro Takada, Gary Bernstein, and Bhuvnesh Jain. Systematic errors in future weak lensing surveys: Requirements and prospects for self-calibration. *Mon. Not. Roy. Astron. Soc.*, 366:101–114, 2006.

[271] D. Huterer, M. Takada, G. Bernstein, and B. Jain. Systematic errors in future weak-lensing surveys: requirements and prospects for self-calibration. *Monthly Notices of the Royal Astronomical Society*, 366:101–114, February 2006.

[272] Michel Chevallier and David Polarski. Accelerating universes with scaling dark matter. *Int. J. Mod. Phys.*, D10:213–224, 2001.

[273] Ian Smail, Richard S. Ellis, and Michael J. Fitchett. Gravitational Lensing of Distant Field Galaxies by Rich Clusters: I. – Faint Galaxy Redshift Distributions. *arXiv e-prints: astro-ph/9402048*, 1994.

[274] Avishai Dekel and Ofer Lahav. Stochastic nonlinear galaxy biasing. *Astrophys.J.*, 520:24–34, 1999.

[275] Antony Lewis, Anthony Challinor, and Anthony Lasenby. Efficient Computation of CMB anisotropies in closed FRW models. *Astrophys. J.*, 538:473–476, 2000.

[276] Sean M. Carroll, William H. Press, and Edwin L. Turner. The Cosmological constant. *Ann. Rev. Astron. Astrophys.*, 30:499–542, 1992.

[277] R. E. Smith et al. Stable clustering, the halo model and nonlinear cosmological power spectra. *Mon. Not. Roy. Astron. Soc.*, 341:1311, 2003.

[278] Andreas Albrecht et al. Findings of the Joint Dark Energy Mission Figure of Merit Science Working Group. *arXiv e-prints: 0901.0721*, 2009.

[279] Anais Rassat, Adam Amara, Luca Amendola, Francisco J. Castander, Thomas Kitching, et al. Deconstructing Baryon Acoustic Oscillations: A Comparison of Methods. *arXiv e-prints: 0810.0003*, 2008. * Brief entry *.

[280] Dragan Huterer and Michael S. Turner. Probing the dark energy: Methods and strategies. *Phys. Rev.*, D64:123527, 2001.

[281] Yun Wang et al. Designing a space-based galaxy redshift survey to probe dark energy. *Mon. Not. Roy. Astron. Soc.*, 409:737, 2010.

[282] Hiroaki Oyaizu. Non-linear evolution of f(R) cosmologies I: methodology. *Phys. Rev.*, D78:123523, 2008.

[283] Hiroaki Oyaizu, Marcos Lima, and Wayne Hu. Non-linear evolution of f(R) cosmologies II: power spectrum. *Phys. Rev.*, D78:123524, 2008.

[284] Fabian Schmidt, Marcos Vinicius Lima, Hiroaki Oyaizu, and Wayne Hu. Non-linear Evolution of f(R) Cosmologies III: Halo Statistics. *Phys. Rev.*, D79:083518, 2009.

[285] Justin Khoury and Mark Wyman. N-Body Simulations of DGP and Degravitation Theories. *Phys. Rev.*, D80:064023, 2009.

[286] Simone Ferraro, Fabian Schmidt, and Wayne Hu. Cluster Abundance in f(R) Gravity Models. *Phys. Rev.*, D83:063503, 2011.

[287] Weiguang Cui, Pengjie Zhang, and Xiaohu Yang. Nonlinearities in modified gravity cosmology I: signatures of modified gravity in the nonlinear matter power spectrum. *Phys. Rev.*, D81:103528, 2010.

[288] Gong-Bo Zhao, Baojiu Li, and Kazuya Koyama. N-body Simulations for f(R) Gravity using a Self-adaptive Particle-Mesh Code. *Phys. Rev.*, D83:044007, 2011.

[289] Philippe Brax, Carsten van de Bruck, Anne-Christine Davis, Baojiu Li, and

Douglas J. Shaw. Nonlinear Structure Formation with the Environmentally Dependent Dilaton. *Phys. Rev.*, D83:104026, 2011.

[290] Mariafelicia De Laurentis, Salvatore Capozziello, Ivan De Martino, and Michelangelo Formisano. Cosmological distance indicators by coalescing binaries. 2011.